VELOCITY MEASUREMENTS IN A TRANSONIC COMPRESSOR USING A CALIBRATED PRESSURE PROBE

Dennis Jay Anderson

NAVAL POSTGRADUATE SCHOOL
Monterey, California

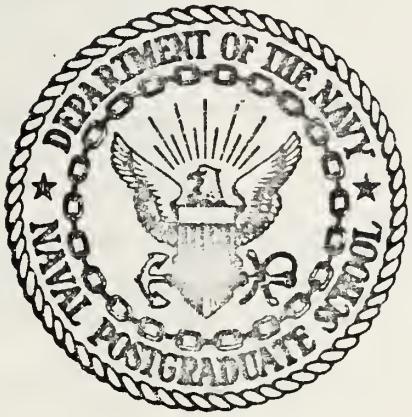

THESIS

Velocity Measurements in a Transonic Compressor Using a Calibrated Pressure Probe

by

Dennis Jay Anderson

Thesis Advisor R. P. Shreeve

SECURITY CLASSIFICATION OF THIS PAGE (When Data Entered)

REPORT DOCUMENTATION PAGE		READ INSTRUCTIONS BEFORE COMPLETING FORM
1. REPORT NUMBER	2. GOVT ACCESSION NO.	3. RECIPIENT'S CATALOG NUMBER
4. TITLE (and Subtitle) Velocity Measurements in a Transonic Compressor Using a Calibrated Pressure Probe		5. TYPE OF REPORT & PERIOD COVERED Master's Thesis: March 1975 6. PERFORMING ORG. REPORT NUMBER
7. AUTHOR(s) Dennis Jay Anderson		8. CONTRACT OR GRANT NUMBER(s)
9. PERFORMING ORGANIZATION NAME AND ADDRESS Naval Postgraduate School Monterey, California 93940		10. PROGRAM ELEMENT, PROJECT, TASK AREA & WORK UNIT NUMBERS
11. CONTROLLING OFFICE NAME AND ADDRESS Naval Postgraduate School Monterey, California 93940		12. REPORT DATE March 1975 13. NUMBER OF PAGES
14. MONITORING AGENCY NAME & ADDRESS(if different from Controlling Office) Naval Postgraduate School Monterey, California 93940		15. SECURITY CLASS. (of this report) Unclassified 15a. DECLASSIFICATION/DOWNGRADING SCHEDULE

16. DISTRIBUTION STATEMENT (of this Report)

Approved for public release: distribution unlimited.

17. DISTRIBUTION STATEMENT (of the abstract entered in Block 20, if different from Report)

18. SUPPLEMENTARY NOTES

19. KEY WORDS (Continue on reverse side if necessary and identify by block number)

Pressure probe calibration
Transonic compressor
Velocity and angle distribution
Rotor inlet and exit

20. ABSTRACT (Continue on reverse side if necessary and identify by block number)

The application is reported of a United Sensor Corporation 5-hole pressure probe to determine the flow field upstream and downstream of the rotor of a transonic compressor operating to near sonic speeds. Calibration of the probe was reduced to a set of equations to allow off-line data reduction and presentation using a Hewlett-Packard Model 9830A Calculator system. The flow velocities and angles measured upstream of the rotor were

DD FORM 1 JAN 73 1473 EDITION OF 1 NOV 65 IS OBSOLETE
S/N 0102-014-6601 |
(Page 1)

SECURITY CLASSIFICATION OF THIS PAGE (When Data Entered)

compared with results of compressible flow calculations. Blockage factors were determined which related analytical approximations of the flow incident at the rotor to the measured flow rate. The measurements downstream of the rotor were compared with those of a second probe of different design. Both probes required corrections to their calibrations which were established in an axial annular flow of similar geometric cross section. It is shown that the results derived from the corrected calibration of the 5-hole probe were the more accurate.

Velocity Measurements in a Transonic Compressor Using a Calibrated Pressure Probe

by

Dennis Jay Anderson
Lieutenant, United States Navy
B.S., Purdue University, 1968

Submitted in partial fulfillment of the requirements for the degree of

MASTER OF SCIENCE IN AERONAUTICAL ENGINEERING

from the

NAVAL POSTGRADUATE SCHOOL
March 1975

ABSTRACT

The application is reported of a United Sensor Corporation 5-hole pressure probe to determine the flow field upstream and downstream of the rotor of a transonic compressor operating to near sonic speeds. Calibration of the probe was reduced to a set of equations to allow off-line data reduction and presentation using a Hewlett-Packard Model 9830A Calculator system. The flow velocities and angles measured upstream of the rotor were compared with results of compressible flow calculations. Blockage factors were determined which related analytical approximations of the flow incident at the rotor to the measured flow rate. The measurements downstream of the rotor were compared with those of a second probe of different design. Both probes required corrections to their calibrations which were established in an axial annular flow of similar geometric cross section. It is shown that the results derived from the corrected calibration of the 5-hole probe were the more accurate.

ACKNOWLEDGEMENT

The experimentation and analysis reported in this paper was supported with countless hours of guidance and counseling by my thesis advisor, Visiting Associate Professor R.P. Shreeve. I wish to express my gratitude for all of his time and genuine interest in this work.

The experimental work would not have been possible without the talents of Mr. J.E. Hammer who supervised and maintained the calibration equipment, compressor test rig and instrumentation. His advice, and knowledge of experimental techniques, was invaluable.

TABLE OF CONTENTS

LIST OF TABLES

ILLUSTRATIONS

ILLUSTRATIONS

ILLUSTRATIONS

ILLUSTRATIONS

TABLE OF SYMBOLS

Latin

c_p	Constant pressure specific heat	(BTU/lbm-^oR)
F_ϕ	5-hole probe calibration factor	(-)
F'_ϕ	5-hole probe calibration function	(-)
F_θ	5-hole probe calibration factor	(-)
F'_θ	5-hole probe calibration function	(-)
F'_λ	5-hole probe calibration function (F'_ϕ/F'_θ)	
H	Normalized distance (y/h)	(-)
h	Distance from hub to outer wall	(in)
K	Constant	(-)
$\bar{K}_\phi$	Pitch angle correction constant	(-)
$\bar{K}_x$	Velocity correction constant	(-)
M	Mach number	(-)
p	Pressure	(lbf/in.^{2})
p_1	Pressure port 1	(in.H_2O)
p_2	Pressure port 2	(in.H_2O)
p_3	Pressure port 3	(in.H_2O)
p_4	Pressure port 4	(in.H_2O)
p_5	Pressure port 5	(in.H_2O)
p_{23}	Average of pressure ports 2 and 3	(in.H_2O)
r	Distance from compressor centerline	(in.)
R	Normalized distance (r/r_o)	(-)
R_G	Gas constant	(ft-lbf/lbm-^oR)
V	Velocity	(ft/sec)
$\dot{w}$	Mass flow rate	(lbm/sec)
$\bar{W}$	$\dot{w}/\rho_t V_t \pi r_o^2$	(-)

X	Non-dimensional velocity (V/V_t)	(-)
y	Distance from hub	(in.)

Greek

Δ	Finite difference	(-)
$\mathcal{E}$	Convergence limit for iteration	(-)
γ	Ratio of specific heats	(-)
λ	Flow pitch angle	(rad.)
ϕ	Flow pitch angle	(deg.)
Φ	Flow function	
$\bar{\Phi}$	Normalized flow function (Φ/Φ_o)	(-)
ρ	Density	(lbm/ft^3)
ξ	Ratio of total non-dimensional flow rate to flow function at the compressor outer wall	(-)

Subscripts

B	Blockage
i	The $i^{\underline{th}}$ value
j	The $j^{\underline{th}}$ value
m	Measured
o	Outer wall
r	Reference
s	Static
t	Total (or stagnation)
1	Station 1 (rotor inlet)

I. INTRODUCTION

The study reported here is an initial part of a program to obtain a full understanding of the flow within a transonic compressor stage, with the ultimate object of obtaining improved designs. Toward this goal, a transonic compressor of the "impulse" type was designed and built by Dr. M.H. Vavra in the Turbopropulsion Laboratories at the Naval Postgraduate School. The work was sponsored by Naval Air Systems Command, Code 310 through the office of Mr. H.J. Mueller. The so-called TRANSX compressor has been operated to 65% of design speed.

The inlet of the TRANSX compressor is designed to contract and to rapidly accelerate the flow in order to generate near uniform conditions, with thin boundary layers, at the rotor face. It is necessary to determine the radial distributions of the flow velocity and angle in order to establish the operating condition and to evaluate the performance of the rotor blading. At or near design speeds, the possibility that wakes in the flow might induce vibrations in the highly stressed rotor blades, prohibits the use of probes just upstream of the rotor. Therefore it is necessary to be able to predict velocity and pitch angle distributions at high speeds from data gathered at lower speeds. Reference 1 gives analytical approximations of the rotor face flow velocity and angle distributions which were obtained from compressible flow calculations. The first goal of the present study was to determine the flow into the rotor by measurement, and to compare the results with the analytical predictions.

A United Sensor 5-hole cylindrical pressure probe was selected for its ability to measure pitch angle and for ease of mounting. The probe calibration was first established in a uniform jet. Following a description of the TRANSX compressor in Section II, the investigation upstream of the rotor is described in Section III of this report.

Measurement of the flow downstream of the rotor is necessary in order to establish blade element performance. The calibrated United Sensor 5-hole probe and a NASA combination probe [Ref. 2] were used simultaneously to conduct radial surveys of the flow downstream of the rotor. In this manner redundant measurements of Mach number and flow angle were obtained using two completely independent probes and their respective calibrations. It was found that the Mach numbers evaluated by the two probes disagreed by as much as 10% when the calibrations, established in the uniform jet, were applied to the probe measurements made downstream of the rotor. Methods were devised for correcting the calibrations established in the uniform jet for application of the probes in the smaller compressor annulus. Following the application of corrections, which were greatest for the NASA probe, the disagreement in Mach number profiles was greatly reduced; in some cases to less than 1%. The measurements carried out downstream of the rotor using the 5-hole probe are described in Section IV.

The calibration of the 5-hole probe and the method devised for correcting the calibration for application in the compressor annulus are described fully in Appendix A.

Inter-related non-linear calibration relations are therein represented by analytic functions which allow computer reduction of probe survey measurements. The methods described in Appendix A can be adapted to other probes and to measurements with the same probe in passages of different geometry.

II. THE TRANSONIC COMPRESSOR

A. DESCRIPTION

A schematic of the compressor test rig is shown in Fig. 1. The test rig consists of an air-turbine drive unit and an induction section containing a filter, a throttle, a settling chamber and a flow measuring nozzle. The air turbine is designed to deliver 450 H.P. at 30,000 RPM. The transonic compressor is designed to operate at 30,460 RPM with a relative tip Mach number of 1.5. The compressor flow rate is controlled by a rotating throttle plate [Fig. 1]. The test rig, located in an explosion proof cell, is controlled by an operator at a remote console. A complete description of the laboratory facilities are given in Ref. 3, and the details of the test rig design is given in Ref. 4. Figure 2 shows the compressor assembly and identifies the instrumentation stations 0 through 3 referred to in the following discussion. As indicated in view J of Fig. 2, peripheral surveys were made by rotating the outer casing.

B. INSTRUMENTATION

The transonic compressor is equipped with stationary probes to provide routine performance data. The measurement of torque was not available at any time during this

investigation, since the honeycomb flow straightener (Fig. 3) was removed to allow higher flow rates. The fixed instrumentation is not discussed in this report.

The results presented here were obtained using a United Sensor DA-125 three dimensional pressure probe. The probe calibration is reported in detail in Appendix A. The probe mounting arrangement is shown in Fig. 3. Radial surveys were taken at a fixed peripheral angle by manually positioning the probe using a traverse unit. Peripheral surveys were made by manually rotating the outer casing, causing the probe to move through an arc at a fixed radius. All pressures were measured by a calibrated transducer in a scanivalve arrangement. Predetermined angular and radial positions were input into the data logging system on thumb wheels.

C. DATA ACQUISITION AND REDUCTION

A data logging system [Ref. 3] was used to scan and record pressure, temperature and position data. The recorded output was on punched paper tape. Reduction of data was carried out using a Hewlett-Packard Model 9830A Calculator system, shown schematically in Fig. 4.

A program, designated TCR Reduction (Station 1), was written to reduce data from rotor inlet flow measurements. Datawere input from the punched tapes. The program calculated and printed the non-dimensional radial probe position, compressor case angle, flow pitch and yaw angles, non-dimensional velocity, velocity and Mach number. These results

were stored on digital magnetic tape and the radial distributions were graphed using the X-Y plotter (Fig. 4).

A program entitled TCR Reduction (Station 2) was written to calculate the flow downstream of the rotor from probe measurements. The program accepted data from magnetic tape, rather than punched paper tape. The paper tape data were therefore transferred to magnetic tape before beginning data reduction. This procedure was selected because data from two different probes were required to be in the same form to allow distribution plots to be made on a common graph. When data had been reduced, the calculated results were stored on magnetic tape and the radial profiles were produced on the X-Y plotter.

III. FLOW INTO THE ROTOR

A. DESCRIPTION OF TESTS

The purpose of these surveys was to measure the flow properties at the rotor inlet and to compare the results with analytical distributions reported in Ref. 1. Preliminary impact pressure surveys were made prior to this investigation, and as a result, a bellmouth inlet fairing was added (Fig. 2) to improve inlet profiles.

The 5-hole probe was positioned ahead of the rotor at station 1. The flow profiles were measured in two separate runs (numbered 33 and 39). All surveys were radial, from hub-to-tip. The speed was set at 50% of design speed in run 33, and varied from 65% to 40% of design speed in run 39.

Throttle settings corresponded to fully open, near surge, or design point for each speed of a given survey. The case angle, or peripheral location of the probe, was not considered to be significant for measurements at this station.

The surveys began with the sensing holes 0.27 inch from the rotor hub. The probe was then withdrawn in 0.1 inch intervals until the total pressure sensing port was flush with the inner surface of the casing. At each point, pressure, temperature and position data were recorded on punched tape. These data were reduced to velocities, angles and non-dimensional position.

B. RESULTS

Radial distributions of the pitch angle and Mach number derived from probe measurements are shown in Fig. 5 to Fig. 11. The measured data were reduced using the probe calibration described in Appendix A, section A2. The radial distribution of pitch angle, derived in Ref. 1, is also shown on the plots. The data were taken in two separate tests. Results from run 33 in Figs. 5-7 show good agreement with the derived profile except at the upper and lower 20% of the distribution. Note the wall effect on pitch angles for radial positions greater than R=0.85. Within the measurement accuracy, distribution of pitch angle is independent of flow rate for all surveys taken in a given test. The results of run 39 (Figs. 9-12) show an overall reduced level of pitch angle, but also shows no dependence upon throttle position or speed. The reason for the reduced levels is not known and should first be confirmed by further measurements.

In order to plot the analytical Mach number distribution as a comparison with the measurements plotted in Fig. 5 to Fig. 11, the area blockage factor must first be determined. Therefore the measured distribution of the mass flux compared with the analytical distribution was chosen to represent the same information, and is presented in the following section.

The calibration correction for application in the compressor annulus does not apply to measurements at the rotor inlet. However, this correction was applied to the profile in Fig. 6, and the results displayed in Fig. 8. The correction applied near the outer wall causes the profile to better match the analytical distribution at the wall. Since the wall angle at the inlet is the same as that in the calibration annulus, the effect brought about by applying the correction supports its validity for this region.

C. DETERMINATION OF BLOCKAGE FACTOR

Details of blockage factor calculations are given in Appendix B. Reference 1 determined a viscous blockage factor, K_{B_1}=0.989, which accounted for wall boundary layer displacement thickness. Figures 13 and 14 show distributions of the non-dimensional mass flux, or flow function obtained from probe measurements and a comparison with the analytical distribution given in Ref. 1 and Appendix B. It is shown in Appendix B that by equating the integral of the measured mass flux, over the region for which the probe measurements are free of wall effects, to the integral of the analytical mass

flux distribution, a blockage factor can be defined. The blockage factors listed in Figures 13 and 14 were obtained in this manner and the analytical distributions are consistent with these values.

The prediction that the mass flux increases with increasing radius is supported by the measurements, but the measured variation is larger than anticipated. This could be the result of the inlet bellmouth velocity profile which has yet to be measured.

The mass flux profiles are quite similar in shape, but considerable variation occurs in the blockage factors deduced from the measurements (.963 to .984). This is possibly due to the measurement of the total mass flow rate, which was observed to vary during the surveys. As shown in Appendix B, an attempt was made to eliminate this effect; however insufficient data was taken to make the process statistically accurate. It is observed that the smallest blockage factors were obtained at the lowest flow rates, for which the measurements are least accurate. However, it is also noted that at highly reduced throttle settings, greater distortion appears in the profiles near the rotor tip, suggesting that an increase in blockage does indeed occur. This question may be resolved by collecting more data with the objective of determining how blockage varies with RPM and throttling conditions.

Figures 15 and 16 show calculated flow distributions into the rotor using the method of Ref. 1 with a blockage factor of 0.98. Note, in Fig. 15, that choking of the inlet

occurs at slightly greater than 21 lb/sec. As blockage increases (decreasing effective cross sectional inlet area) choking occurs at lower flow rates. Figure 16 shows that the rotor blade relative Mach number is subsonic everywhere at the speeds encountered thus far. At design speed (30,460 RPM) 80% of the blading will see supersonic relative velocities, assuming a blockage factor of approximately 0.98.

IV. FLOW DOWNSTREAM OF THE ROTOR

A. DESCRIPTION OF TESTS

The United Sensor probe and a NASA combination probe [Ref. 2] were mounted at station 2, separated peripherally by a 45° angle. There was a 1.5° difference in the position of each probe with respect to a stator blade leading edge. Peripheral surveys were plotted such that peripheral angle displacement of each probe was measured with a stator blade leading edge as reference. During radial surveys the two probes were moved outwards and data from both were taken simultaneously.

Three separate runs, numbered 43, 44 and 45 are reported. The tests consisted of one radial survey and one peripheral survey at the passage centerline for each of the three runs. Runs 43 and 44 were conducted at the same RPM, but at different throttle settings. Runs 44 and 45 were conducted at the same throttle setting, but at different speeds.

The purpose of these surveys was to verify measurements

through redundancy and to calculate rotor performance. Agreement was obtained only after probe calibrations were corrected, as described in Appendix A. The verification of the measurements themselves is described in this section, and the procedure for calibration, correction and application to the 5-hole pressure probe is described in Appendix A. The evaluation of rotor blade element performance will be reported separately.

B. RESULTS

Figure 17 shows a comparison of Mach numbers for run 45, point 3, evaluated from 5-hole and NASA probe measurements using calibrations established in a uniform jet. Approximately 10% disagreement between the measured Mach numbers was observed. Since neither the static pressure distributions calculated from the 5-hole probe calibration nor that from the NASA probe calibration were consistent with the measured compressor hub and tip wall pressures, the Mach number distributions shown in Fig. 17 were not acceptable. It had also been observed from surveys of the uniform jet, described in Appendix A, that the probes indicated uniform flow profiles over different regions of the flow. In particular, the NASA probe failed to indicate uniform conditions until it was traversed radially more than 3 inches into the flow. The effect of "immersion" or "wall effect" on the calibration of the two probes was the probable cause of the observed disagreement exhibited in Fig. 17. Since the magnitude of the immersion effect, in the uniform jet, was quite

different for each probe, the approach taken was to first devise separate corrections to the calibrations of the two probes. Agreement between the corrected survey measurements with both probes, and consistency of the calculated static pressure distributions with the measurements at the hub and tip walls were sought. The corrections were based upon survey measurements made in an annular axial flow passage which was similar in size to the compressor annulus downstream of the rotor. The procedure for correcting the 5-hole probe calibration is described in Section A3 of Appendix A.

The results shown in Fig. 18 to Fig. 29 were obtained following the application of corrections to the measurements of both probes. The upper sections of Figs. 18-23 show the impact pressure (to the right) and indicated static pressure (dashed lines) measured by the probes. The solid lines toward the left are the distributions of static pressure evaluated from the probe measurements after the annulus corrections were applied. The lower sections of Fig. 18 to Fig. 23 compare Mach number and flow angles derived from the probe measurements. Figures 24 to 29 show pitch angle distributions from the 5-hole probe measurements.

The results shown in Figs. 18 to 29 were from the three tests mentioned above. Figures 18, 19 and 20 show radial surveys at 50% of design speed and design incidence (determined from Fig. 15), 50% speed near surge and 65% speed near design incidence, respectively. Figures 21, 22 and 23 show peripheral surveys of the centerline of the channel at the

same test conditions. Figures 24 to 29 show the resulting pitch angle distributions corresponding to tests shown in Figs. 18 to 23.

C. DISCUSSION

1. Radial Surveys

The radial surveys are shown in Figs. 18 to 20. The Mach number comparison between the two probes is in much better agreement than the uncorrected results of Fig. 17. The differences close to the hub are a result of the static pressure, rather than total pressure measurements. It was noted that corrected static pressure measurements for the 5-hole probe tended toward measured hub and tip wall pressures, whereas the NASA probe corrected static pressure tended to values that were too high. As an example, for the test shown in Fig. 20, the measured hub and tip wall pressures were -5.3 and 23.1 inches of water respectively. Therefore, the Mach number calculated from the 5-hole probe measurements is considered to be more accurate than that given by the NASA probe.

Yaw angle measurements of flow behind the rotor are in agreement to better than one degree. The reason for the residual disagreement is not clear. It was noticed that the largest and most consistent disagreement occurred at the highest speed and flow rate (Fig. 20). In Fig. 21 the flow angle at the rotor tip is large; corresponding to a low axial velocity component. This suggests a stalled condition at the rotor tips.

Total pressure measurements do not agree as well as in

the steady flow in which the probes were calibrated (Appendix A). Leaks were thought to have been eliminated from the scanivalve and pressure transducer data system. There is a possibility that the total pressure differences were caused by the unsteady nature of the flow. This argument is supported by Fig. 19, corresponding to a near stall condition, for which additional unsteadiness might be expected. However, at the higher frequencies associated with the higher RPM in Fig. 20, the disagreement is greater. Such would not be the case if the increased differences were caused by the unsteady response of the probes.

2. Peripheral Surveys

Figures 21 to 23 show the results of peripheral surveys taken at the passage centerline, corresponding to test conditions shown in Figs. 18 to 20. In Figs. 21 and 23, the impact pressure difference is small and uniform with respect to angular position. (For these tests, profiles hub-to-tip, were also similar). At the near stall condition in Fig. 22, a variation in impact pressure with peripheral position is evident. The two measurements agree only over a small portion of a blade space.

The peripheral variation in corrected static pressure, as indicated by both probes, was quite pronounced. With the stagnation pressures being relatively constant, a variation in Mach number proportional to the probe static pressure differences was measured. Inspection of these figures leads to the conclusion that the stator bladesvere affecting the flow upstream. The minimum Mach number and flow angle

(Fig. 22) was measured in line with the leading edge of a stator blade, at a case angle of approximately 363°. That angle is consistent with the geometry of the flow into the stator. It is clear that peripheral variations in flow properties must be taken into account for specification of rotor performance from probe measurements at station 2. This is particularly true at reduced throttle settings, as in Fig. 22.

The distribution of static pressure from the NASA probe shown in Fig. 22 is similar in shape to those from both probes in Figs. 21 and 23. The more uniform distribution of the 5-hole probe static pressure is a marked departure from the distributions of Figs. 21 and 23. Since the probes were separated by 3 stator blade passages, it is possible that the stator passage downstream of the 5-hole probe contained a separation, or local stalled condition, whereas the passage downstream of the NASA probe was unaffected.

3. Pitch Angle Measurement

The pitch angle distributions measured downstream of the rotor are shown in Figs. 24 to 29 and correspond to the surveys of Figs. 18 to 23. The variation of pitch angle with radius was nearly linear at design throttle settings (Figs. 24 and 26). The pitch angle is indicated to be approximately -1° close to the outer wall, as might be expected due to boundary layer effects. These measurements, which rely upon the annulus corrections described in Appendix A, are remarkably consistent with the expected distribution. At the point where probe measurements were taken, the hub wall angle was

$+12^{o}$. Extrapolation of the angle distribution to the wall, in Figs. 24 and 26, is consistent with this value. The results in Fig. 25, for the near surge condition, shows a region of nearly constant pitch angle near the inner wall and a tendency to increase rapidly toward the 12^{o} hub wall angle. This is consistent with rake measurements of impact pressure taken at the stator exit, which indicated a region of separated flow at the hub wall. This would have the effect of creating a large pitch angle gradient near the hub. The larger region of negative pitch angle near the tip would be consistent with an increase in wall boundary layer thickness. This region also exhibits a large pitch angle gradient when compared to the center 50% of the distribution.

Peripheral variations in pitch angle, shown in Figs. 27 to 29 indicate little change at or near design conditions. However, near surge(Fig. 28) the flow angle increased on one side of the stator blade and decreased on the other side. Though it appears to be a significant effect, the variation is no more than one degree either side of the mean line and would not be significant in rotor performance calculations.

V. CONCLUSION

In this study a 5-hole pressure probe was used successfully to determine the distribution of velocity and flow angle upstream of a compressor rotor. Blockage factors were determined from measurements, which allow the use of analytical expressions to relate the measured flow rate to the incident flow properties at the rotor.

The same probe was applied downstream of the rotor. The measurements were compared to those of a NASA probe, which did not provide a measurement of pitch angle. Part of the differences in the Mach number distributions, seen near the hub, was probably for this reason. The 5-hole probe gave more accurate Mach number distributions mainly because the static pressure corrections for passage effects were smaller than those for the NASA probe.

The differences in the radial distributions of impact pressure were partially the effect of the difference in the location of the probes with respect to the nearest stator blade leading edge. Although that difference was only 1.5°, at decreased throttle settings the peripheral variations in the indicated flow profiles became significant. In future tests radial surveys should be conducted with both probes in the flow simultaneously, at fixed speed and throttle setting; then the probes should be interchanged and the surveys repeated without changing conditions. The resulting plots would differ only as they are affected by the slight peripheral displacement of the probes. Peripheral survey variations must

be accounted for if probe measurements at station 2 are to be used for derivation of rotor performance.

The effects of unsteady response on probe measurements should also be examined. It is reported that the average indicated total pressure in unsteady flow can be greater than the time average of the total pressure [Ref. 6]. This implies that two different probes in the same steady flow could measure identical total pressures, and when placed in unsteady flow might disagree as a function of speed and throttle setting. While using Reference 6, this effect was calculated to be small for the probes and conditions in the present study. The differences in the measurements suggest that this conclusion should be re-examined.

The correction devised to compensate for wall effect on the 5-hole probe pitch angle measurements was very effective judging from the plotted pitch angle distributions at station 2. The overall effect of correcting the 5-hole probe calibration for application to the specific flow geometry of the transonic compressor, points out the necessity of careful calibration of pressure probes used for making measurements of internal flows.

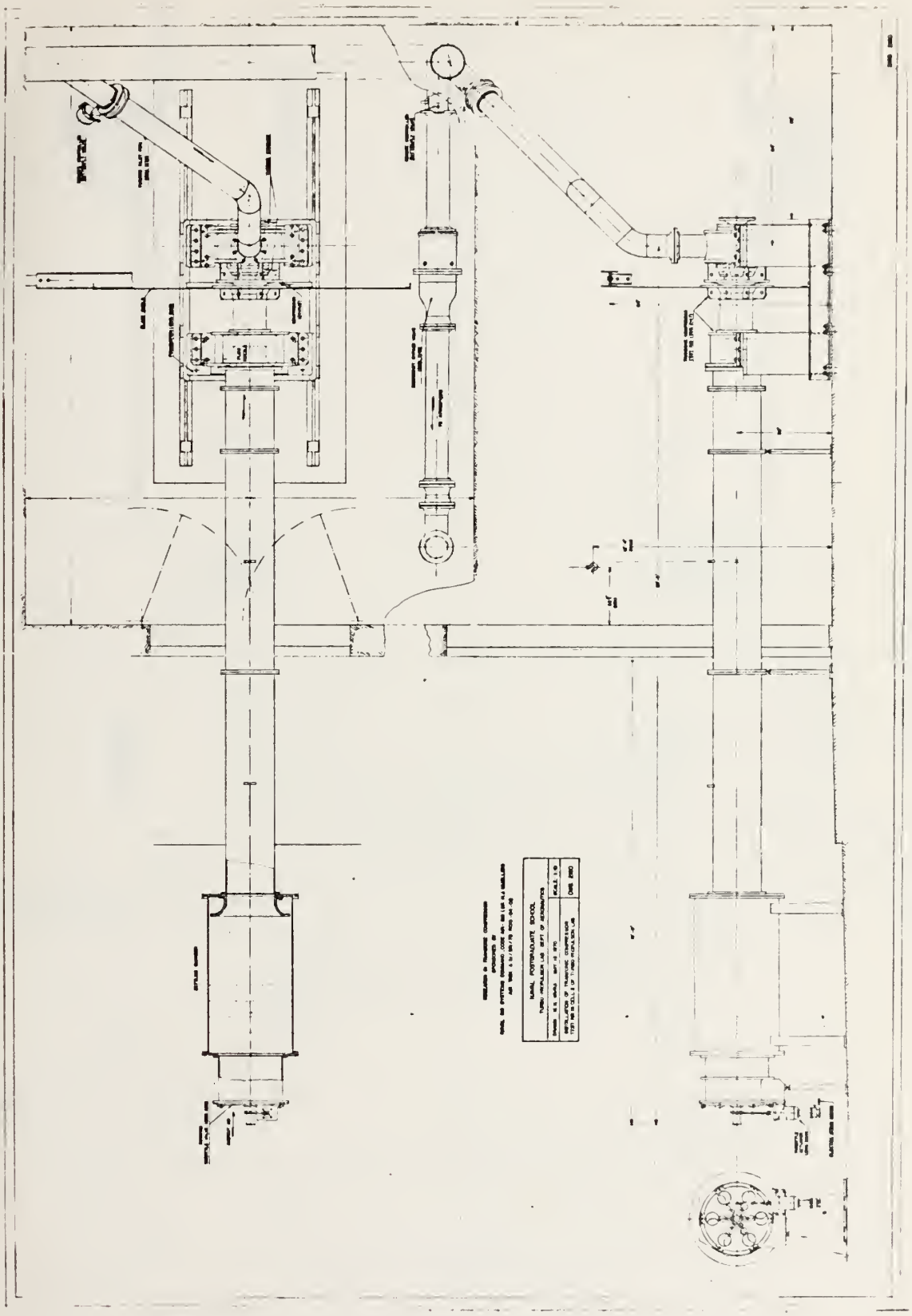

Figure 1. The Compressor Test Rig

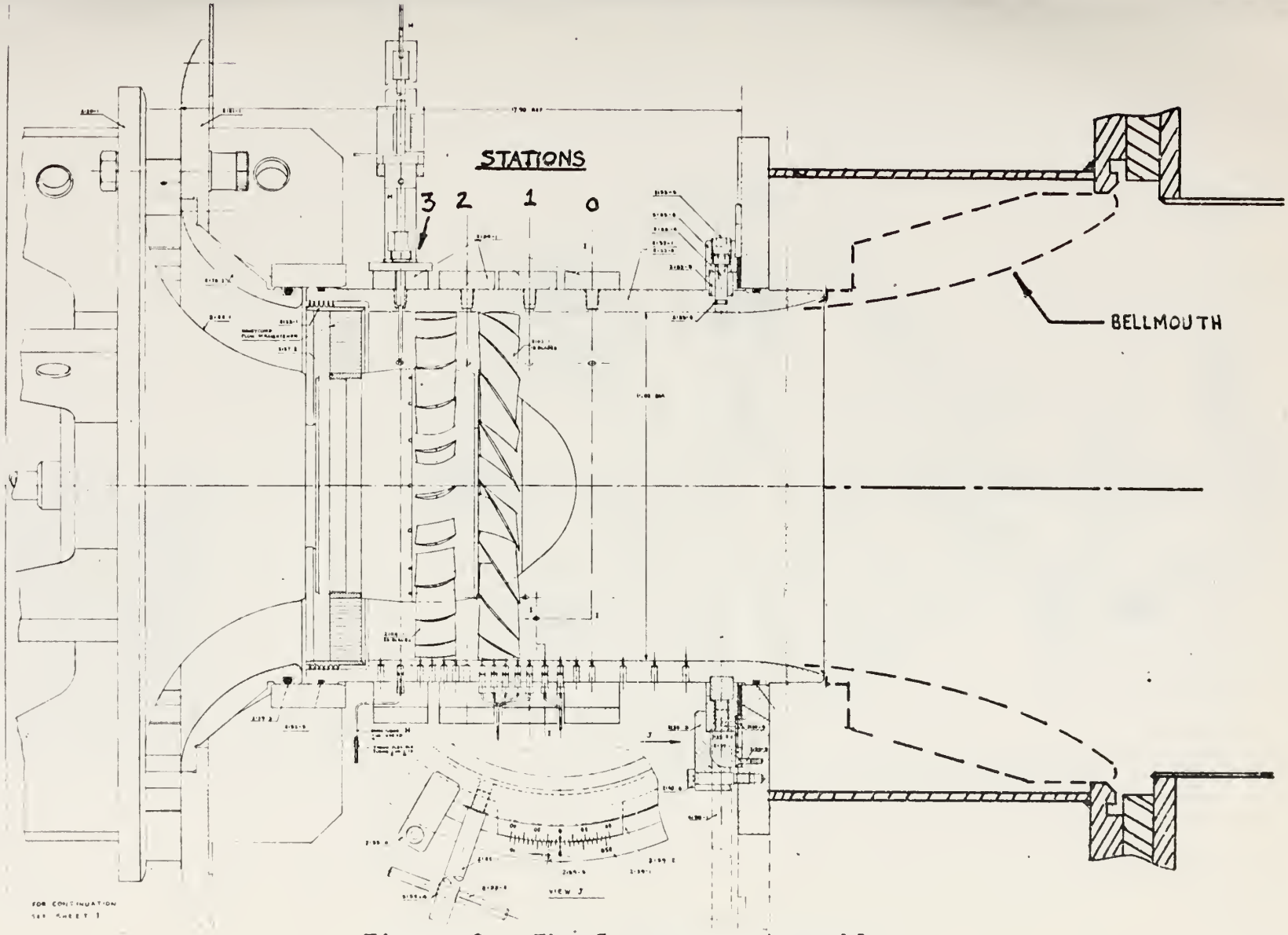

Figure 2. The Compressor Assembly

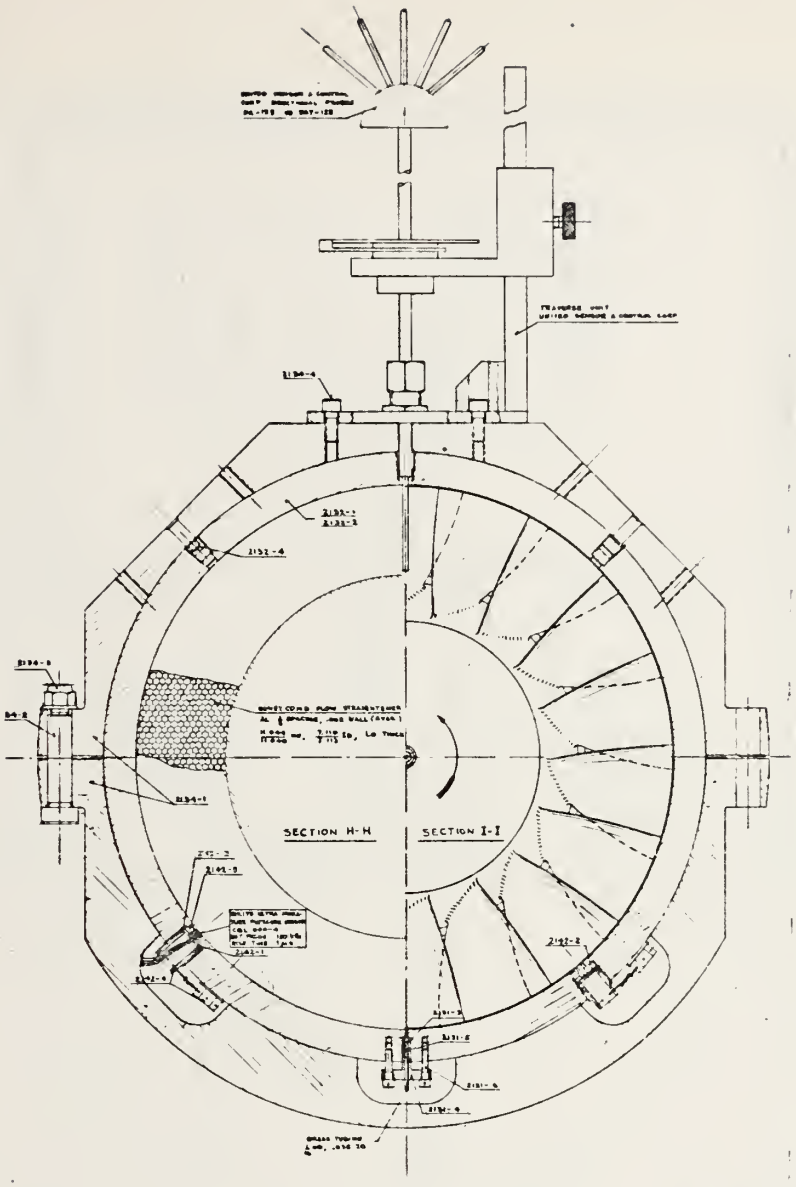

RESEARCH IN TRANSONIC COMPRESSORS SPONSORED BY
NAVAL AIR SYSTEMS COMMAND, CODE AIR-310 (DR H J MUELLER)
AIR TASK A3F-310/551/70, R010-04-02

NAVAL POSTGRADUATE SCHOOL DEPT OF AERONAUTICS, TURBO-PROPULSION LABORATORY		
DRAWN M H VAVRA, DEC 10, 1969	SCALE FULL	
ASSEMBLY OF TRANSONIC COMPRESSOR TEST RIG	DWG NO 2147-2	SHEET 2 of 2

Figure 3. End View of Compressor Assembly

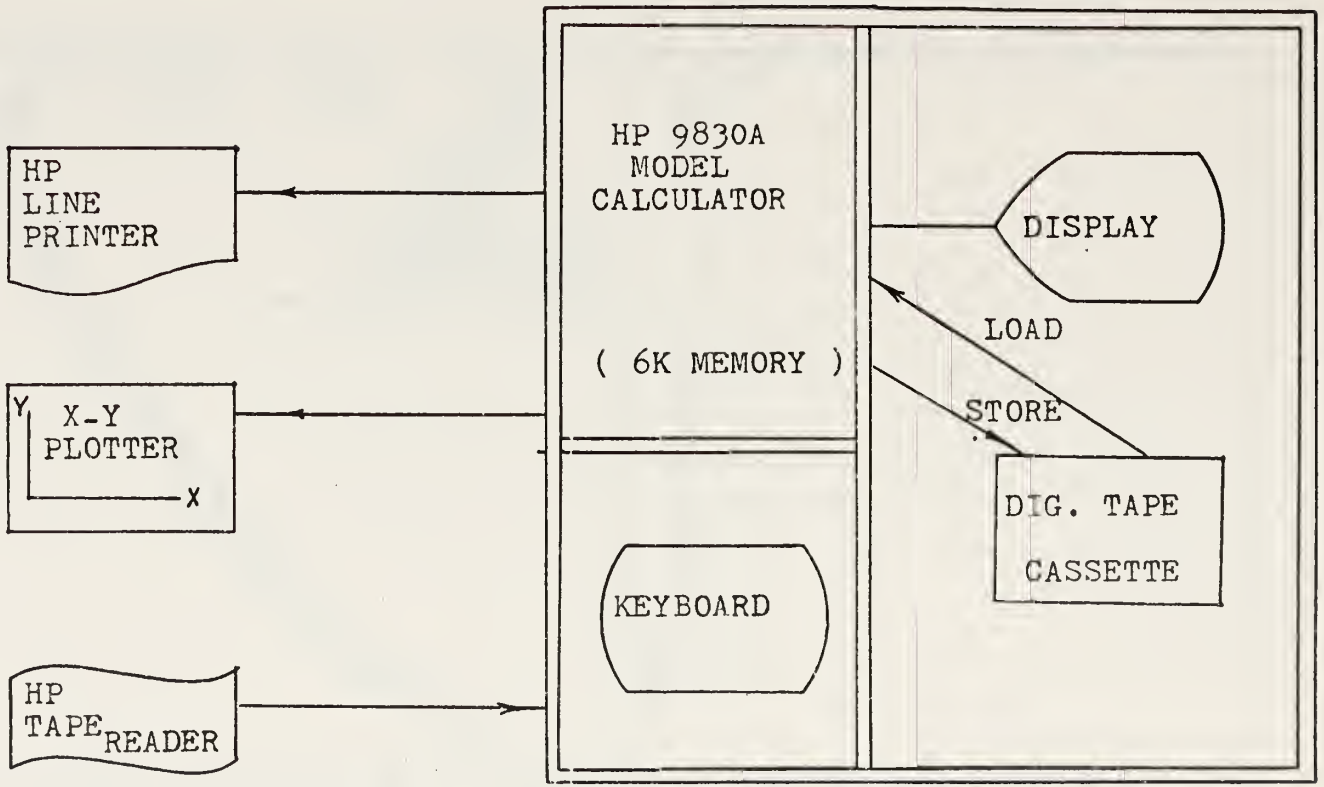

Figure 4. Schematic of the Hewlett-Packard Model 9830A Calculator System

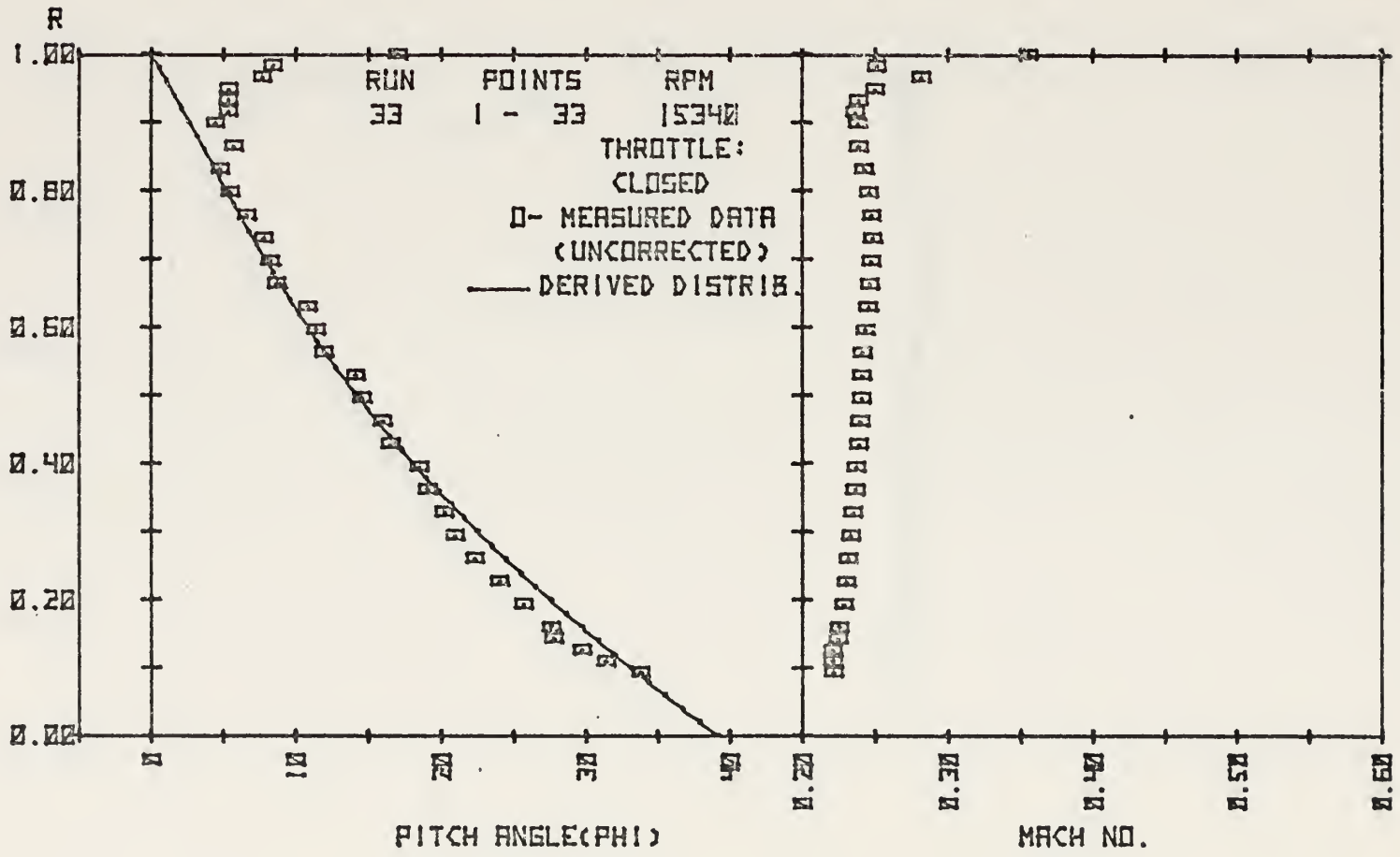

FIGURE 5. PITCH ANGLE AND MACH NO. DISTRIBUTION AT STATION 1.

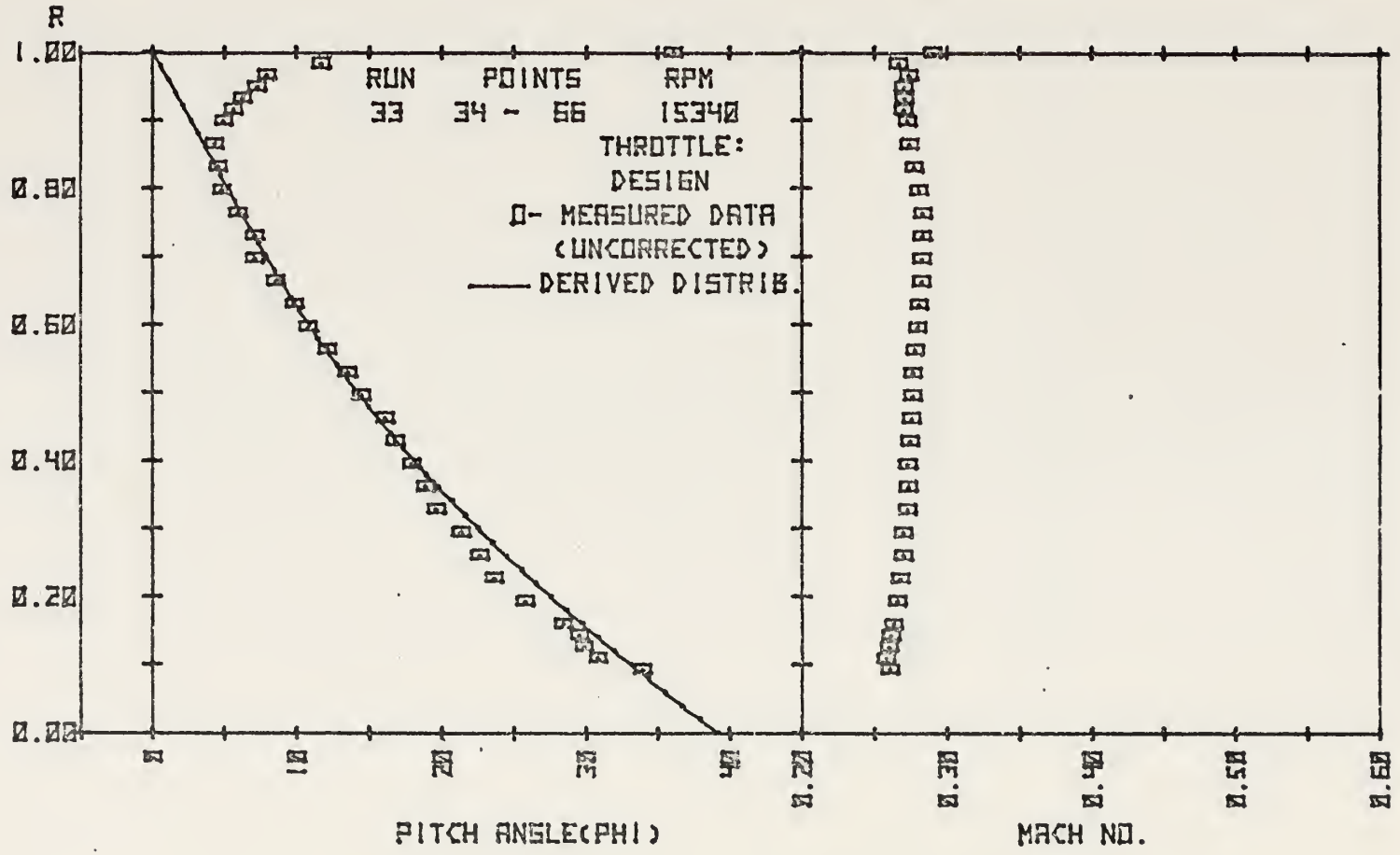

FIGURE 6. PITCH ANGLE AND MACH NO. DISTRIBUTION AT STATION 1.

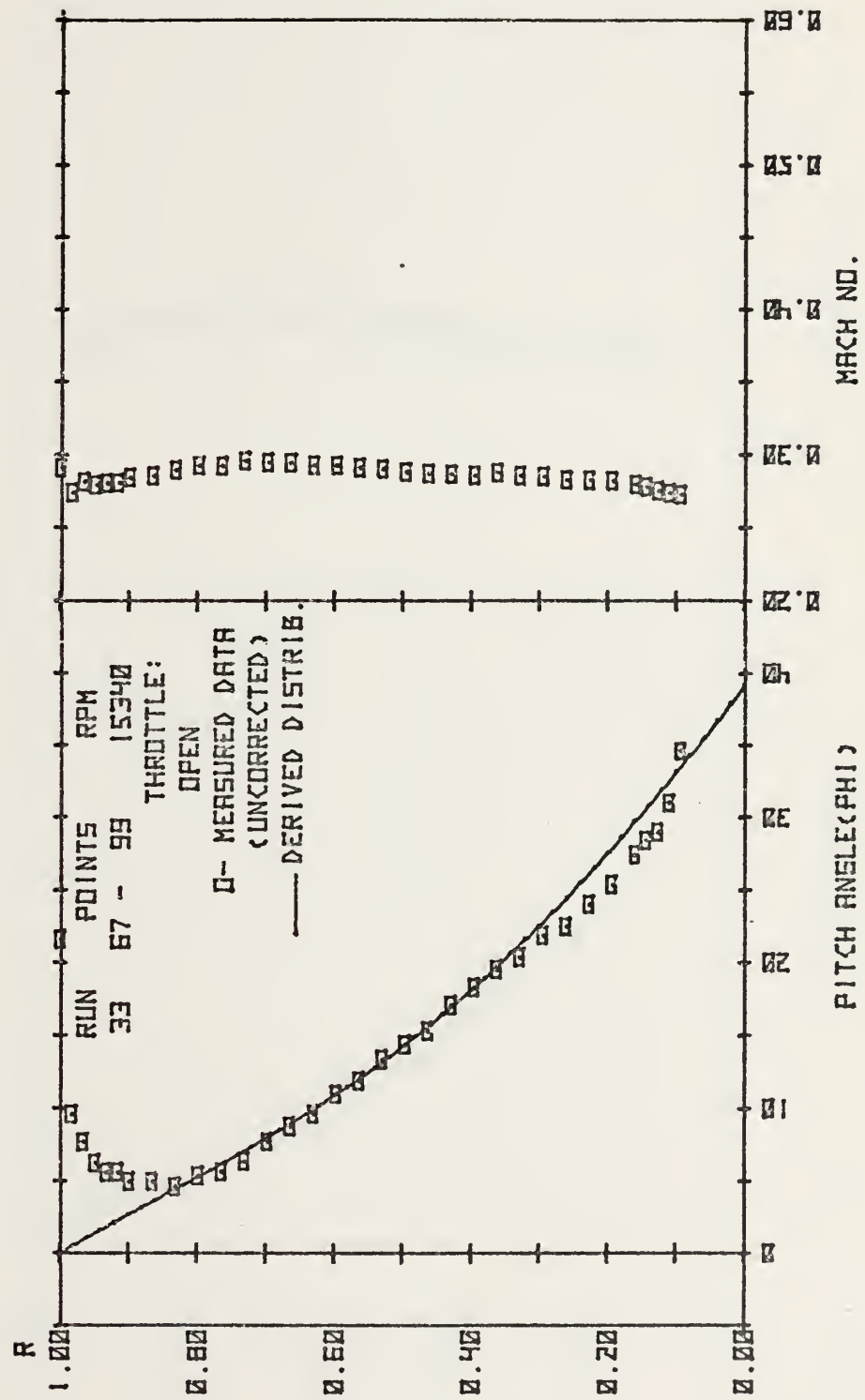

FIGURE 7. PITCH ANGLE AND MACH NO. DISTRIBUTION AT STATION 1.

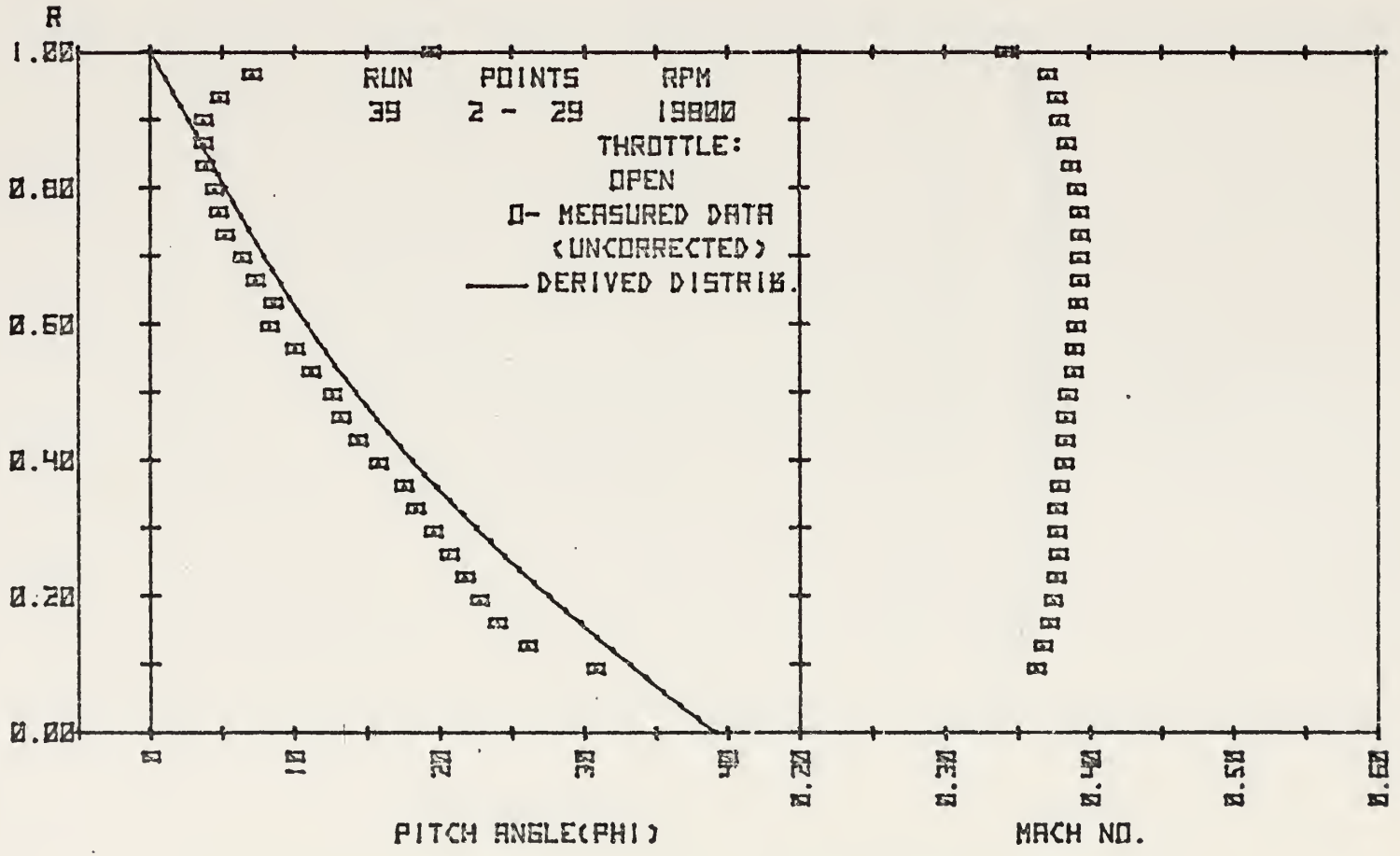

FIGURE 8. PITCH ANGLE AND MACH NO. DISTRIBUTION AT STATION 1.

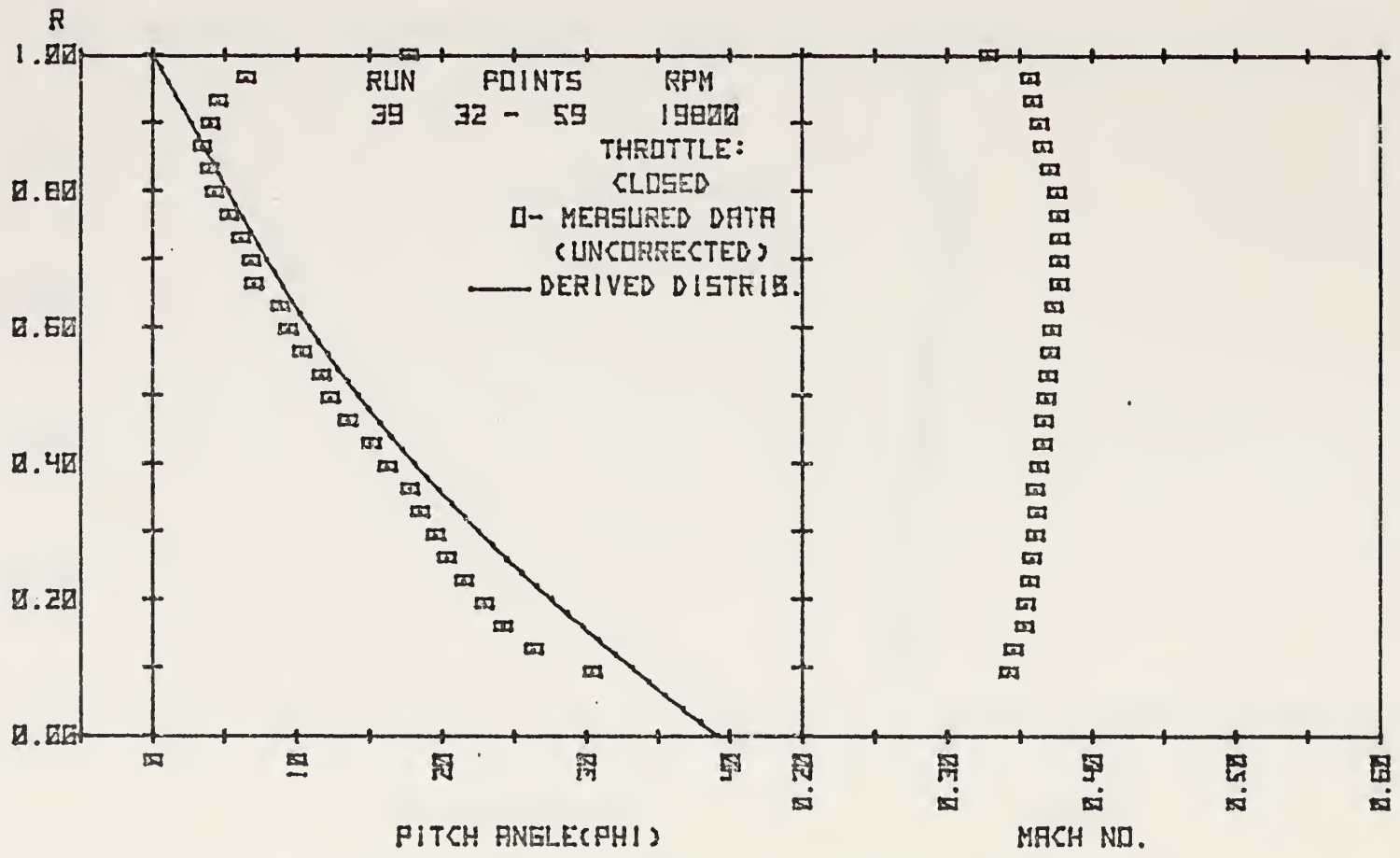

FIGURE 9. PITCH ANGLE AND MACH NO. DISTRIBUTION AT STATION 1.

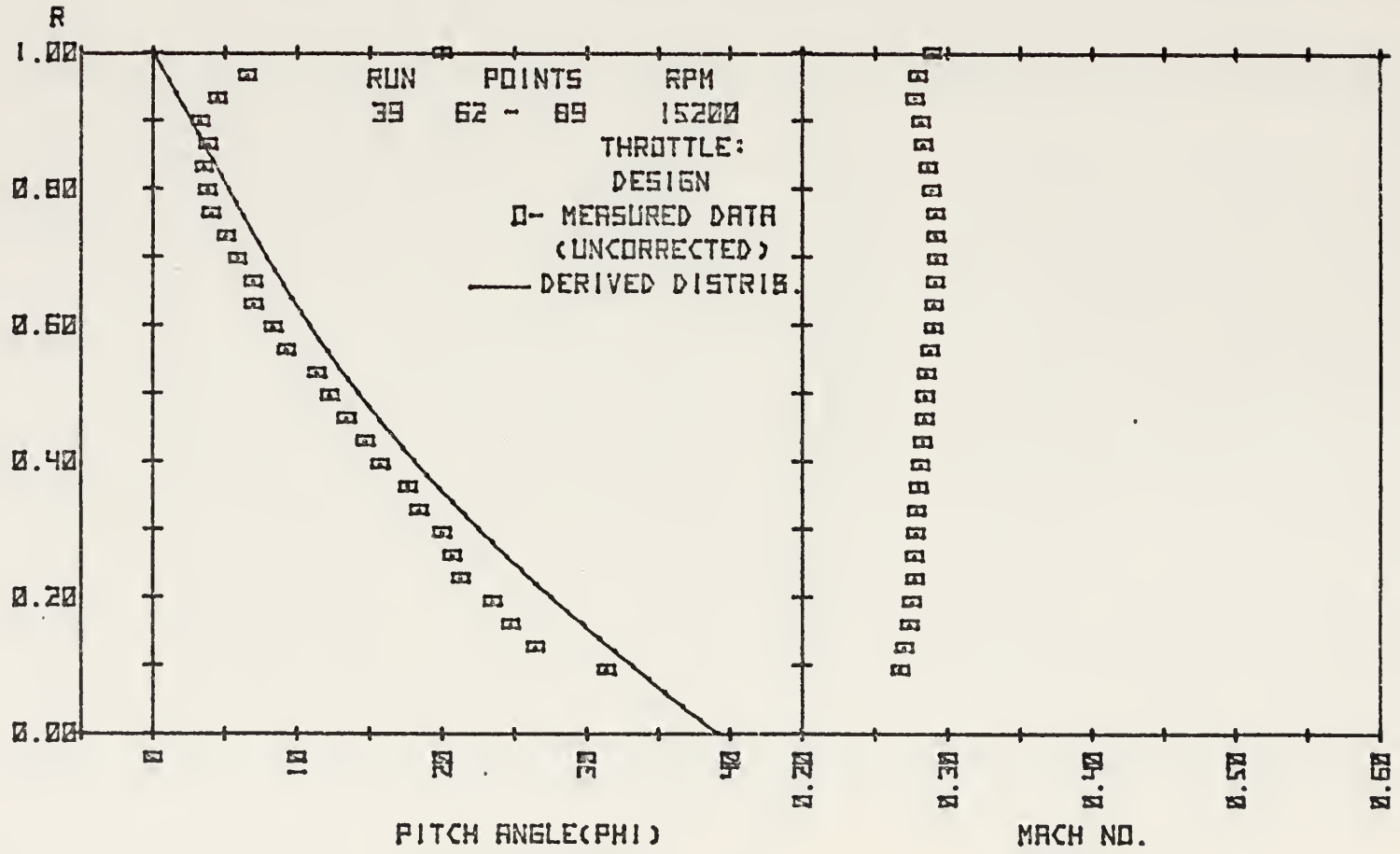

FIGURE 10.PITCH ANGLE AND MACH NO. DISTRIBUTION AT STATION 1.

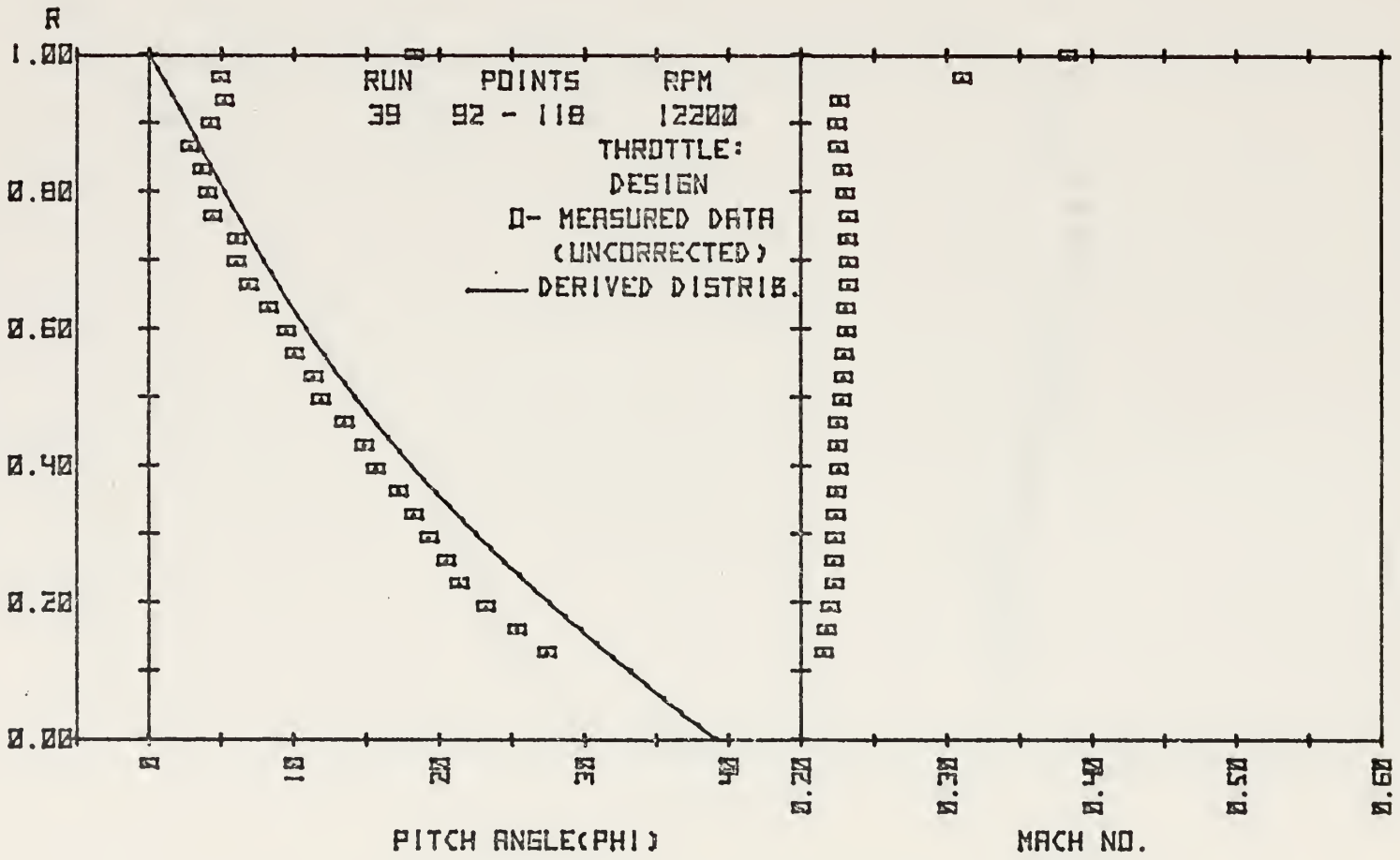

FIGURE 11. PITCH ANGLE AND MACH NO. DISTRIBUTION AT STATION 1.

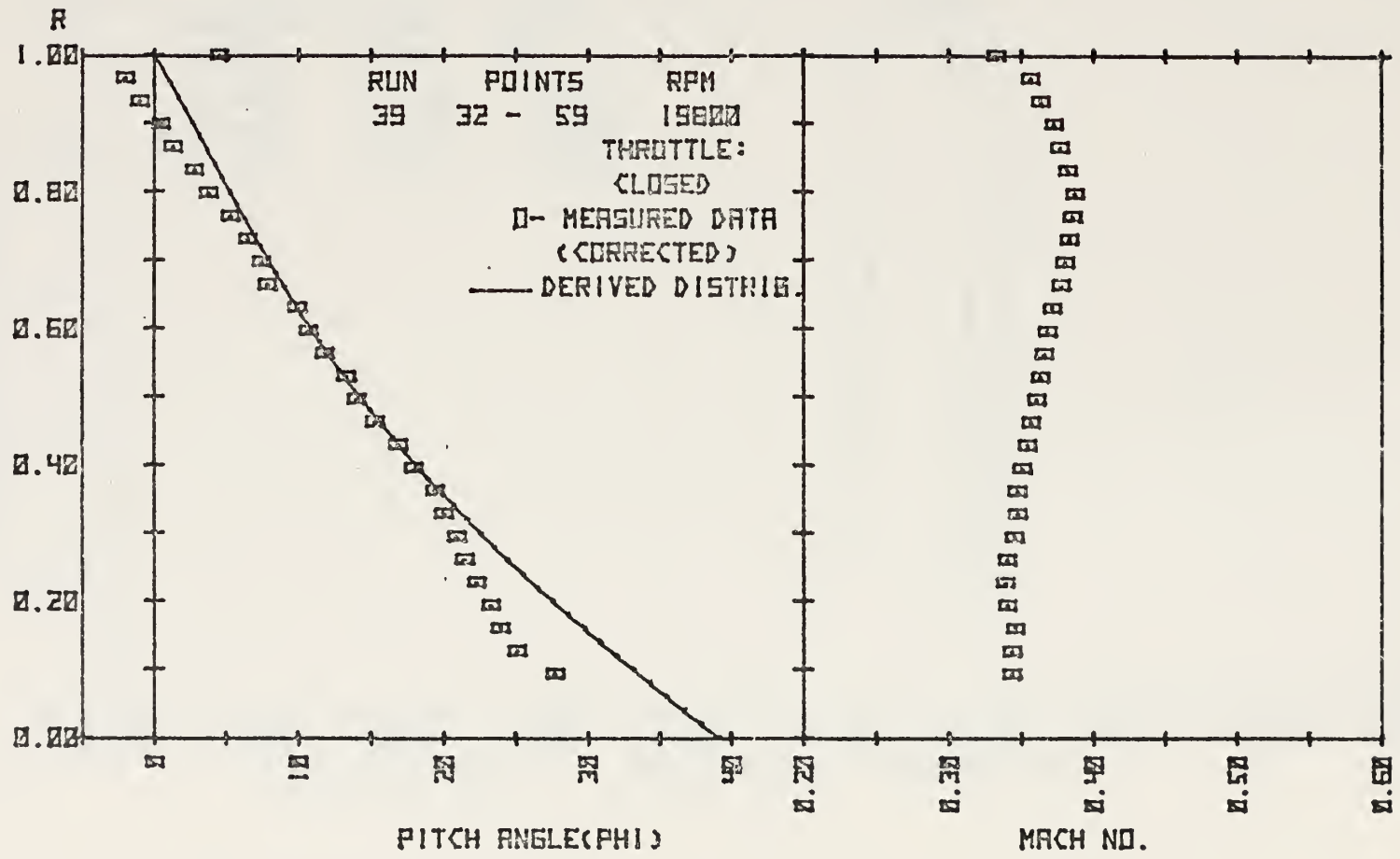

FIGURE 12. PITCH ANGLE AND MACH NO. DISTRIBUTION AT STATION 1.

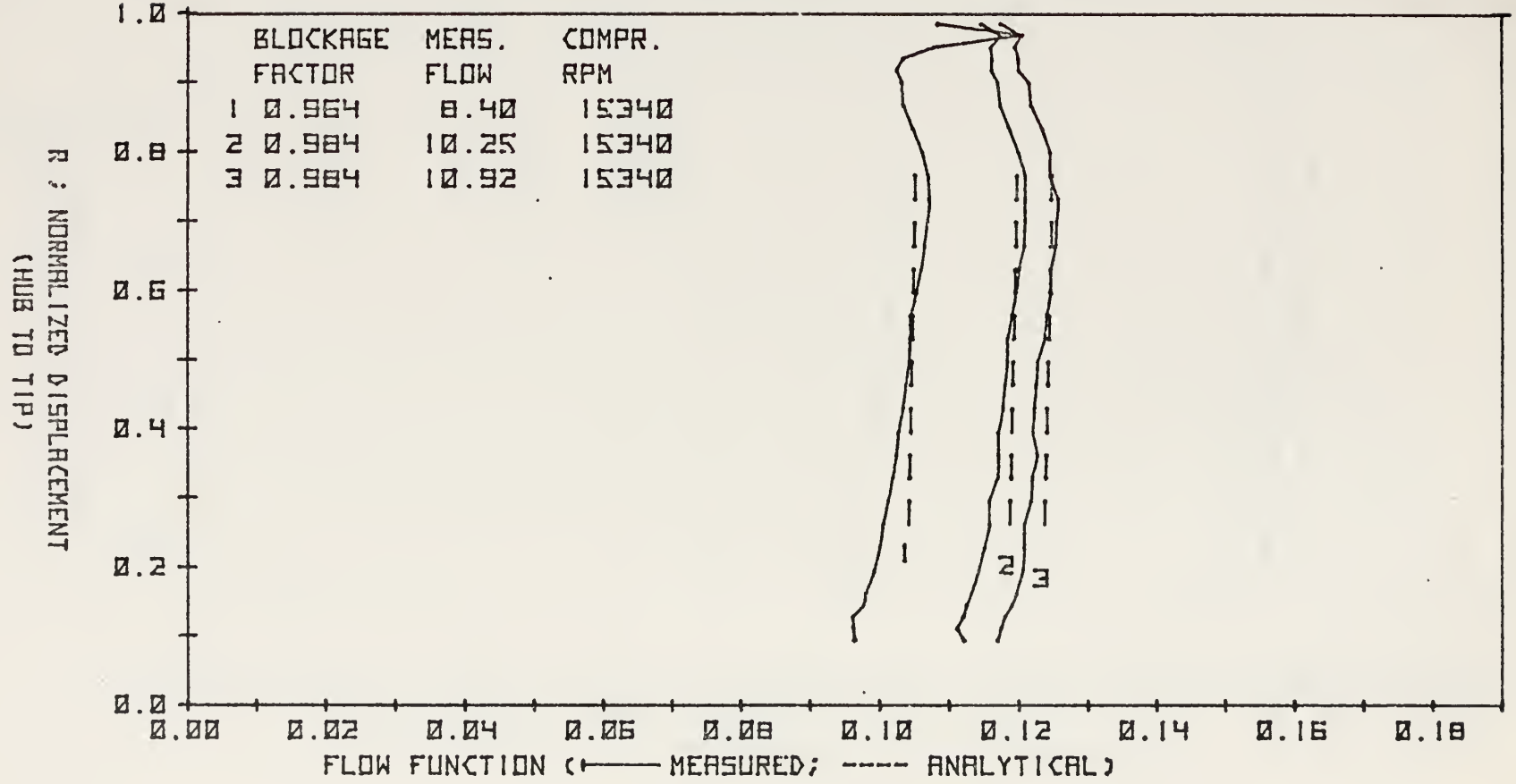

FIG.13. DISTRIBUTION OF FLOW FUNCTION AHEAD OF THE ROTOR.

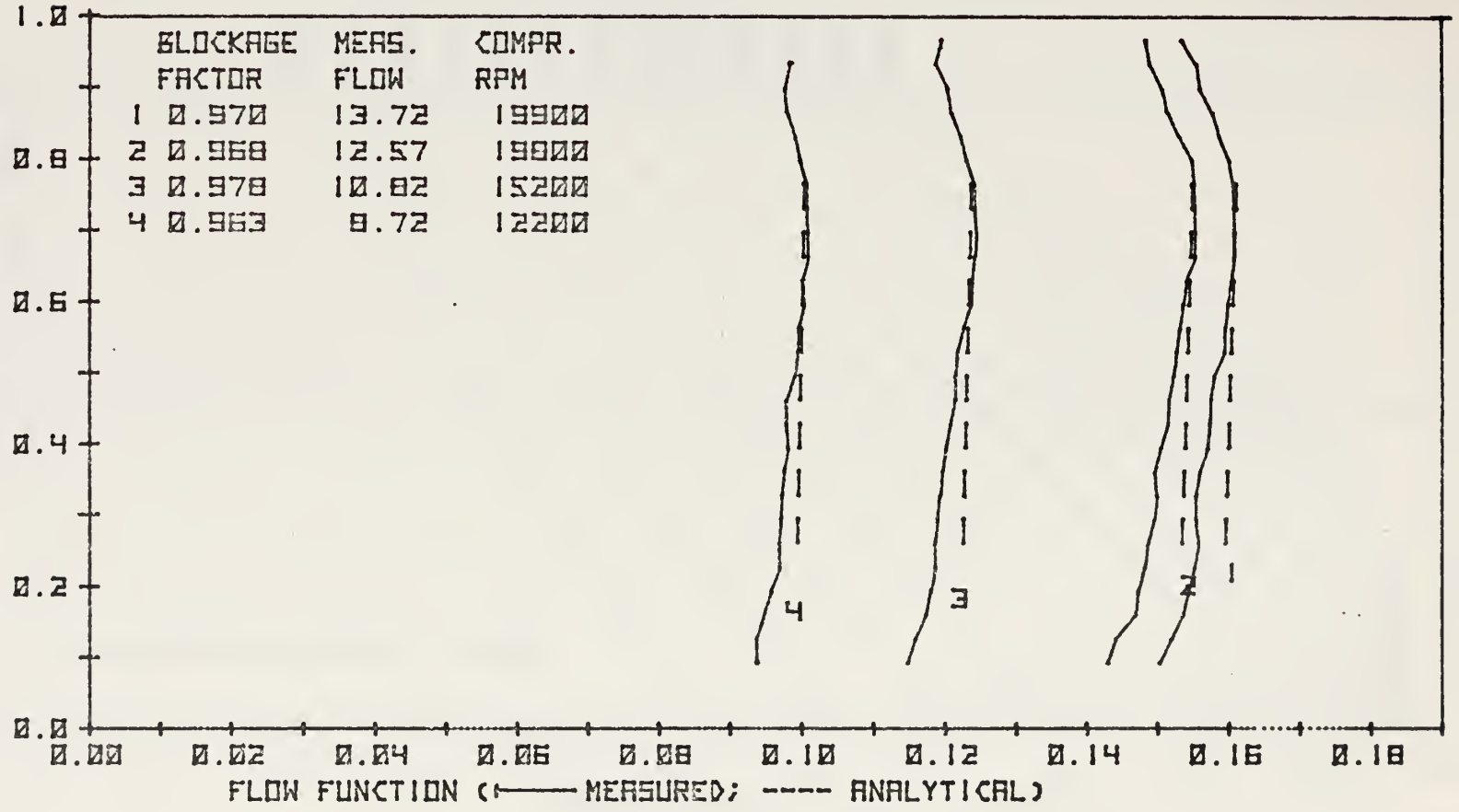

FIG.14. DISTRIBUTION OF FLOW FUNCTION AHEAD OF THE ROTOR.

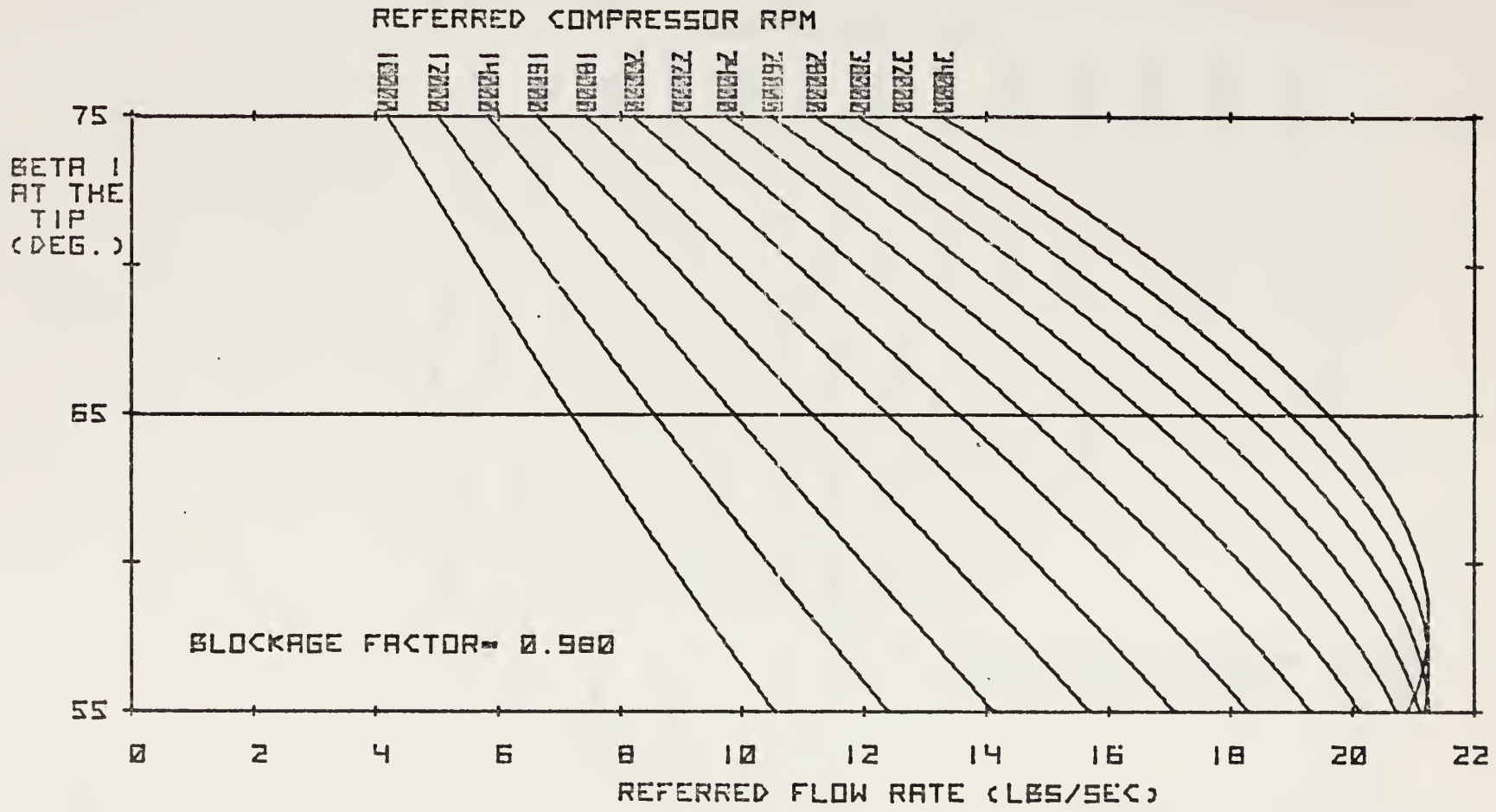

FIG. 15. TRANSONIC COMPRESSOR - CALCULATED FLOW INTO THE ROTOR

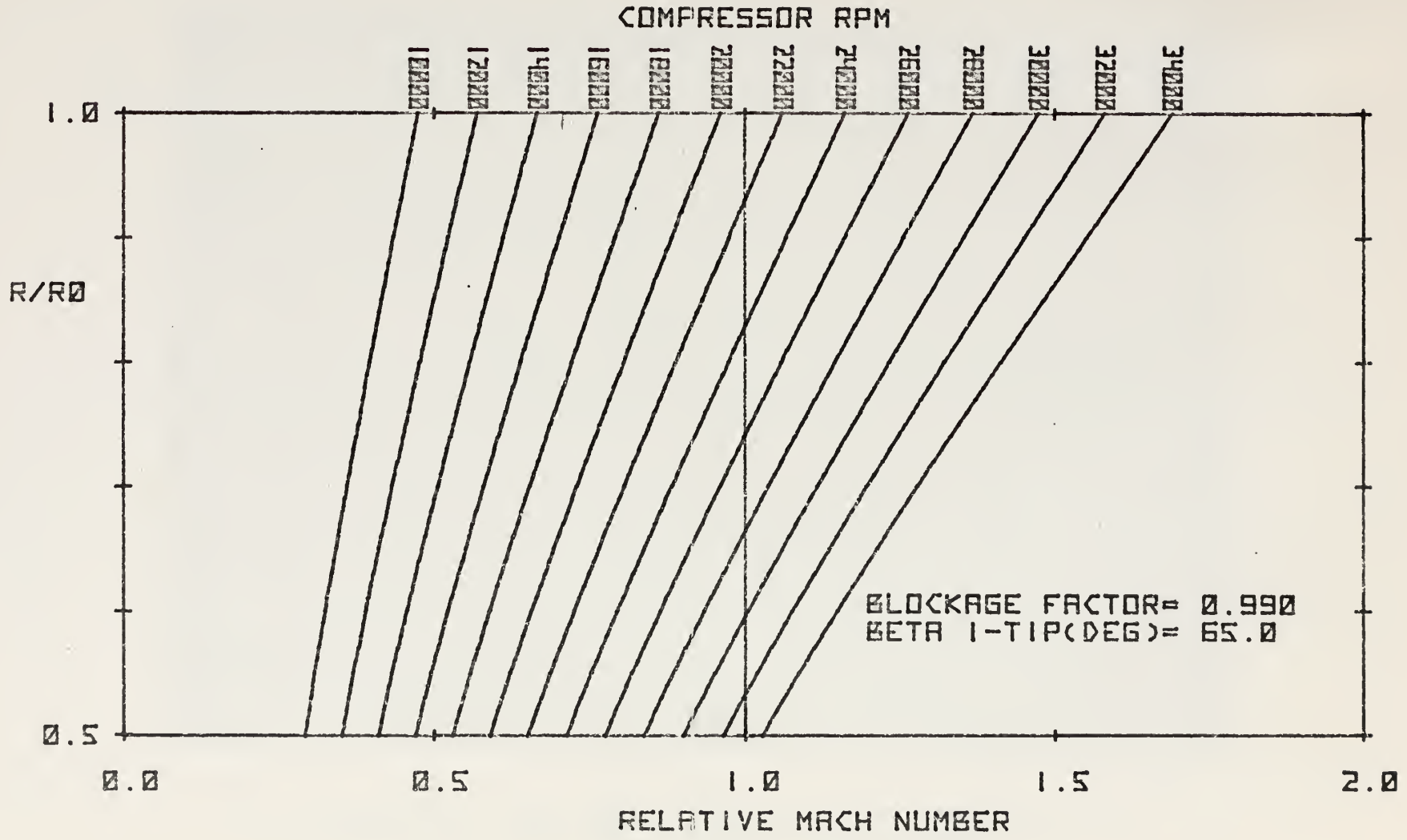

FIG. 16. TRANSONIC COMPRESSOR - CALCULATED FLOW INTO THE ROTOR

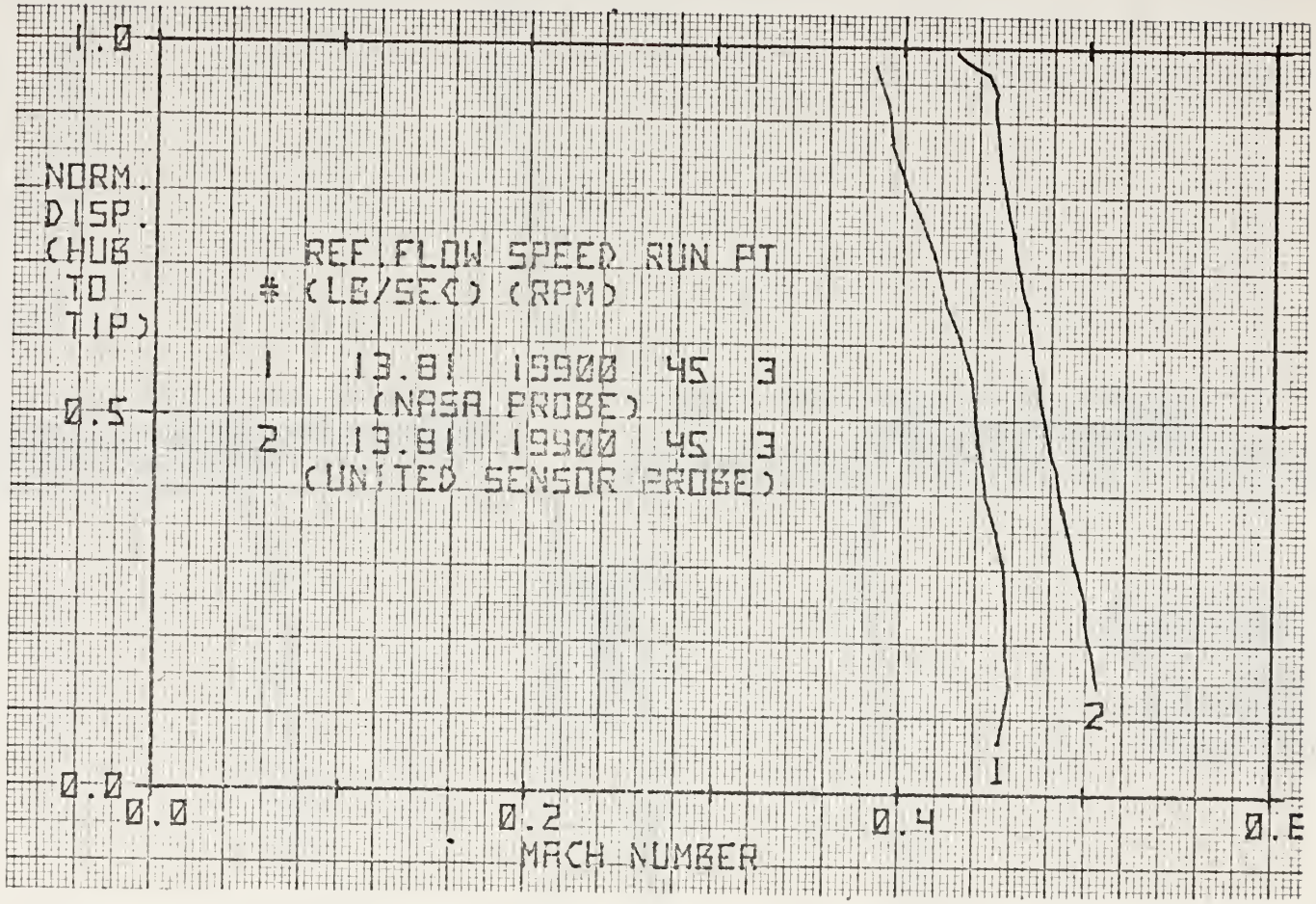

Figure 17. Mach Number Distribution Prior To Application of the Annulus Corrections

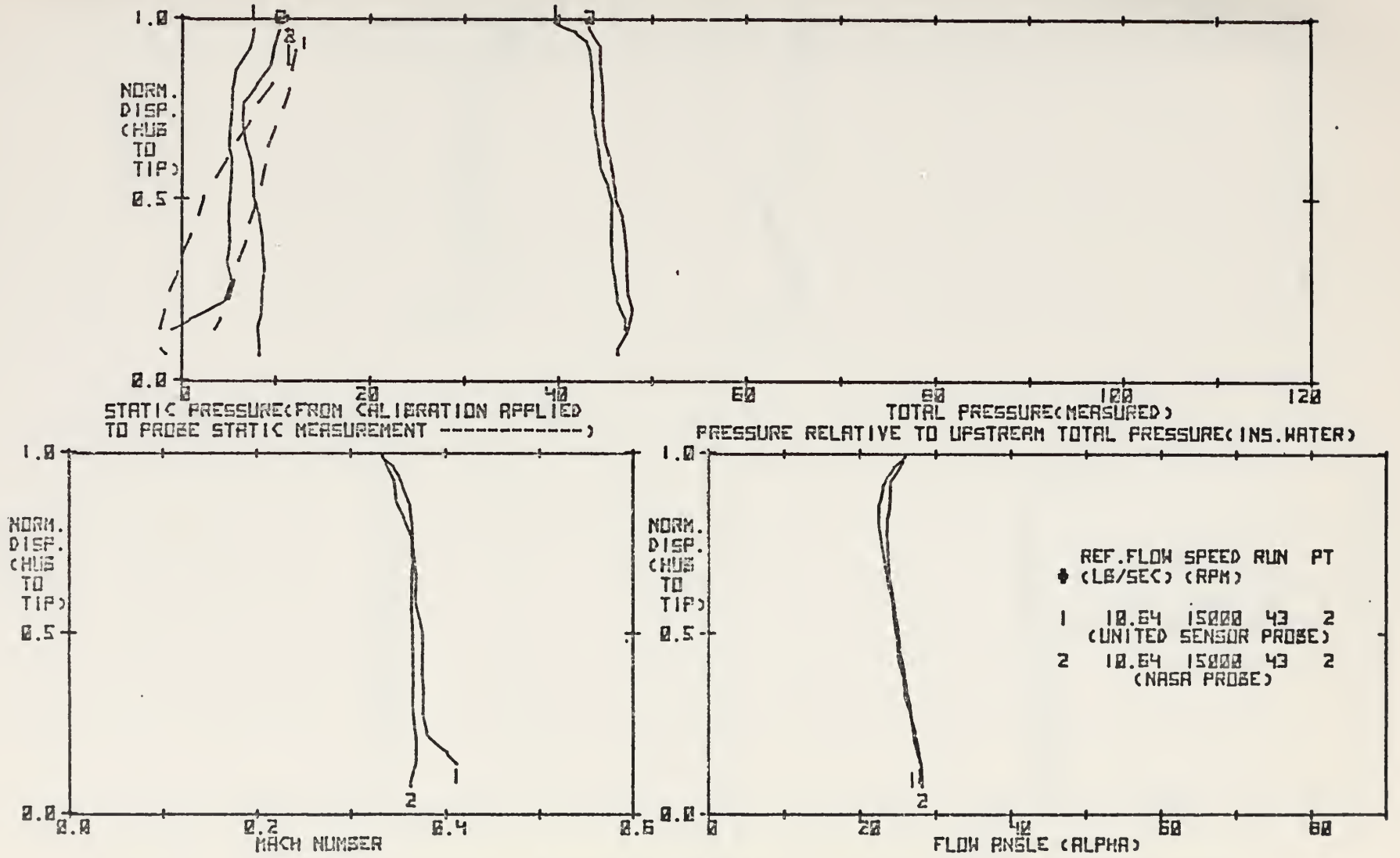

FIGURE 18. RESULTS OF PROBE SURVEYS DOWNSTREAM OF THE TRANSONIC COMPRESSOR ROTOR

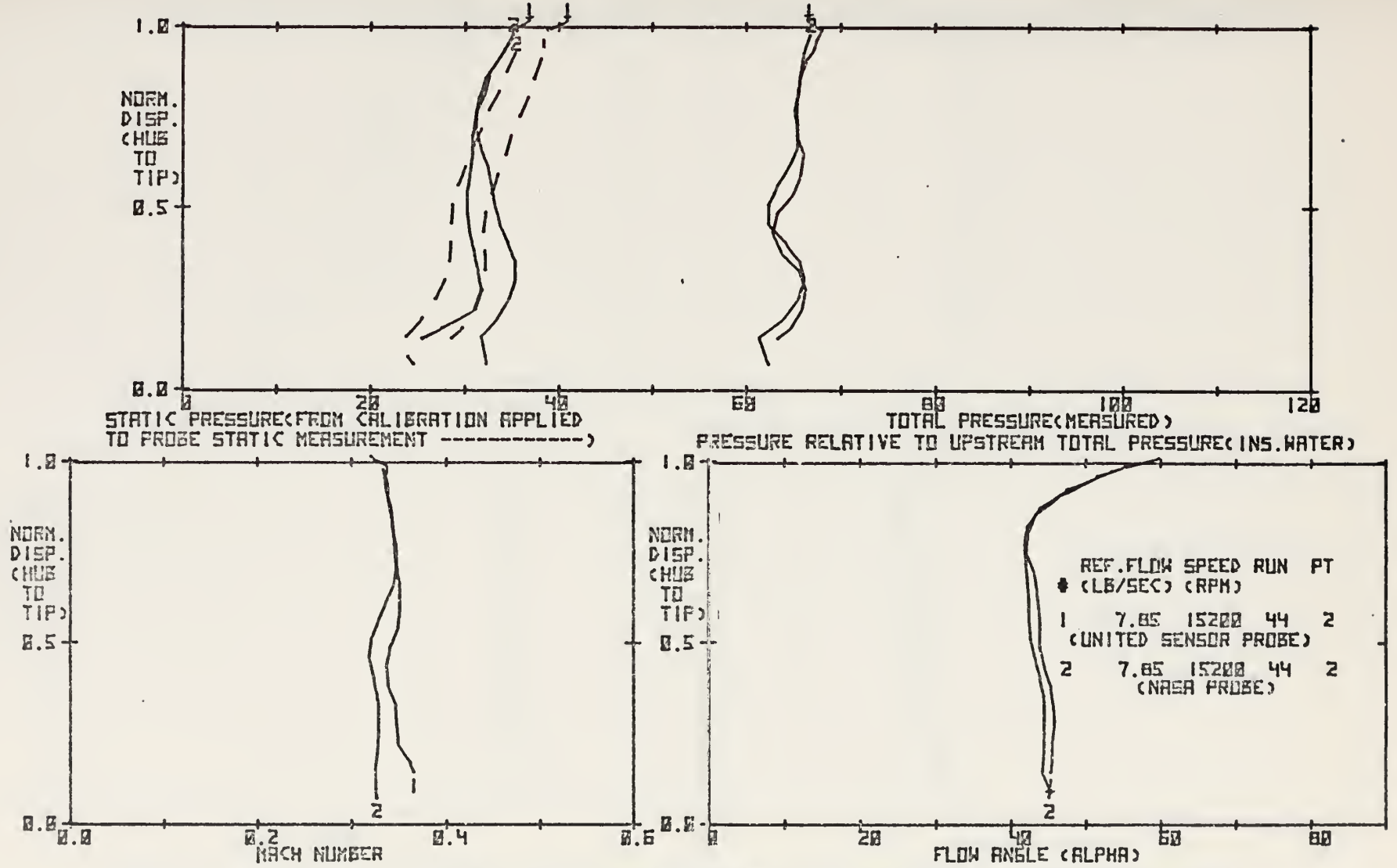

FIGURE 19. RESULTS OF PROBE SURVEYS DOWNSTREAM OF THE TRANSONIC COMPRESSOR ROTOR

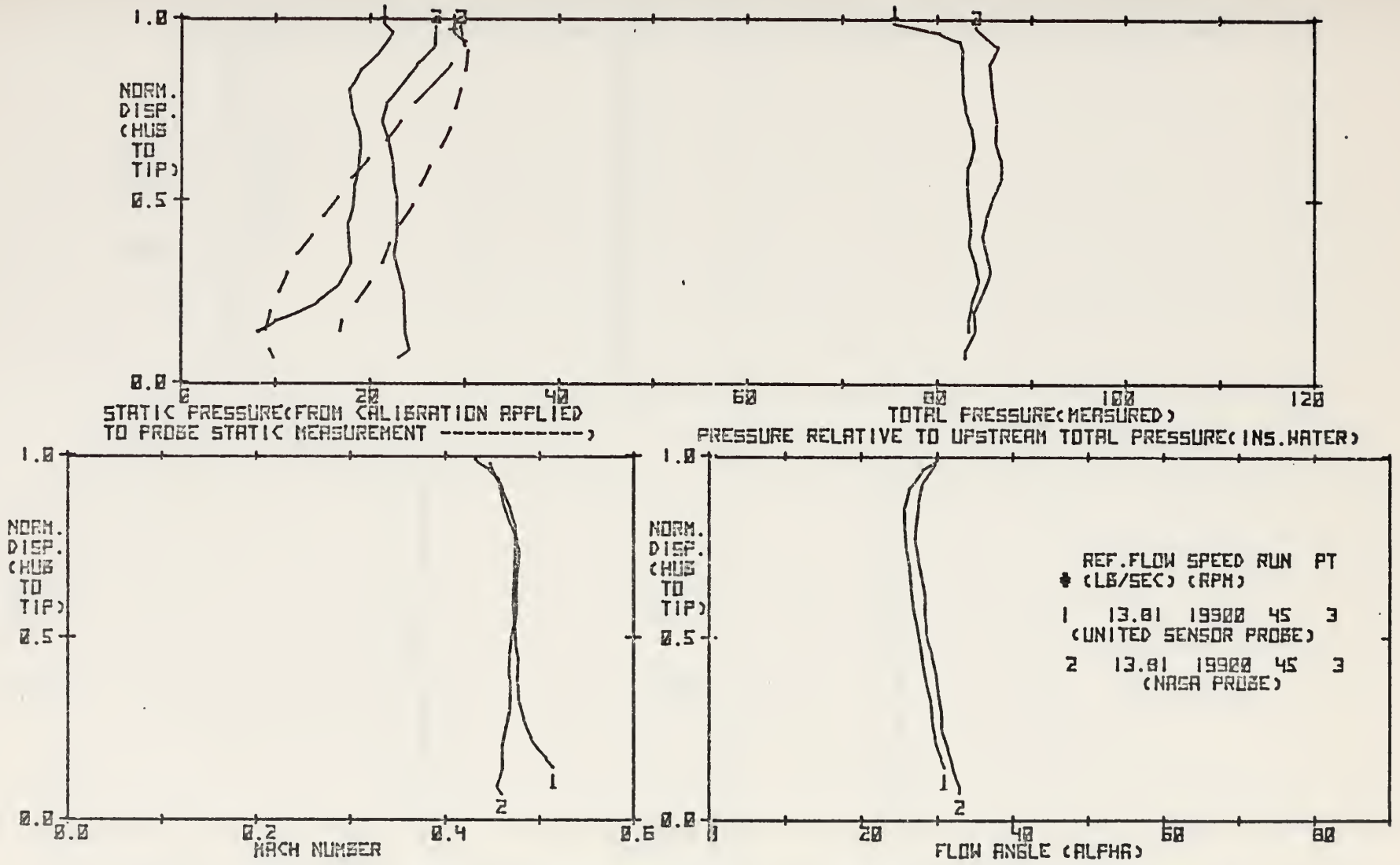

FIGURE 20. RESULTS OF PROBE SURVEYS DOWNSTREAM OF THE TRANSONIC COMPRESSOR ROTOR

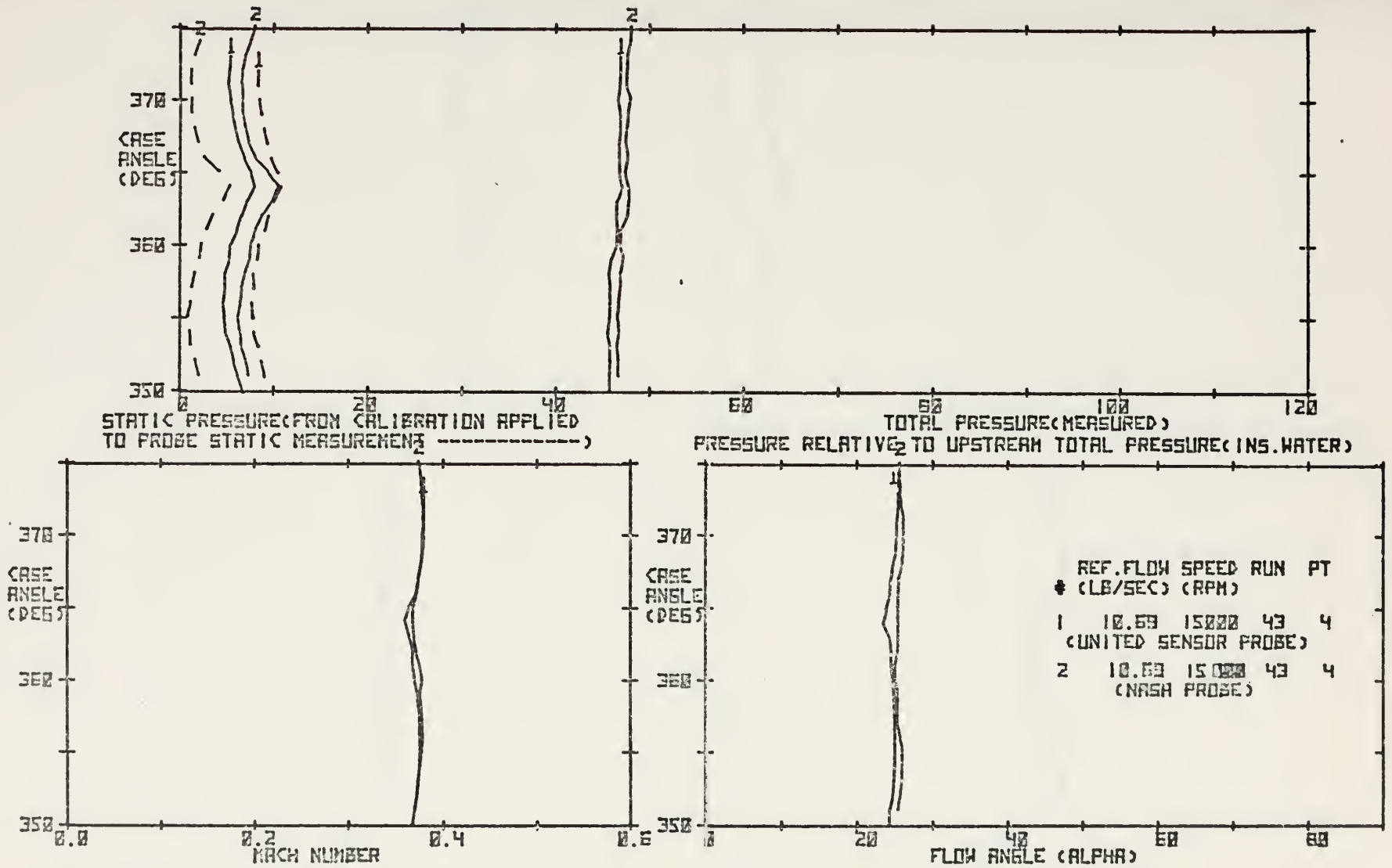

FIGURE 21. RESULTS OF PROBE SURVEYS DOWNSTREAM OF THE TRANSONIC COMPRESSOR ROTOR

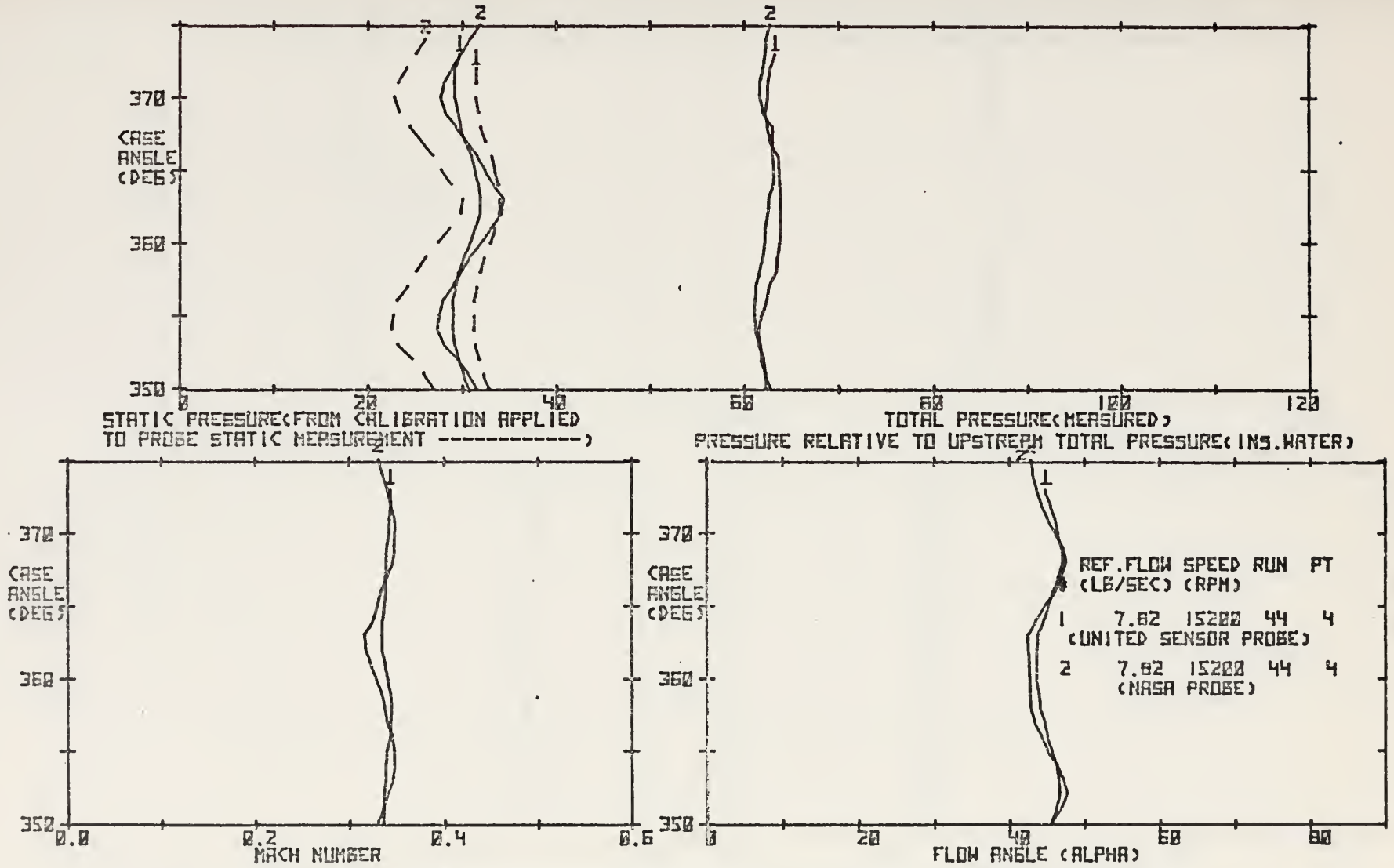

FIGURE 22. RESULTS OF PROBE SURVEYS DOWNSTREAM OF THE TRANSONIC COMPRESSOR ROTOR

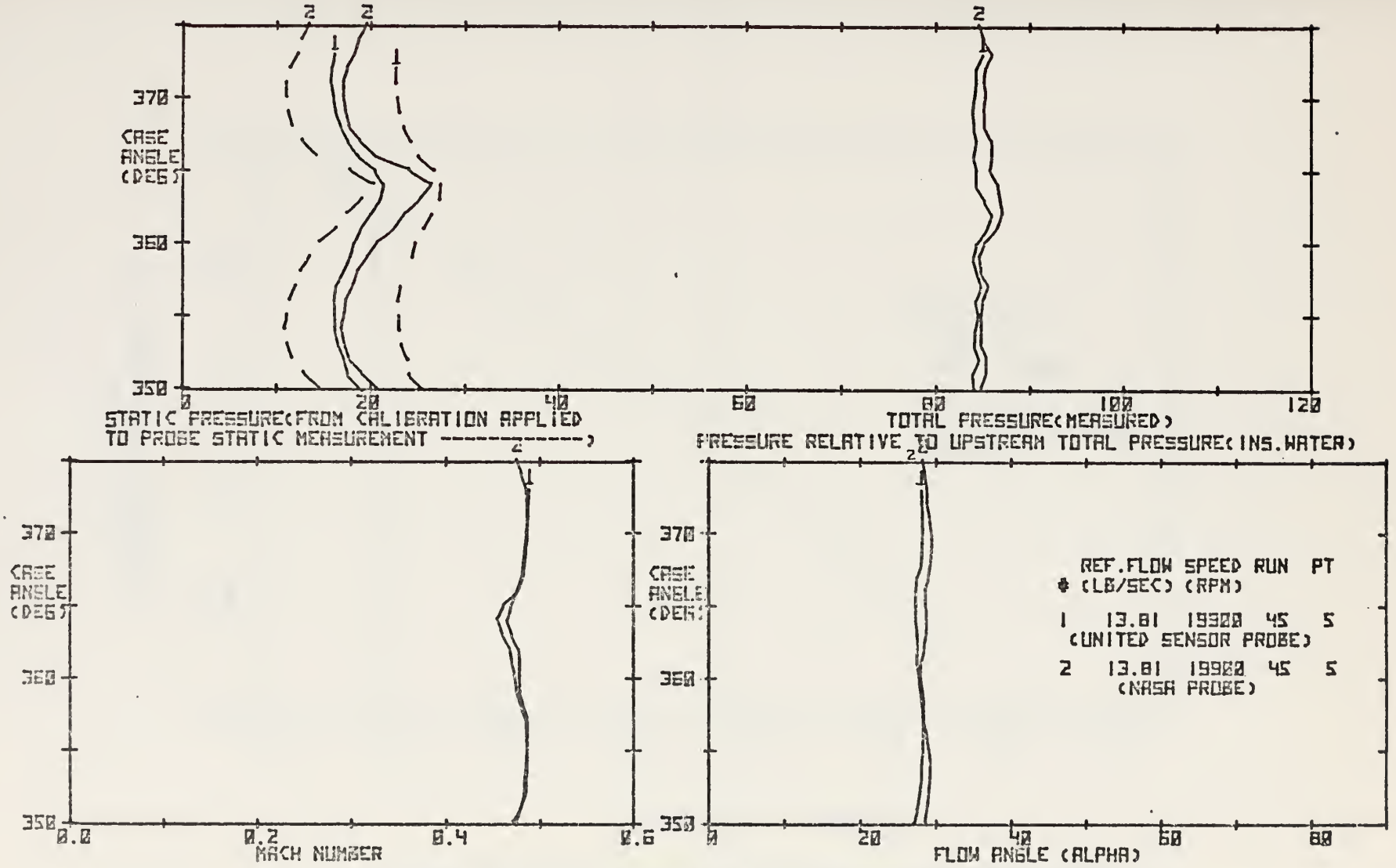

FIGURE 23. RESULTS OF PROBE SURVEYS DOWNSTREAM OF THE TRANSONIC COMPRESSOR ROTOR

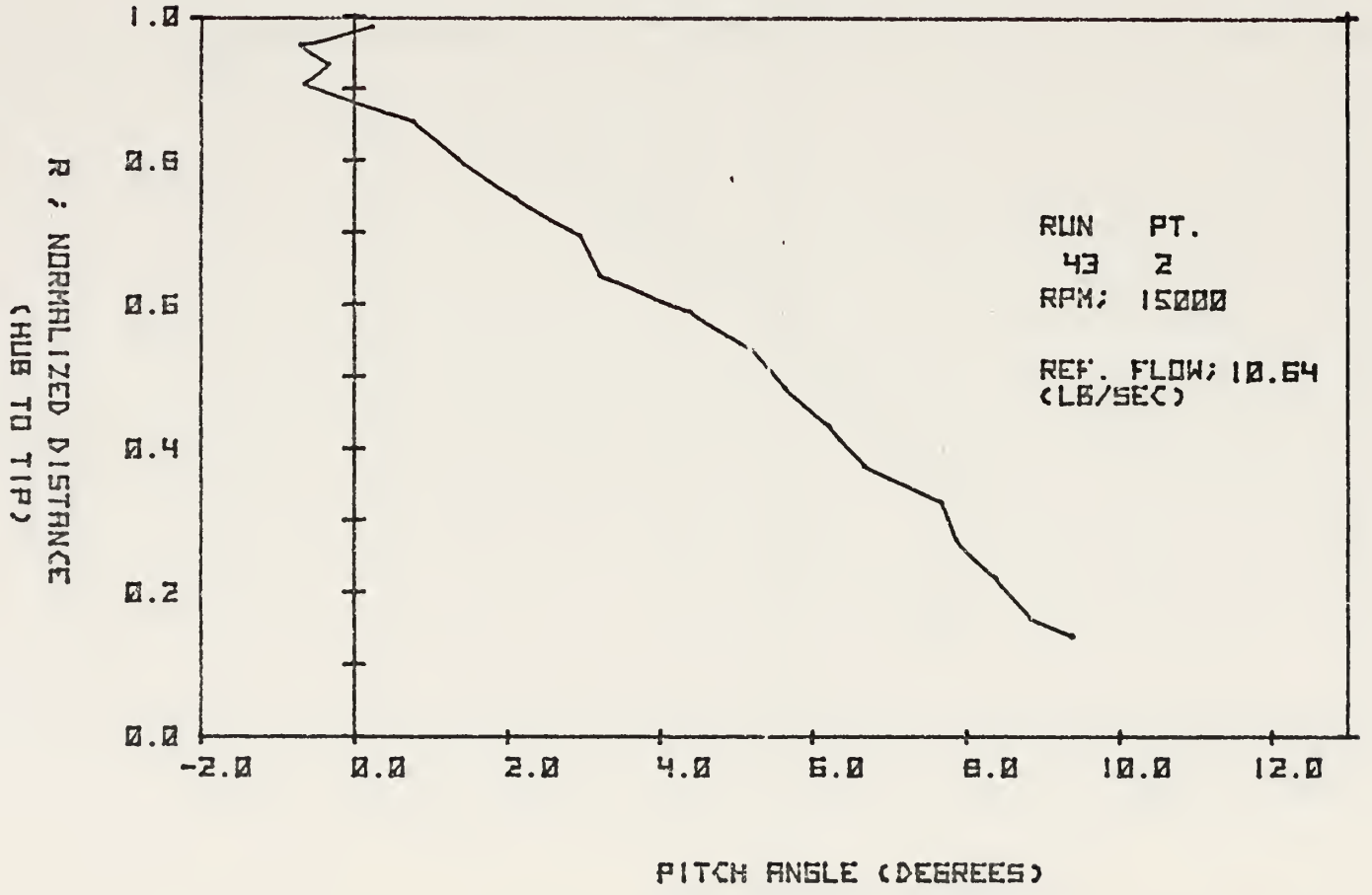

FIGURE 24. PITCH ANGLE DISTRIBUTION BEHIND THE ROTOR.

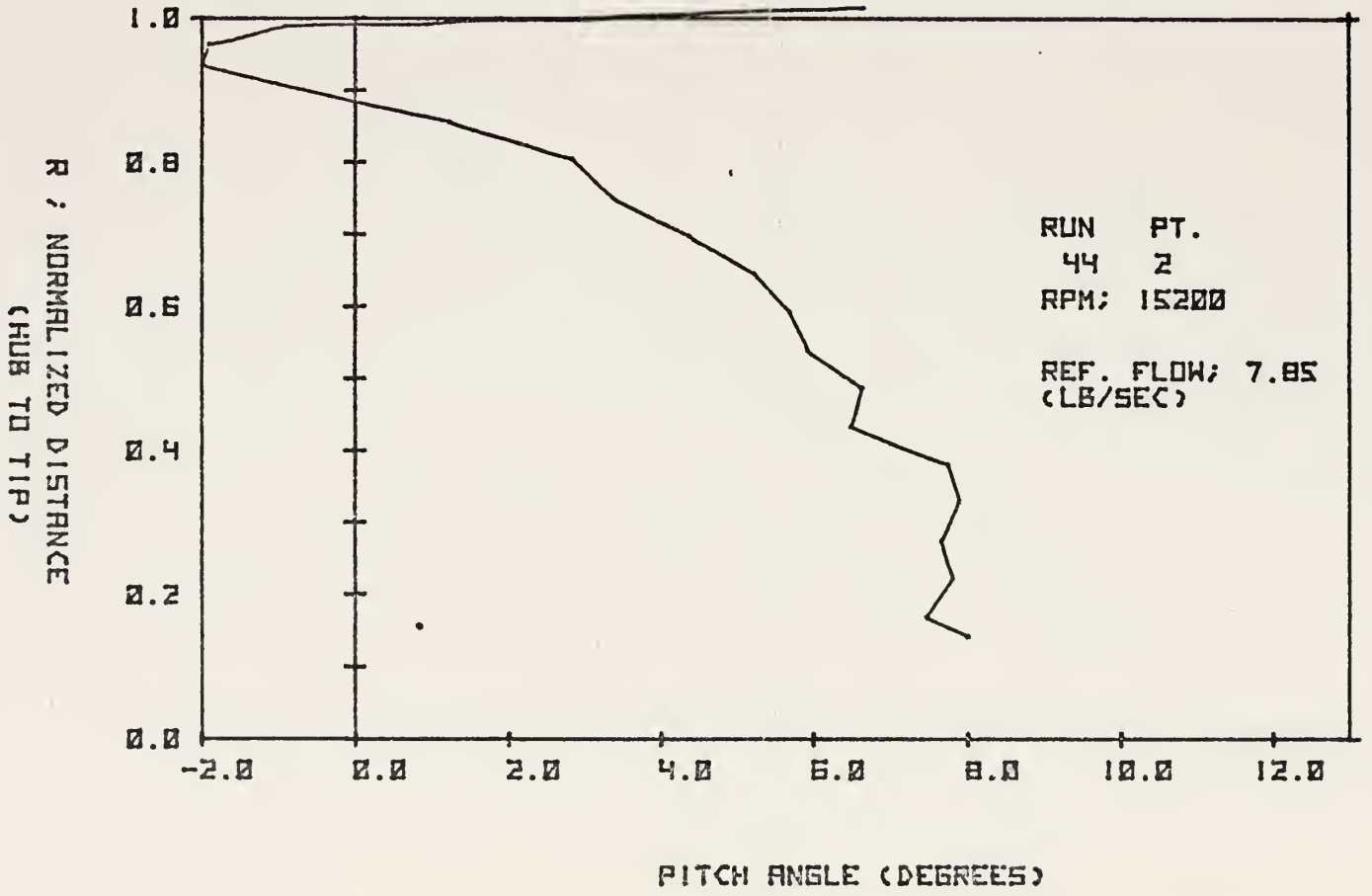

FIGURE 25. PITCH ANGLE DISTRIBUTION BEHIND THE ROTOR.

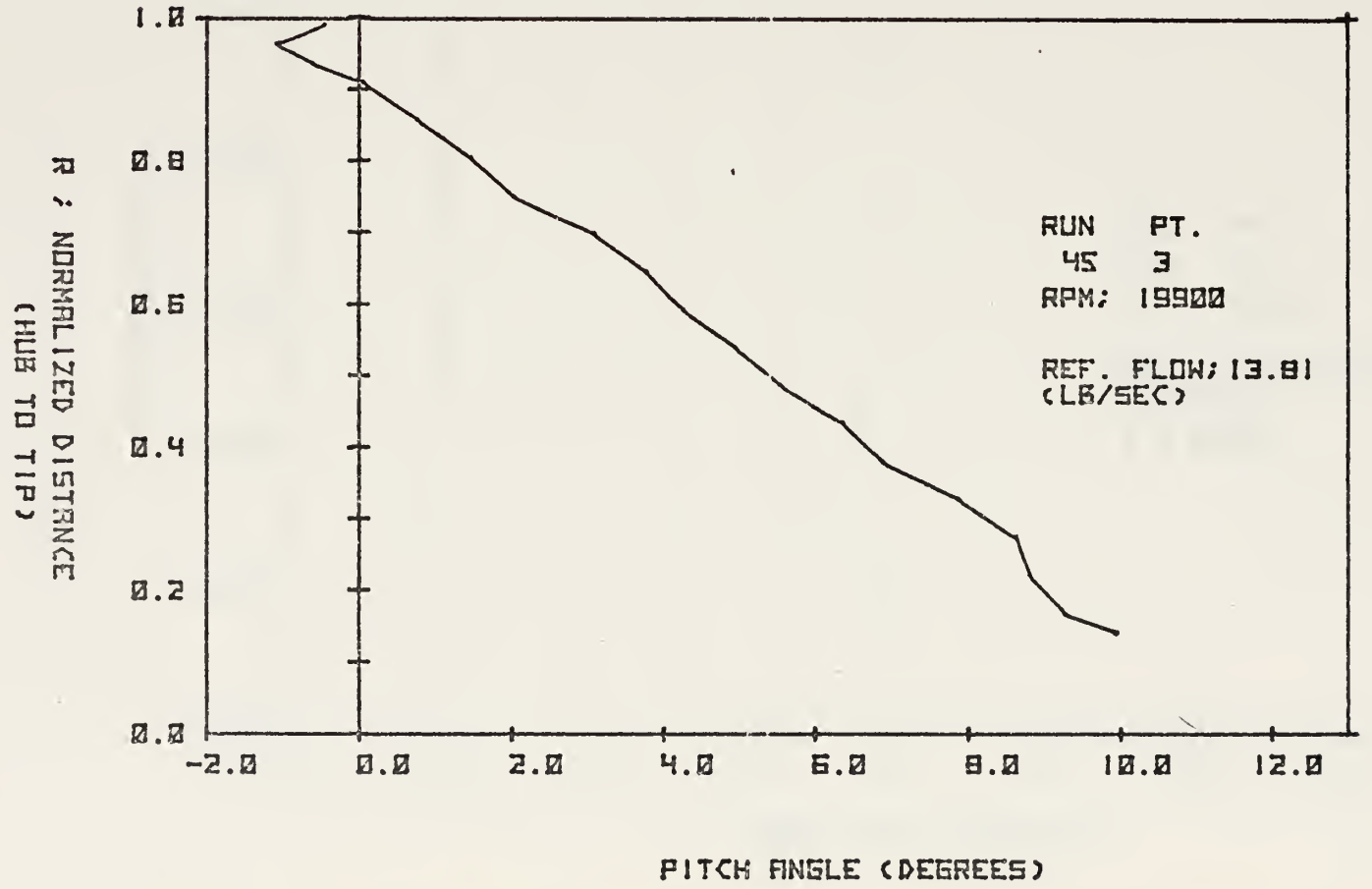

FIGURE 26. PITCH ANGLE DISTRIBUTION BEHIND THE ROTOR.

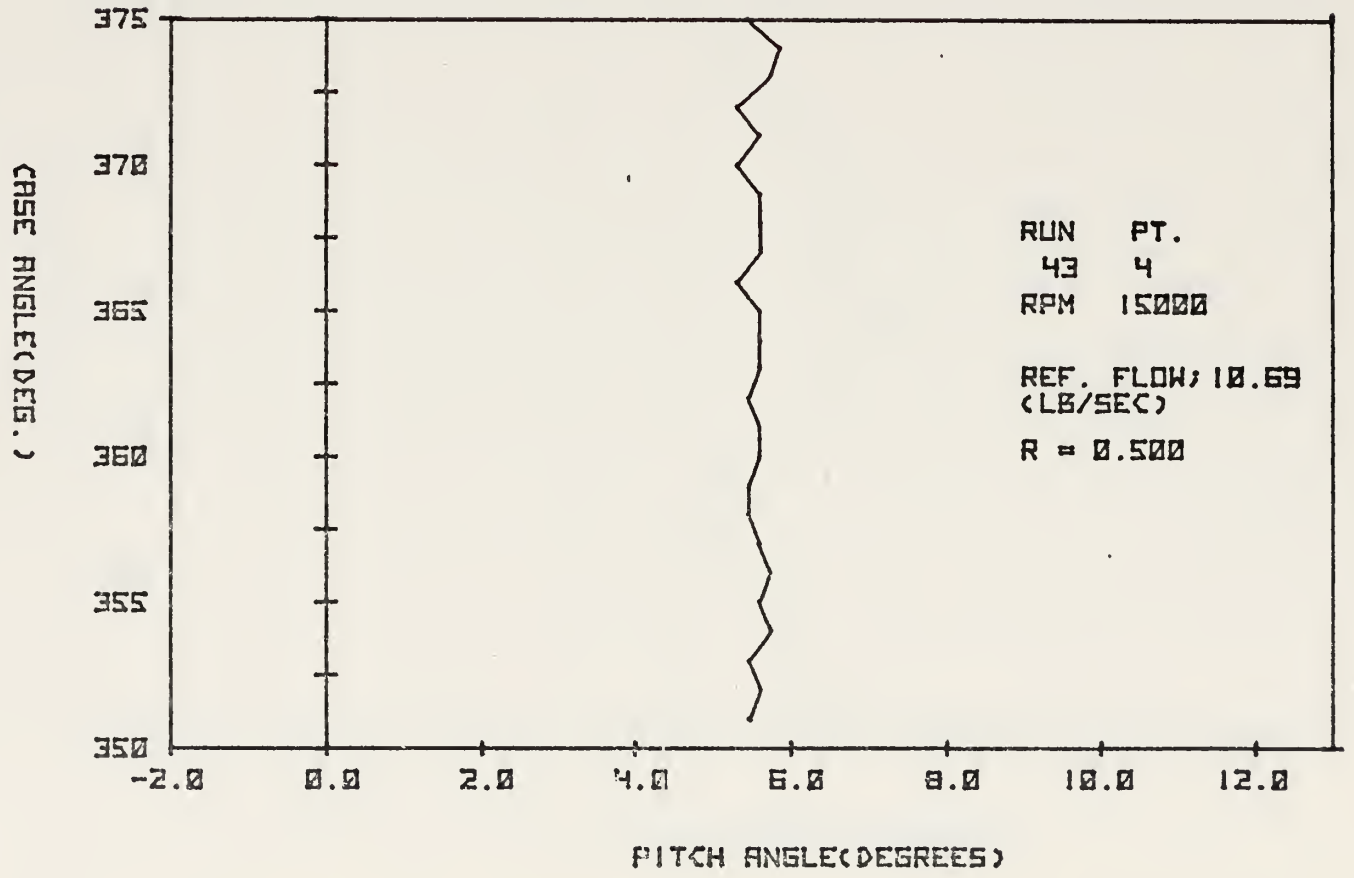

FIGURE 27. PITCH ANGLE DISTRIBUTION BEHIND THE ROTOR.

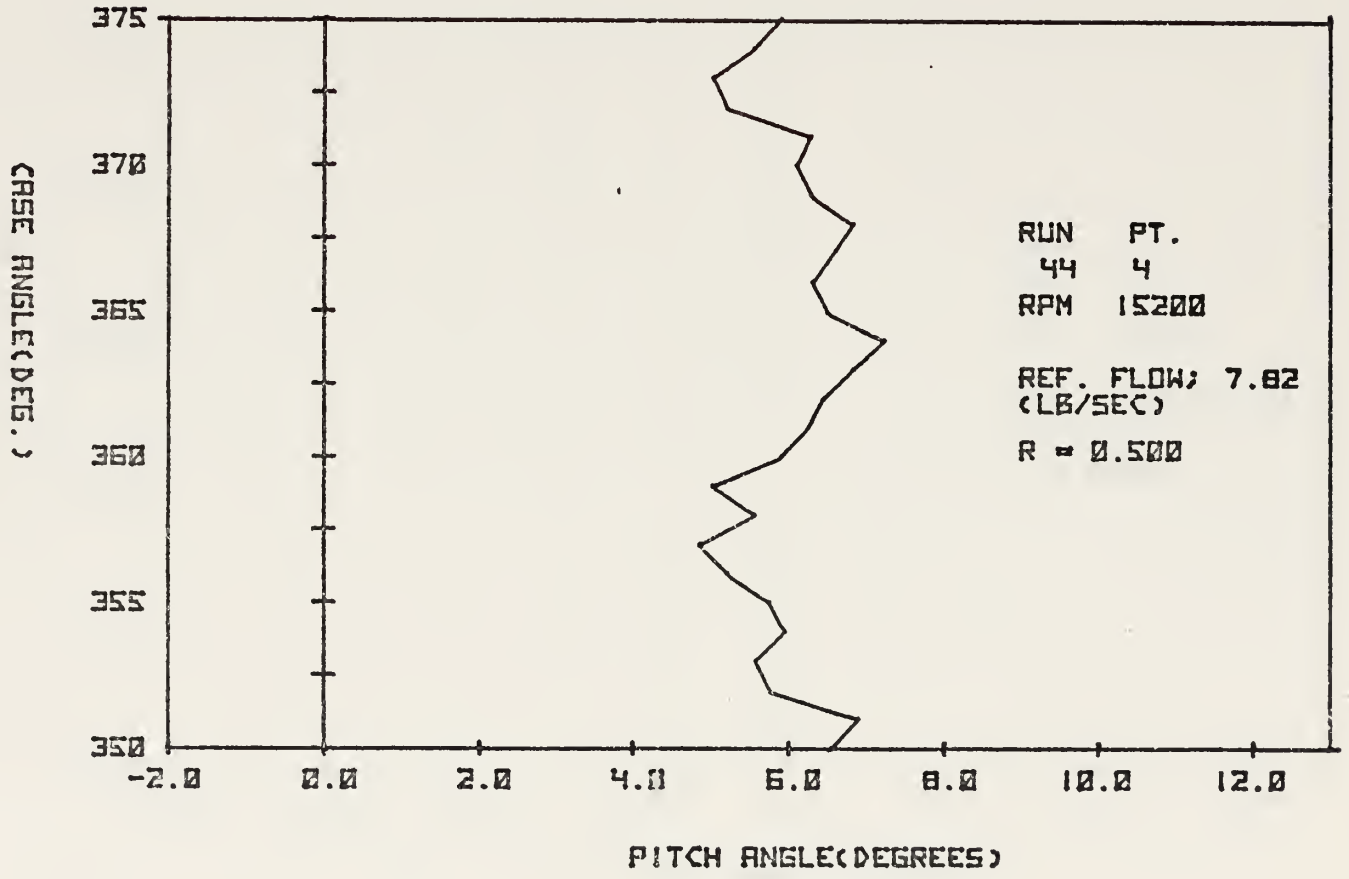

FIGURE 28. PITCH ANGLE DISTRIBUTION BEHIND THE ROTOR.

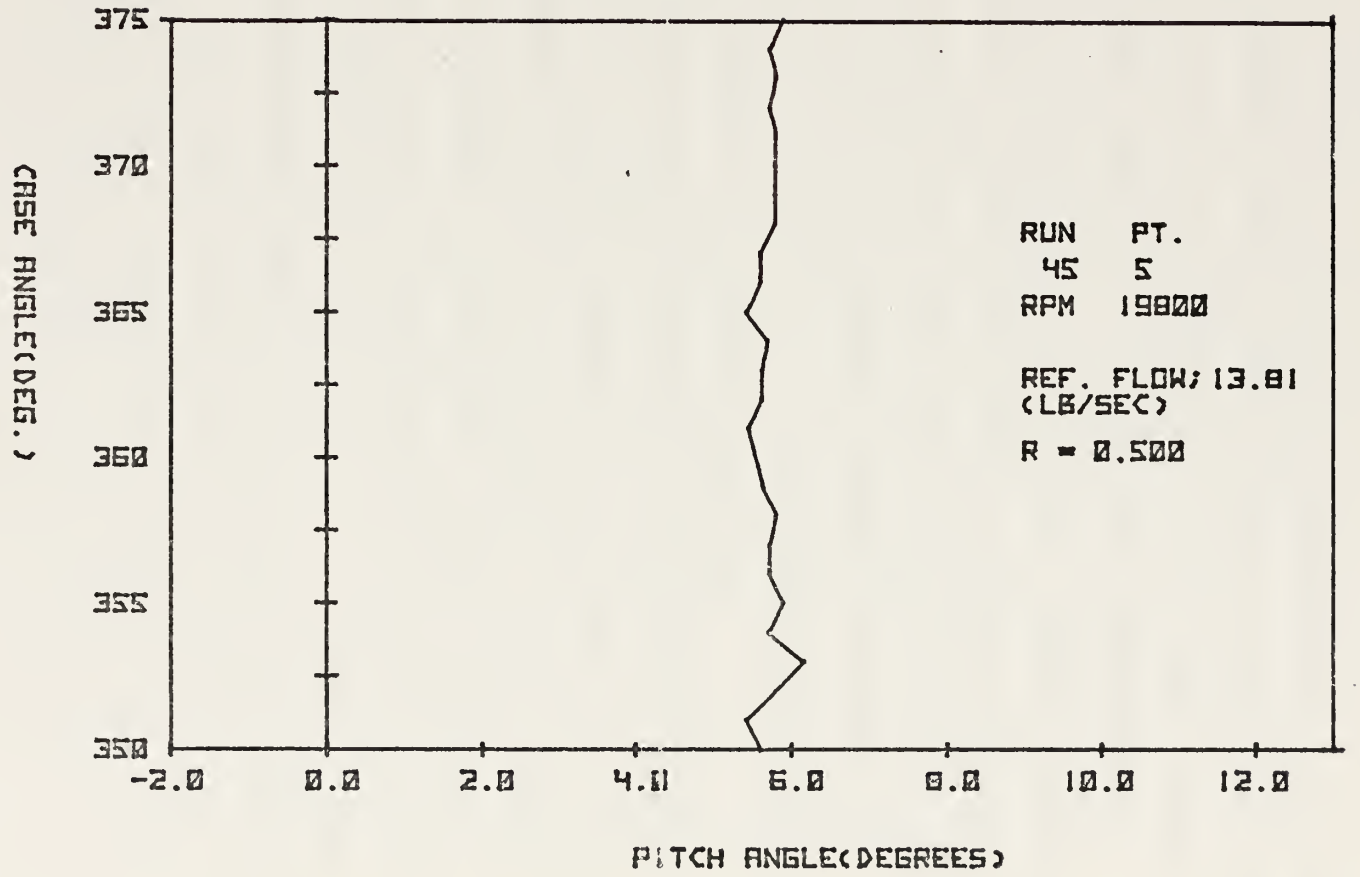

FIGURE 29. PITCH ANGLE DISTRIBUTION BEHIND THE ROTOR.

Appendix A: Determination of Velocity Vector From 5-Hole Pressure Probe Measurements

A.1 Method of Approach

The limited axial space available for instrumentation in most turbomachinery flow passages severely limits the types and sizes of pressure probes which can be used. The United Sensor DA-125, 5-hole pressure probe is designed for this application. The probe, when calibrated, will measure flow velocity, yaw angle and pitch angle. A major drawback of the probe has been the tedious labor required to extract velocity and angle data from non-linear, and inter-related calibration curves. The purpose of this appendix is to document a method for calibrating the United Sensor 5-hole probe such that, in application, data reduction can be performed by computer at the time of acquisition.

Results are given here for a particular probe which was used to measure profiles in the TRANSX. compressor. It was found to be necessary to correct the measurements made in the compressor annulus for effects altributable to the passage size and shape. The method is therefore in two parts. First, the probe was calibrated with reference to a Prandtl probe in a jet contained within a larger pipe. Analytical approximations were found which were represented as a function of the radial position in the annulus. These steps are described in section A2 and section A3 respectively, where methods of applying the calibration with and without the passage correction are also given.

A.2 Calibration and Application Free of Wall Effects

A.2.1 Probe Description and Analysis

The 5-hole probe is shown in Fig. A1. Characteristics of this and similar probes are given in the manufacturer's catalogue (8). Briefly, the probe is rotated in the flow until the pressure indicated by ports 2 and 3 (p_1 & p_3) are equal. The yaw angle (α) is then read on a vernier scale attached to the top of the probe. (Fig. A2). The average of pressures p_2 and p_3 (p_{23}, obtained pneumatically through a mixing value) is referred to as the "indicated static" pressure of the probe. Port 1 (p_1) measures "indicated total" pressure and the difference between the pressures p_4 and p_5 is a measure of the pitch angle. However, the relationship of p_{23}, and ($p_4 - p_5$) to actual static pressure, total pressure and pitch angle must be established by calibration in a known flow. Indicated static pressure is known to be more subject to errors than total pressure, particularly when the sensing holes are within about ten probe diameters of a boundary.

The calibration of the probe is expected to depend on flow Mach number. It is more convenient however to non-dimensionalize the velocity using the "limiting" velocity, $V_t = \sqrt{2C_pT_t}$ (for a perfect gas), when the stagnation temperature is a constant in the flow. The use of limiting velocity is discussed in Appendix A of reference 7 . The non-dimensional velocity is given by

$$X = V/V_t \qquad A(1)$$

where $V_t = 109.62\sqrt{T_t}$ ft/sec. for air when the stagnation temperature, T_t, is in°R. As shown in reference 7 , the relationships between the static and stagnation gas properties become

$$\frac{T}{T_t} = 1 - X^2$$

$$\frac{p}{p_t} = (1 - X^2)^{\frac{\gamma}{\gamma-1}} \qquad A(2)$$

$$\frac{\rho}{\rho_t} = (1 - X^2)^{\frac{\gamma}{\gamma-1}}$$

The relationship between Mach number and X is given by

$$X^2 = \frac{\frac{\gamma-1}{2} M^2}{1 + \frac{\gamma-1}{2} M^2} \qquad A(3)$$

The calibration of the 5-hole probe can be represented in the form of two functions of Mach number (or X) and pitch angle, ϕ.

If p_t and p are the true stagnation and static pressures, then define

$$F_\theta (X, \phi) = \frac{p_1 - p_{23}}{p_t - p} \qquad A(4)$$

and

$$F_\phi (X, \phi) = \frac{p_4 - p_5}{p_t - p} \qquad A(5)$$

to be the required calibration functions, where it is understood that the probe pressures are taken when $p_2 = p_3$.

The value of X is obtained from true static and stagnation pressures using Eq. A(2):

$$X = 1 - \left(\frac{p}{p_t}\right)^{\frac{\gamma-1}{\gamma}} = 1 - \left[1 - \frac{(p_t - p)}{(p_t - p_A) + p_A}\right]^{\frac{\gamma-1}{\gamma}} \qquad A(6)$$

where p_A = atmospheric pressure, and the pressure differences can be measured by manometers.

To calibrate, the probe must be placed in a flow at a known pitch angle and the true static and impact pressures measured by a reference probe. From the measured pressures, the value of X is calculated from Eq. A(6) and the values of F_θ and F_ϕ from Eq. A(4) and Eq. A(5). However, in applying the probe in an unknown flow, expressions relating only 5-hole probe measurements to the unknowns X and ϕ are required. Rearranging Eq. A(4) and using Eq. A(2),

$$\frac{p_1 - p_{23}}{p_1} = \left(\frac{p_t}{p_1}\right) F_\theta (X, \phi) \left[1 - \frac{p}{p_t}\right] = \left(\frac{p_t}{p_1}\right) F_\theta (X, \phi) \left[1 - (1-X^2)^{\frac{\gamma}{\gamma-1}}\right] \qquad A(7)$$

Define

$$F'_\phi (X,\phi) = F_\theta (X,\phi) \left[1 - (1-X^2)^{\frac{\gamma}{\gamma-1}}\right] \qquad A(8)$$

and, similarly

$$F'_\phi (X,\phi) = F_\phi (X, \phi) \left[1 - (1-X^2)^{\frac{\gamma}{\gamma-1}}\right] \qquad A(9)$$

The two functions F'_θ and F'_ϕ can be tabulated as functions of X and ϕ using the values obtained in the calibration for F_θ and F_ϕ at each value of X. If, in addition, it can be shown that $p_{t/p_1} = 1.0$ to within the desired accuracy over the range of X and ϕ of interest, then, from Eq. A(7)

$$F'_\theta (X, \phi) = \frac{(p_1 - p_{23})}{(p_1 - p_A) + p_A} \qquad A(10)$$

and similarly

$$F'_\phi (X, \phi) = \frac{p_4 - p_5}{(p_1 - p_A) + p_A} \qquad A(11)$$

In using the calibration expressed by Eq. A(10) and Eq. A(11), it is necessary to interpolate in the tables established for F'_θ and F'_ϕ to find values of X and ϕ for which Eq. A(10) and Eq. A(11) are simultaneously satisfied by the measurements. Alternatively, analytical approximations can be derived for F'_θ and F'_ϕ which can be solved by iteration. The analytical approximation technique was chosen here.

A.2.2 Calibration Tests in a Jet

The 5-hole probe was calibrated as shown in Fig. A3. An A.S.M.E. flow nozzle, 7 inches in diameter, was flanged between two 36 inch lengths of 10 inch diameter steel pipe. (The internal contour of the nozzle was chrome plated and polished to a maximum roughness of 32 micro inches). Air was supplied to the 10" pipe at controlled flow rates from an industrial compressor (3) via a 4 ft. diameter settling chamber and entrance bellmouth. A 12" long bundle of $\frac{1}{2}$" diameter tubing removed any swirl remaining in the flow from the plenum. The flow from the pipe downstream of the flow nozzle exhausted into the laboratory.

A Prandtl probe was used to obtain the reference measurements of static and total pressures. The 5-hole and Prandtl probe tips were positioned on opposite sides of the flow centerline at a radius of one inch. The measuring station was 2 inches downstream of the nozzle exit face. The 5-hole probe was mounted through an aluminum block as shown in Fig. A4. The block allowed the pitch angle to be set in 5° increments from - 10° to + 10° and in 10° increments from - 40° to + 40° with no change in the tip location. All pressure differences were measured using U-tube water manometers. The stagnation temperature was measured using an iron-constantarn thermocouple probe in the flow upstream of the flow nozzle.

The flow at the measuring plane was first surveyed using the Prandtl probe with the 5-hole probe removed. The result in Fig. A5 showed that the velocity (X) was uniform over a 4" diam core, and therefore that the flow at the reference probe tip and the 5-hole probe tip were the same to within measurement accuracy.

The procedure for the calibration tests was the following: The flow rate from the compressor was set and allowed to stabilize. The 5-hole probe was then inserted in turn at each desired value of the pitch angle. Pressure differences were recorded by hand from the manometer for the Prandtl and 5-hole probes. The thermocouple probe reading and barometric pressure were also recorded.

To cover the range required in the probe application, ϕ was varied from -5° to $+40^{\circ}$ in 7 steps. Nine values of X were set giving dynamic pressures between 9 and 75 inches of water column. If ± 0.025 inches in the accuracy of reading each manometer column, the pressure differences are measured to ± 0.05 inches of water. However, unsteadiness in the air supply over the recording time period can be expected to reduce to overall accuracy to ± 0.1 inches water.

A.2.3 Analysis of the Results

The recorded data is given in Table A1. The ratio (p_1/p_t) was calculated to be within 0.2% of unity over the complete range of X and ϕ measured and hence was set equal to unity in representing and applying the calibration results. Using the data in Table A1, values of F'_θ and F'_ϕ were calculated using Eq. A(8) and Eq. A(9), where F_θ and F_ϕ were obtained from Eq. A(4) and Eq. A(5) and X was calculated using Eq. A(6). The remaining task was to find analytical approximations for the values of F'_θ and F'_ϕ as functions of X and ϕ, and to devise an iterative computer solution.

F'_θ and F'_ϕ were plotted as functions of ϕ for each value of X. The results are shown in Fig. A6 and Fig. A7. Using polynomial regression on the Hewlett-Packard 9830A calculator, F'_θ at constant X was satisfactorily fit by a 4th order polynomial in ϕ. F'_ϕ at constant X was satisfactorily fit by a 2nd order polynomial in ϕ. This representation however was found to be unsuitable in solving iteratively for X and ϕ with F'_θ and F'_ϕ given. Instead, expressions were found for

$$F'_\phi = F'_\phi\ (\phi)\ |_{X\ =\ \text{const}}$$

as in Fig. A7, and

$$X = X\ (F'_\theta)\ |_{\phi\ =\ \text{const}}$$

Fig. A8 shows the results plotted in the latter form. Quadratic functions were found to represent the data satisfactorily.

Since data was taken for 9 values of X and 7 values of ϕ, the two sets of functions were expressed as

$$F'_{\phi_i}\ (\phi) = a_i(X) + b_i(X)\ \phi + c_i(X).\ \phi^2 \qquad A(12)$$

where i = 1, 2 --- 9 and a_i, b_i and c_i are coefficients which depend on the value of X, and

$$X_j(F'_\theta) = f_j(\phi) + g_j(\phi).\ [F'_\theta] + h_j(\phi).[F'_\theta]^2 \qquad A(13)$$

where j = 1, 2 --- 7 and f_j, g_j and h_j are coefficients which depend on the value of ϕ.

Next, the coefficients a_i, b_i and c_i from the 9 equations represented by Eq. A(12) were approximated by a polynomial expansion in X, and the coefficients f_j, g_j and h_j from the 7 equations represented by Eq. A(13) by

a polynomial expression in ϕ. Thus coefficients were found for the expressions

$$a_i(X) = A_1 + A_2X_i + A_3X_i^2 + - - - - -$$

$$b_i(X) = B_1 + B_2X_i + B_3X_i^2 + - - - - - \qquad A(14a)$$

$$c_i(X) = C_1 + C_2X_i + C_3X_i^2 + - - - - -$$

$$f_j(\phi) = F_1 + F_2\phi_j + F_3\phi_j^2 + - - - - -$$

$$g_j(\phi) = G_1 + G_2\phi_j + G_3\phi_j^2 + - - - - - \qquad A(14b)$$

$$h_j(\phi) = H_1 + H_2\phi_j + H_3\phi_j^2 + - - - - -$$

which gave the best fit to the 9 values of a_i, b_i, c_i and to the 7 values of f_j, g_j and h_j. This results in a single equation (Eq. A(12)) for $F'_\phi(\phi)$ in which the coefficients are analytic functions of X, and a single equation (Eq. A(13)) for $X(F'_\theta)$ in which the coefficients are analytic functions of ϕ. The coefficients in Eq. A(14) are given in Table A3.

In application, the probe measurements give values to F'_θ and F'_ϕ through Eq. A(10) and Eq. A(11). Equation A(12) and Eq. A(13) must be solved for the unknown ϕ and unknown X. An initial estimate of the pitch angle was devised in the following way. A new function of the probe pressure differences was defined such that

$$F'_\lambda(X,\phi) \equiv \frac{F'_\phi}{F'_\theta} \equiv \frac{p_4 - p_5}{p_1 - p_{23}} \qquad A(15)$$

When ϕ was plotted as a function of F'_λ for each value of X, it was observed that the curves were nearly linear with similar slopes. Therefore the average of the 9 values of F'_λ at each value of ϕ was calculated and a third order polynomial was found to fit the 7 average values when ϕ was plotted

as a function the average F'_λ (Fig. A9). This gave

$$\phi_1 (F'_\lambda) = J + K (F'_\lambda) + L (F'_\lambda)^2 + M (F'_\lambda)^3 \qquad A(16)$$

where ϕ_1 is the desired initial estimate of the pitch angle and F'_λ is obtained from the probe measurements using Eq. A(15). The coefficients J, K, L & M are given in Table A4.

A2.4 Application

When applying the 5-hole probe to measure an unknown flow, the pressure differences read when p_2 and p_3 are balanced are reduced to the three factors F'_θ, F'_ϕ and F'_λ using Eq. A(10), Eq. A(11) and Eq. A(15). X and ϕ are evaluated using the calibration relations derived in the preceeding section. The yaw angle is read directly from the probe scale. The velocity is obtained from the product of X and V_t which requires the input of the stagnation temperature.

The reduction to velocity and pitch angle was programmed for the Hewlett-Packard Model 9830A calculator. A flow chart of the program is shown in Fig. A10. The program first calculates the initial estimate of ϕ ($=\phi_1$) using Eq. A(16). The initial estimate of X ($=X_1$) is calculated from Eq. A(13) using ϕ_1 in Eq. A(14b) to evaluate the coefficients f, g and h. The coefficients a, b and c in Eq. A(12) are then calculated using X_1 in Eq. A(14a). In general the value of F'_ϕ which could be calculated using these coefficients in Eq. A(12) would not be equal to the value calculated from the input data. An iterative procedure is begun using ϕ_1 and X_1 as initial values.

In the adopted procedure, Eq. A(12) is viewed as an equation to be solved for an unknown ϕ in terms of a known F'_ϕ and known X. Equation A(13) is treated as an equation for X in terms of a known ϕ. Equation A(12) is solved by fixed point iteration (9) beginning with the initial values ϕ_1 and X_1. In this

method, the $(i+1)^{th}$ value of ϕ in the iteration is given in terms of the i^{th} value by rewriting Eq. A(12) as

$$\phi_{i+1} = [F'_{\phi} - a - c\,\phi_i^2]/b \qquad A(17)$$

For a fixed value of $X(=X_i)$, which fixes the coefficients a, b, and c, successive values of ϕ are calculated using Eq. A(17) until $|\phi_{i+1} - \phi_i| < \epsilon_{\phi}$ is satisfied. ϵ_{ϕ} is a small quantity. A new value of $X(=X_{i+1})$ is then calculated using $\phi = \phi_{i+1} = \phi_i$ in Eq. A(13) and the process repeated until $|X_{i+1} - X_i| < \epsilon_x$, where ϵ_x is a small quantity.

The steps in the solution may be summarized as follows:

1) Calculate ϕ from Eq. A(16)
2) Calculate X_1 from Eq. A(13)
3) Calculate ϕ_{i+1} from Eq. A(17)
4) If $|\phi_{i+1} - \phi_i| < \epsilon_{\phi}$ do step 5), otherwise go to step 3)
5) Calculate X_{i+1} from Eq. A(13) using $\phi = \phi_{i+1} = \phi_i$
6) If $|X_{i+1} - X_i| < \epsilon_x$ stop, otherwise go to step 3).

A.3 Corrections to the Calibration for Application in an Annulus

A3.1 Introduction

The calibration described above was carried out where the presence of flow boundaries would not be expected to influence the probe readings. A change in the calibration of the probe is expected when measurements are made within about ten probe diameters of a boundary, and when the probe size is significant compared to the flow passage area. A precise correction which would allow the use of the probe in any flow field is a difficult task and not attempted here. Instead, a calibration of the probe in an axial annular flow of similar geometry to the compressor annulus was carried out, and corrections to the "wall-free" calibration of section A2 were derived which were represented as a function of radial position. The test of the success of this proceedure was to compare measurements made in the compressor using two different types of probes. Agreement in the velocity profiles derived from the two probes would be expected if the corrections applied to each calibration were valid. Also, the distribution of true static pressure derived from the probe calibrations should be consistent with wall tap measurements on the tip and hub surfaces. In the following sections, the calibration tests are described and the derivation of corrections to the "wall-free" calibration is presented. The application of the revised calibration to compressor measurements is then given.

A3.2 Calibration Tests in an Annulus

An annular axial flow was generated as shown in Fig. A11. An axisymmetric body with a maximum diameter of 6"over 28"of its length was supported in the center of a 10" pipe. At the upstream end, four thin airfoil struts were positioned ahead of the contoured nose section which generated a smooth contraction of the flow passage to a 2" annulus. Heavy struts supported the

centerbody at the outlet flange where the flow exhausted into the laboratory. A view of the apparatus is shown in Fig. A12. Six equally spaced wall pressure taps were provided in the 10" pipe at each of 3 axial stations. Corresponding pressure taps were provided on the centerbody surface. Provision for radial probe surveys was made at the same three axial stations.

It was established in preliminary surveys that the wall pressures at station 1 in Fig. A11 were uniform around the periphery to ± 0.34% of the average dynamic head. The outer (tip) wall pressures were consistently lower than inner (hub) wall pressures by 0.45% of the dynamic head. The flow was measured to be axial to within the sensitivity of the 5-hole probe yaw angle measurement (± .1°). Probe calibration was therefore carried out at station 1. Static pressure was assumed to vary linearly between hub and tip values, and the pitch angle was taken to be zero.

Radial surveys were made from hub to tip at fixed flow rates using the 5-hole probe, a Kiel probe and a pitot-static probe in succession. Readings were taken at the same radial locations with each probe. Intervals of 0.2", decreasing to 0.05" near the walls, were used. Dynamic pressure was varied from 27 to 73 inches of water in 7-8 inch increments. The data for seven surveys is given in Table A2.

A3.3 Analysis of the Results

An example of the distribution of pressures measured by the three probes is given in Fig. A13. It was observed that the probes gave the same values of impact pressure at corresponding points to within the accuracy of the measurements except close to the outer wall where the velocity gradients were large. The static pressure indicated by the pitot static probe was observed to vary very little across the annulus, and was in agreement with a linear

variation of the true static pressure between hub and tip measurements at the wall. Also, the wall pressures at hub and tip away from the traverse station were not measurably affected by the prove movement. Consequently, the 5-hole probe indicated total presure (P_1) and a static pressure obtained by a linear interpolation between measurements at the walls were used to calculate the actual velocity (X) at the probe location. By applying the methods of section A2, the 5-hole probe pressure measurements were reduced to "wall-free" values of velocity and pitch angle, ($\bar{X}$ and $\bar{\phi}$), which in general were different from the actual values, (X and ϕ) at the probe location.

A velocity correction factor, $\bar{K}_x$, was defined and examined as a function of position in the annulus and the indicated velocity, thus:

$$\bar{K}_x\ (H,\bar{X}) = \frac{X - \bar{X}}{\bar{X}} \qquad A(18)$$

where H = y/h, y is the distance outwards from the hub wall and h is the annulus depth. At each value, H_i, of the probe position the dependence of $\bar{K}_x$ on $\bar{X}$ was approximated by a polynomial

$$\bar{K}_{x_i} = q_i + r_i \bar{X} + s_i \bar{X}^2 + \qquad A(19)$$

where i = 1, 2, --- 12, and H_i = 0.125, 0.15, --- 0.975. The coefficients in Eq. A(19) are listed in Table A5.

The pitch angle at each probe position, H_i, was found to be independent of X. A pitch correction factor, $\bar{K}_\phi$ was defined which was then a function of position only: thus

$$\bar{K}_\phi\ (H) = \frac{(\phi + \beta) - (\bar{\phi} + \beta)}{(\phi + \beta)} \qquad A(20)$$

where β is a constant angle introduced to avoid division by zero. Since

$\phi = 0$ in the calibration test, Eq. A(20) with $\beta = 180^\circ$ becomes

$$\bar{K}_\phi(H) = - \frac{\bar{\phi}}{180} \qquad A(21)$$

The values of $\bar{K}_\phi$ obtained for the tests in the annulus using Eq. A(21) were approximated by a 6^{th} order polynomial,

$$\bar{K}_\phi (H) = z_1 + z_2 H + z_3 H^2 + z_4 H^3 + z_5 H^4 + z_6 H^5 + z_7 H^6 \qquad A(22)$$

to .995 root mean square. The coefficients in Eq. A(22) are listed in Table A6.

A3.4 Application

It is assumed that the corrections required to the calibration free of wall effects when the 5-hole probe is used to determine the flow field in a compressor annulus, are those established for an axial flow in the annulus of similar geometry. The probe readings are first reduced to values of $\bar{X}$ and $\bar{\phi}$ using the methods given in Section A2. Then, from Eq. A(18) and Eq. A(20) with $\beta = 180^\circ$, the corrected velocity and pitch angle are given by

$$X = \left(\frac{1}{1 - \bar{K}_x}\right). \bar{X} \qquad A(23)$$

and

$$\phi = \left(\frac{1}{1 - \bar{K}_\phi}\right). \phi + 180 \left(\frac{\bar{K}_\phi}{1 - \bar{K}_\phi}\right) \qquad A(24)$$

At any probe position, H, the value of $\bar{K}_\phi$ in Eq. A(24) is given by Eq. A(22) for which the coefficients are given in Table 6.

The value of $\bar{K}_x$ in Eq. A(23) must be obtained by interpolation. The uncorrected velocity $\bar{X}$ is known at the probe position H; however, the correction factor $\bar{K}_x$ can be evaluated using Eq. A(19) only at discreet locations H_i. The method adopted is a form of quadratic interpolation for uneven

intervals (10). First the value of i is found such that H is located in the interval between H_i and H_{i+1} as shown in Fig. A(14). The values of $\bar{K}_{x_{i-1}}$, $\bar{K}_{x_i}$, $\bar{K}_{x_{i+1}}$ and $\bar{K}_{x_{i+2}}$ are calculated from Eq. A(19) using the coefficients given in Table A5. The coefficients of quadratics for $\bar{K}_x$ passing through each of the two sets of three points H_{i-1}, H_i, H_{i+1} and H_i, H_{i+1}, H_{i+2} are calculated and each quadratic is used to calculate a value for $\bar{K}_x$ at H. The arithmetic mean of the two values is taken for the interpolation. In the first or the last interval, or to extrapolate outside the given range, only one quadratic is used.

The data reduction with corrections was programmed for the Hewlett-Packard Model 9830A calculator. The flow chart is given in Fig. A(15). The steps are summarized as follows:

1) Input probe pressure data, probe position, flow stagnation temperature, atmospheric pressure.
2) Calculate $\bar{\phi}$ and $\bar{X}$ using the steps given in Section A2.4.
3) Calculate $\bar{K}_\phi$ with Eq. A(22).
4) Calculate $\bar{K}_x$ using quadratic interpolation between $\bar{K}_{x_i}$ values given by Eq. A(19).
5) Calculate X and ϕ using Eq. A(23) and Eq. A(24).

This proceedure was applied to the calibration data as described in Section A3.2 and listed in Table A2. The results for one survey are shown for illustration in Table A7. At each probe position in the annulus, H, the uncorrected indicated velocity, X(UNMOD), the measured actual velocity, X(ACTUAL), and the corrected velocity, X(MOD) are compared. The largest error between the corrected and actual values was less than 0.3% for all points in all surveys taken.

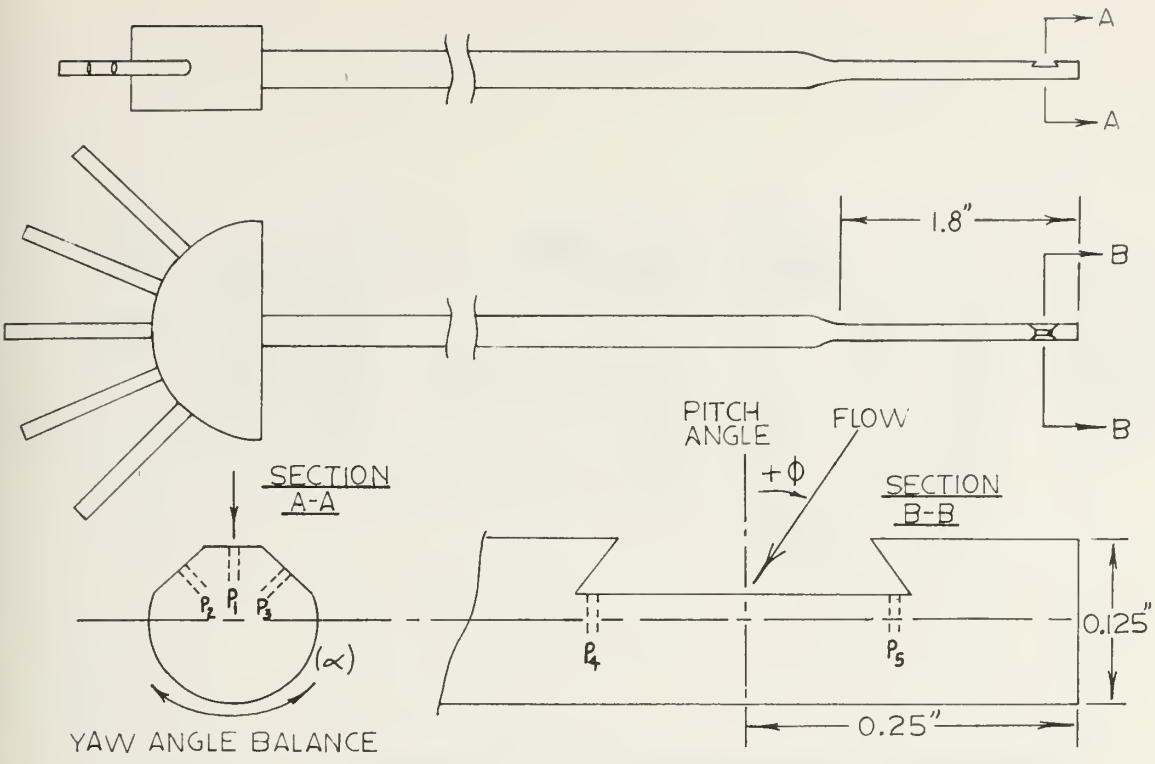

FIGURE A1. SCHEMATIC OF THE 5-HOLE PROBE

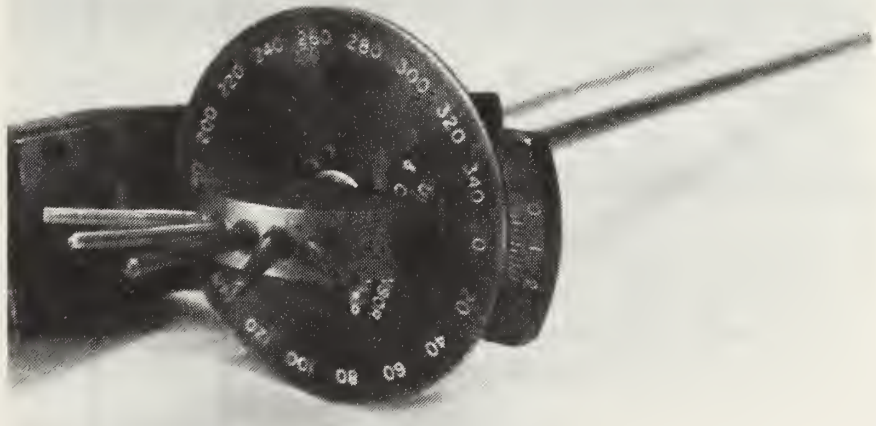

FIGURE A2. VIEW OF THE 5-HOLE PROBE SHOWING YAW ANGLE SCALE

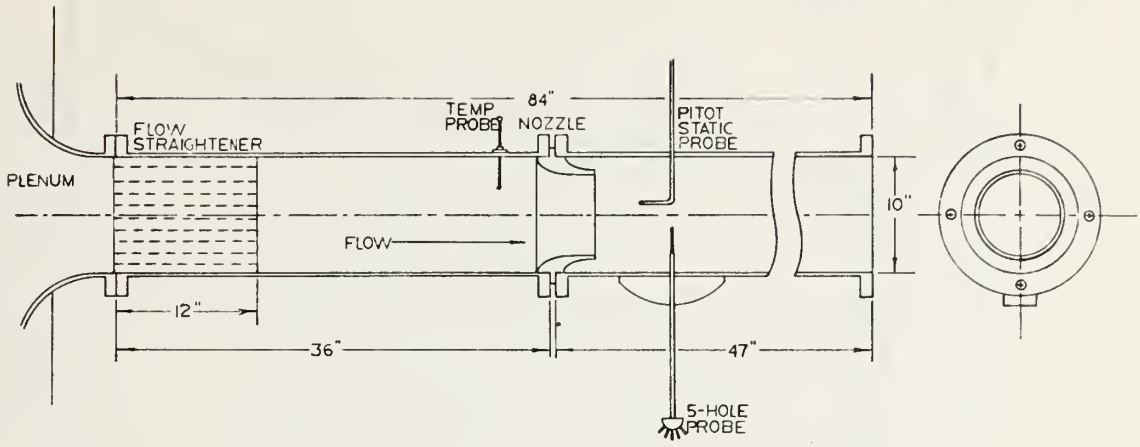

FIGURE A3. SCHEMATIC OF THE APPARATUS FOR PROBE CALIBRATION FREE OF WALL EFFECT

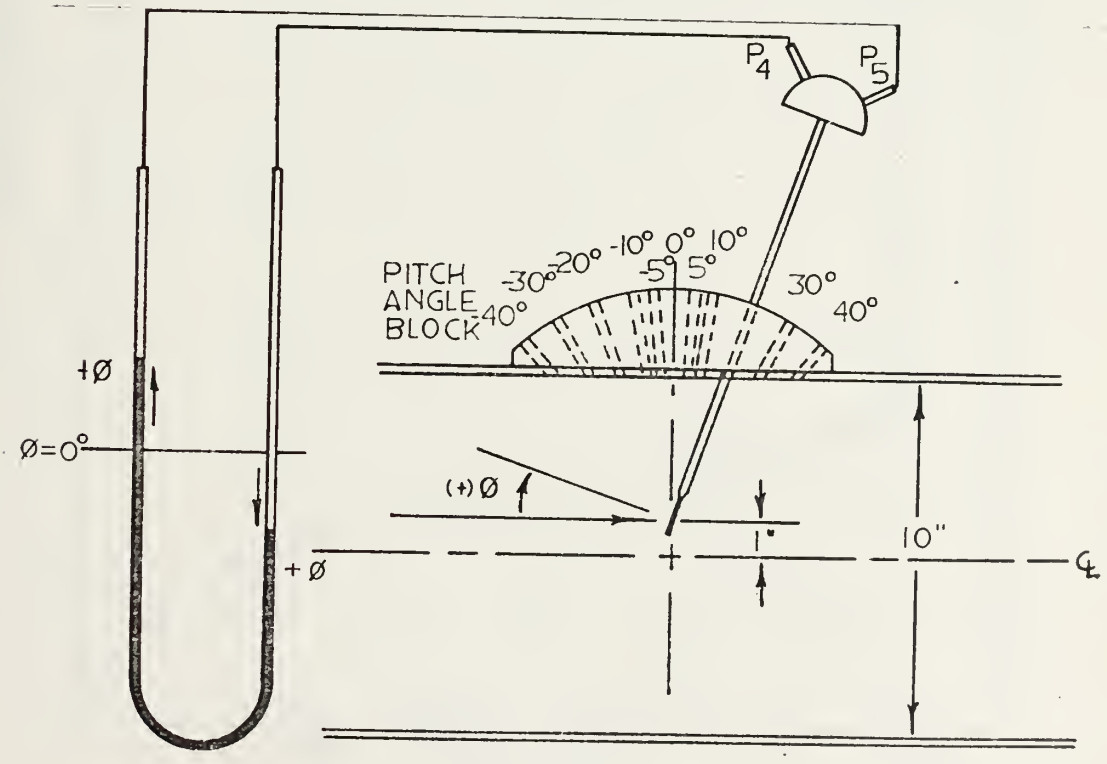

FIGURE A4. PITCH ANGLE BLOCK

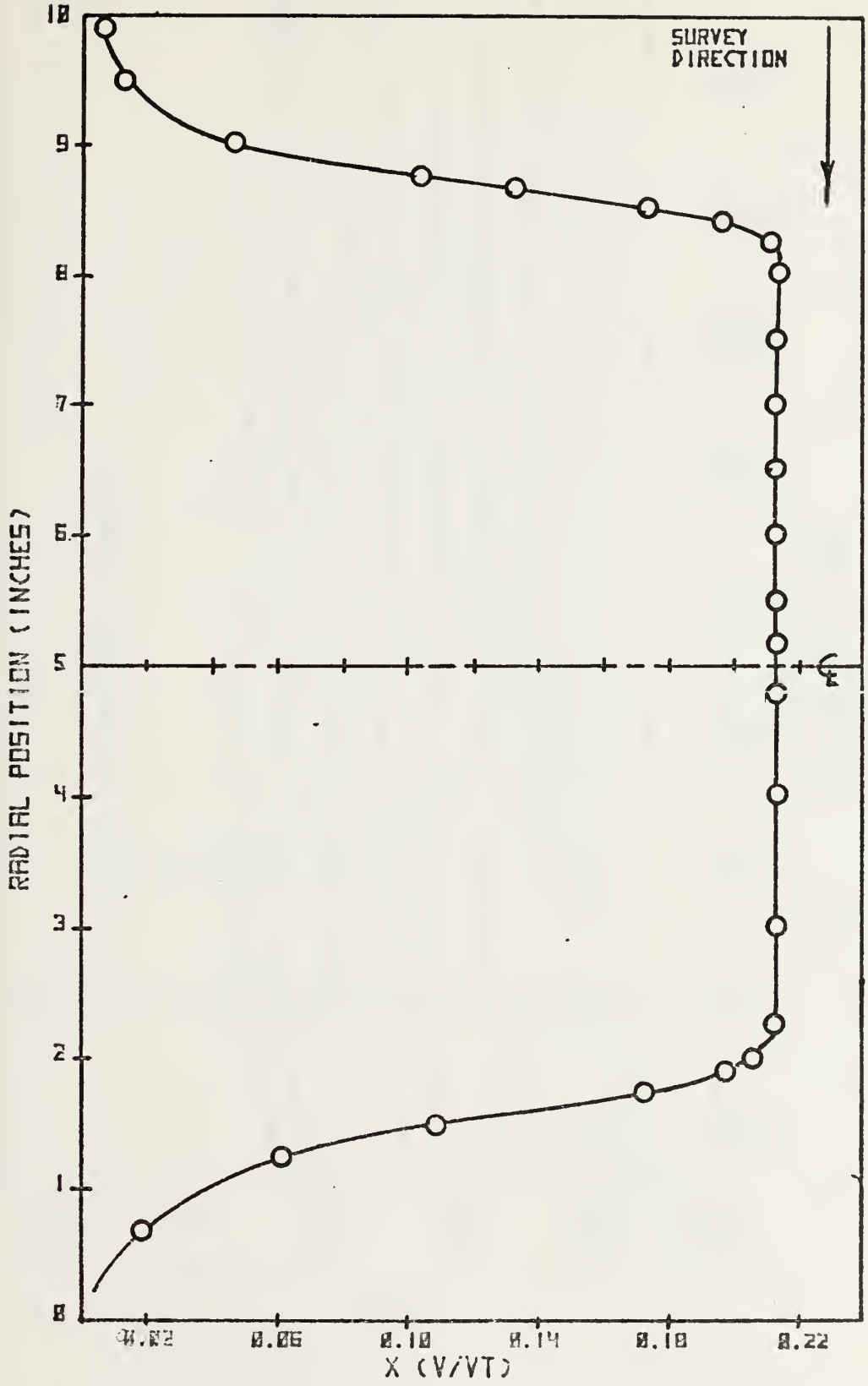

FIGURE A5. VELOCITY PROFILE IN THE MEASUREMENT PLANE.

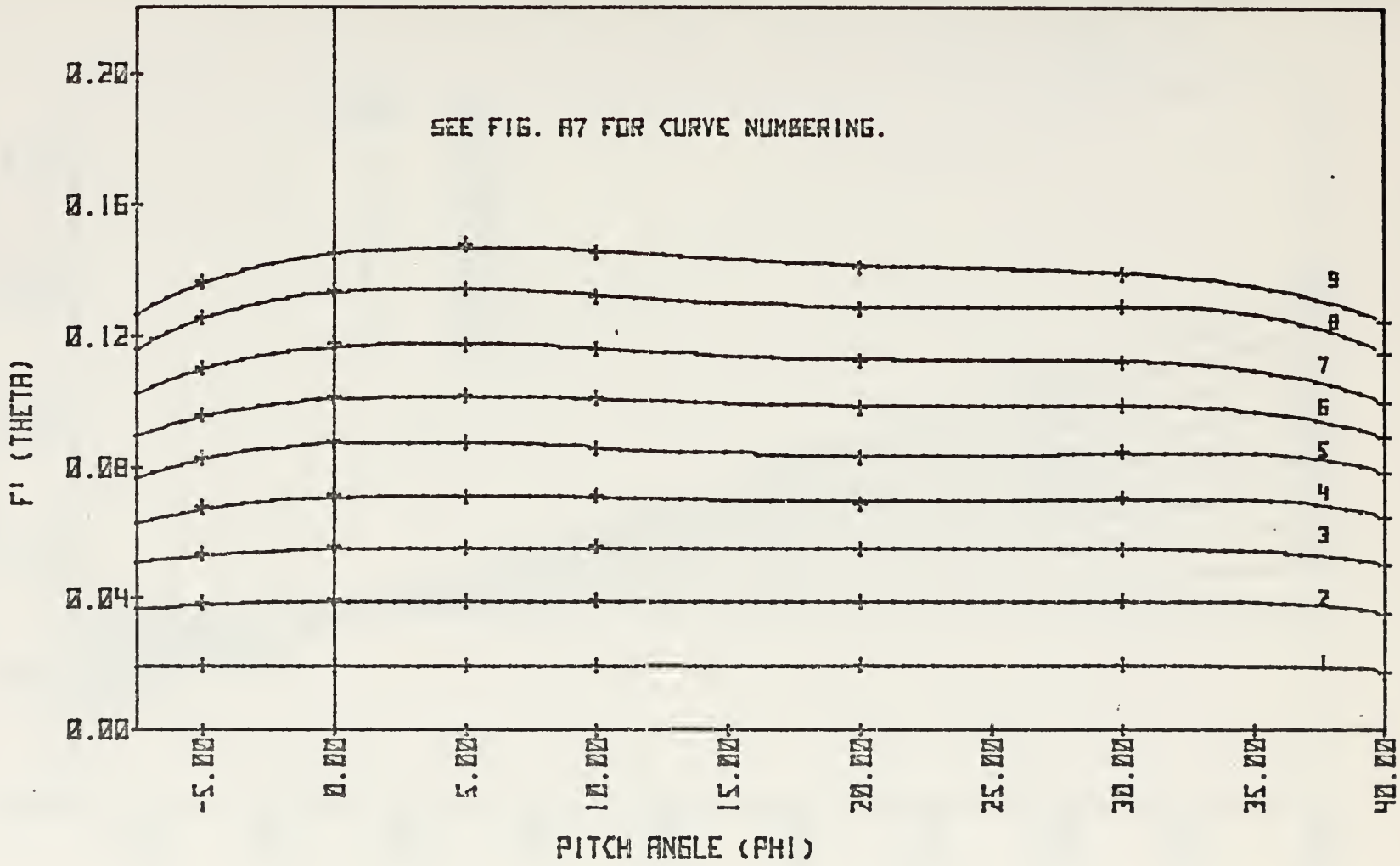

FIGURE A6. F'(THETA) VS. PHI DATA POINTS AND POLYNOMIAL CURVE FITS.

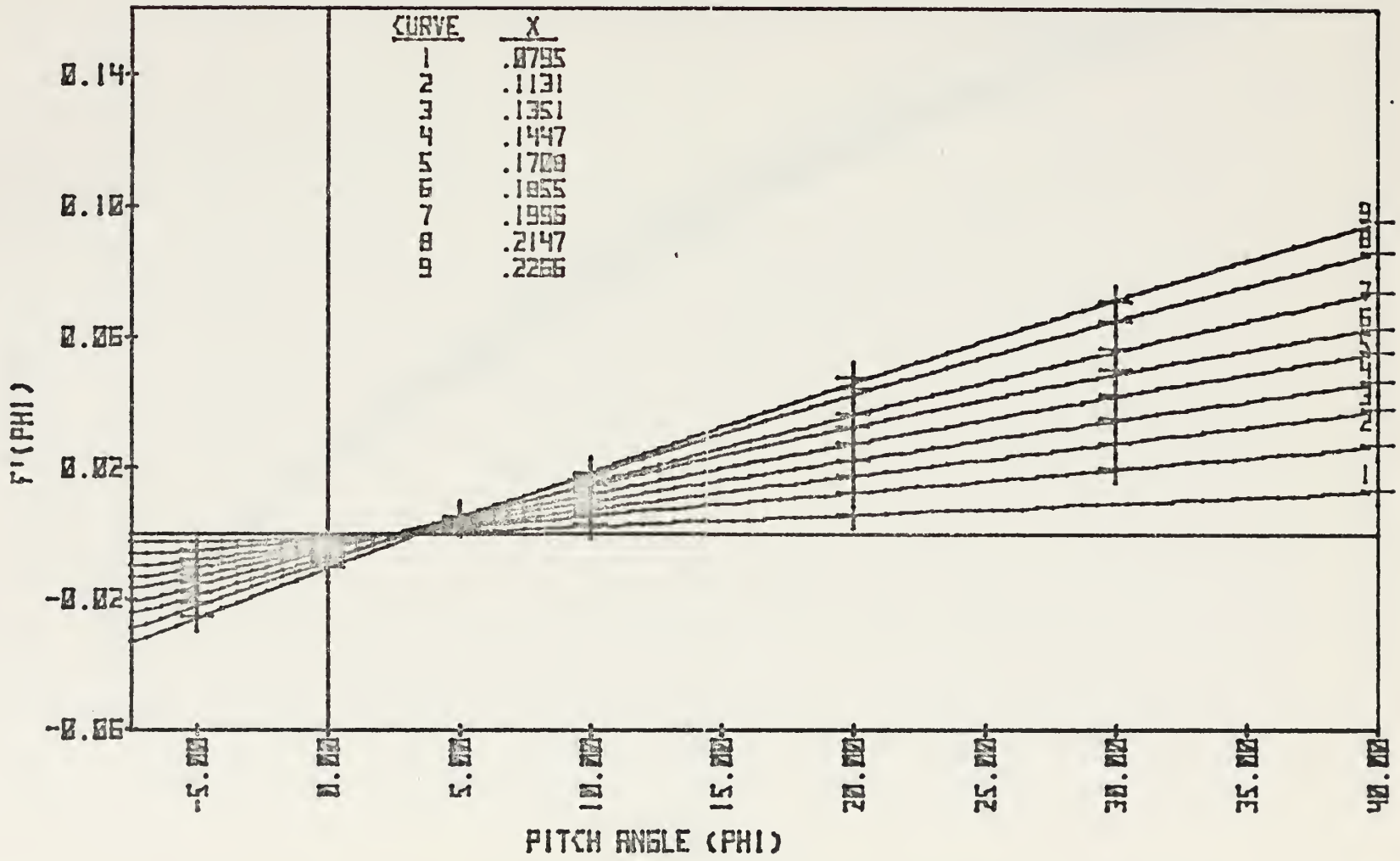

FIGURE A7. F'(PHI) VS. PHI DATA POINTS AND POLYNOMIAL CURVE FITS.

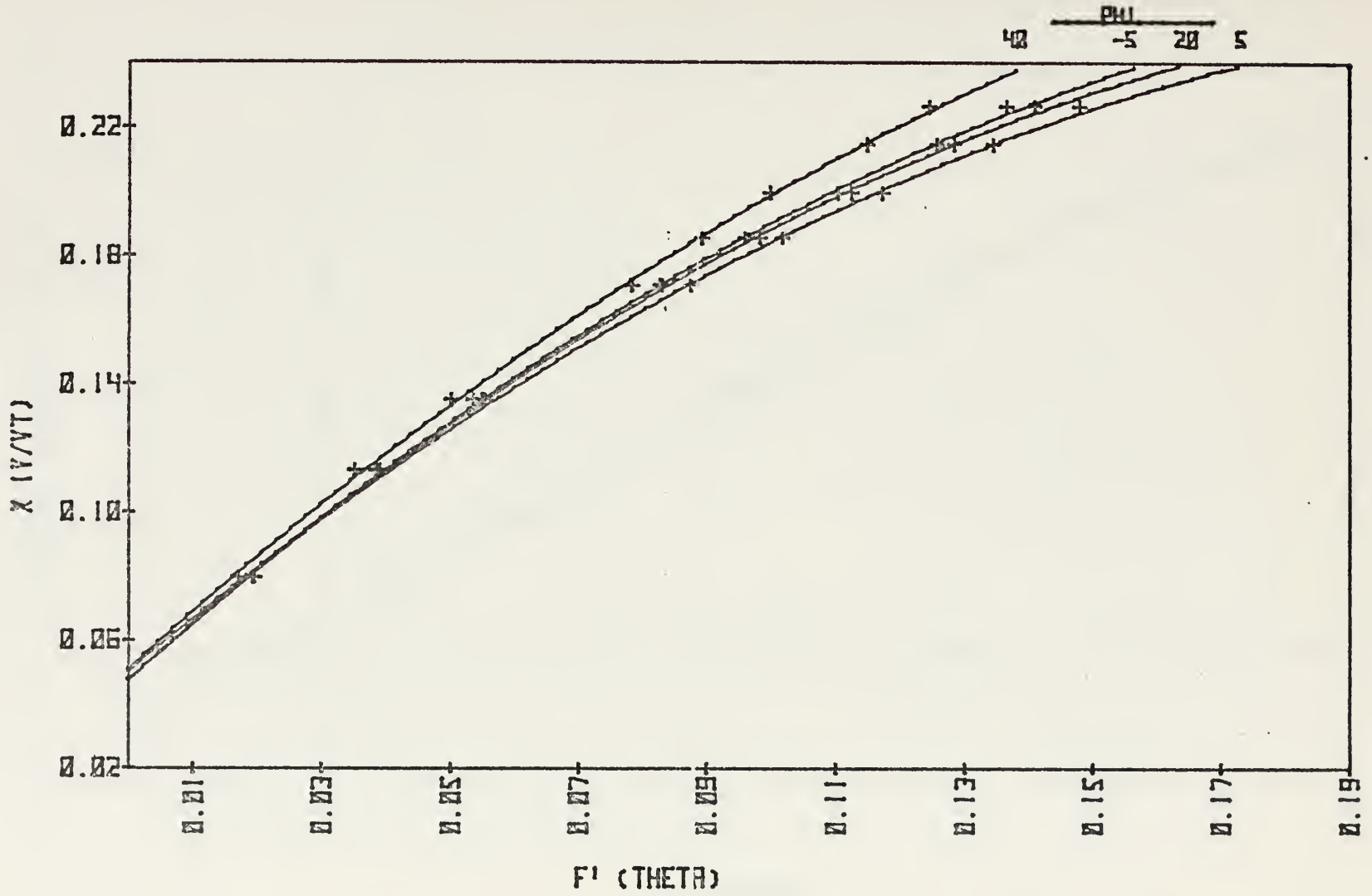

FIGURE A8. X VS F'(THETA) DATA POINTS AND POLYNOMIAL CURVE FITS.

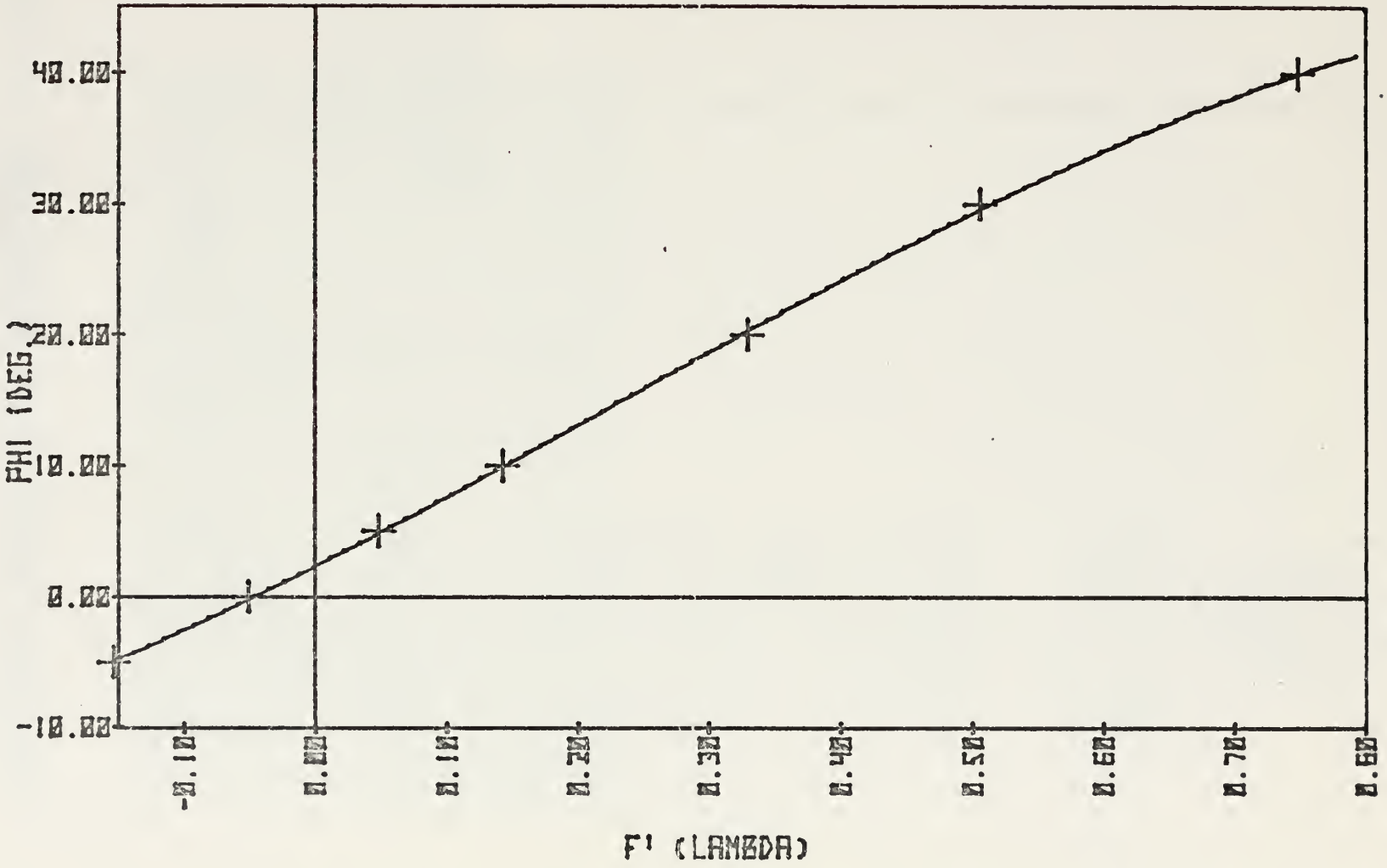

FIGURE A9. PHI VS. AVERAGE F'(LAMBDA) AND POLYNOMIAL CURVE FITS.

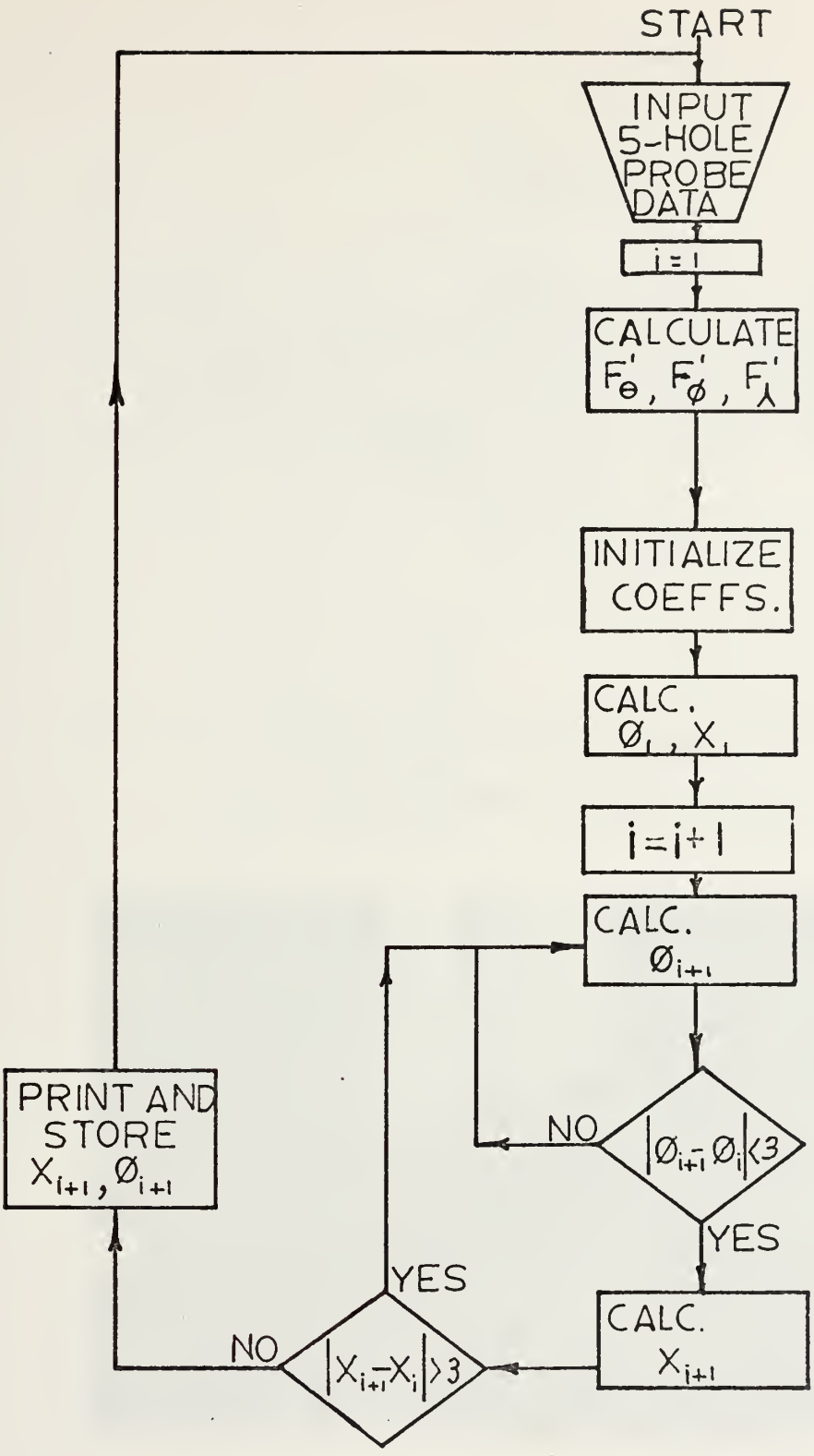

FIGURE A10. FLOW CHART FOR THE REDUCTION OF 5-HOLE PROBE MEASUREMENTS TO VELOCITY AND PITCH ANGLE.

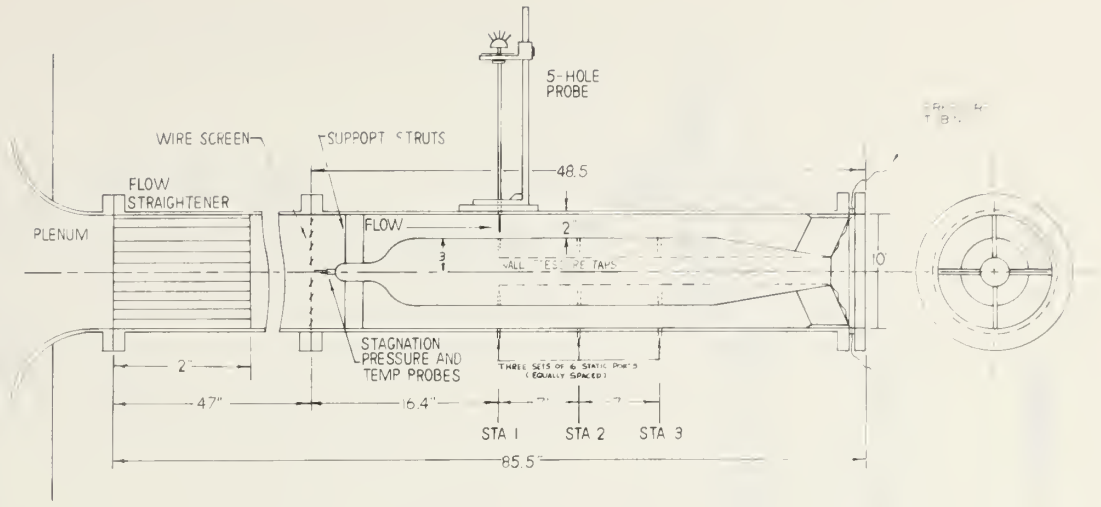

FIGURE A11. SCHEMATIC OF THE APPARATUS FOR PROBE CALIBRATION IN AN ANNULUS

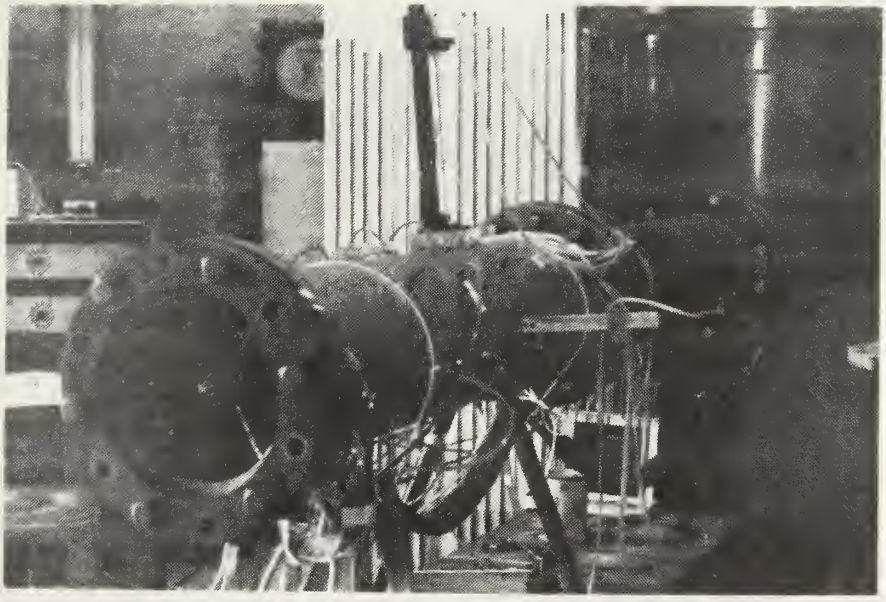

FIGURE A12. VIEW OF THE CALIBRATION APPARATUS

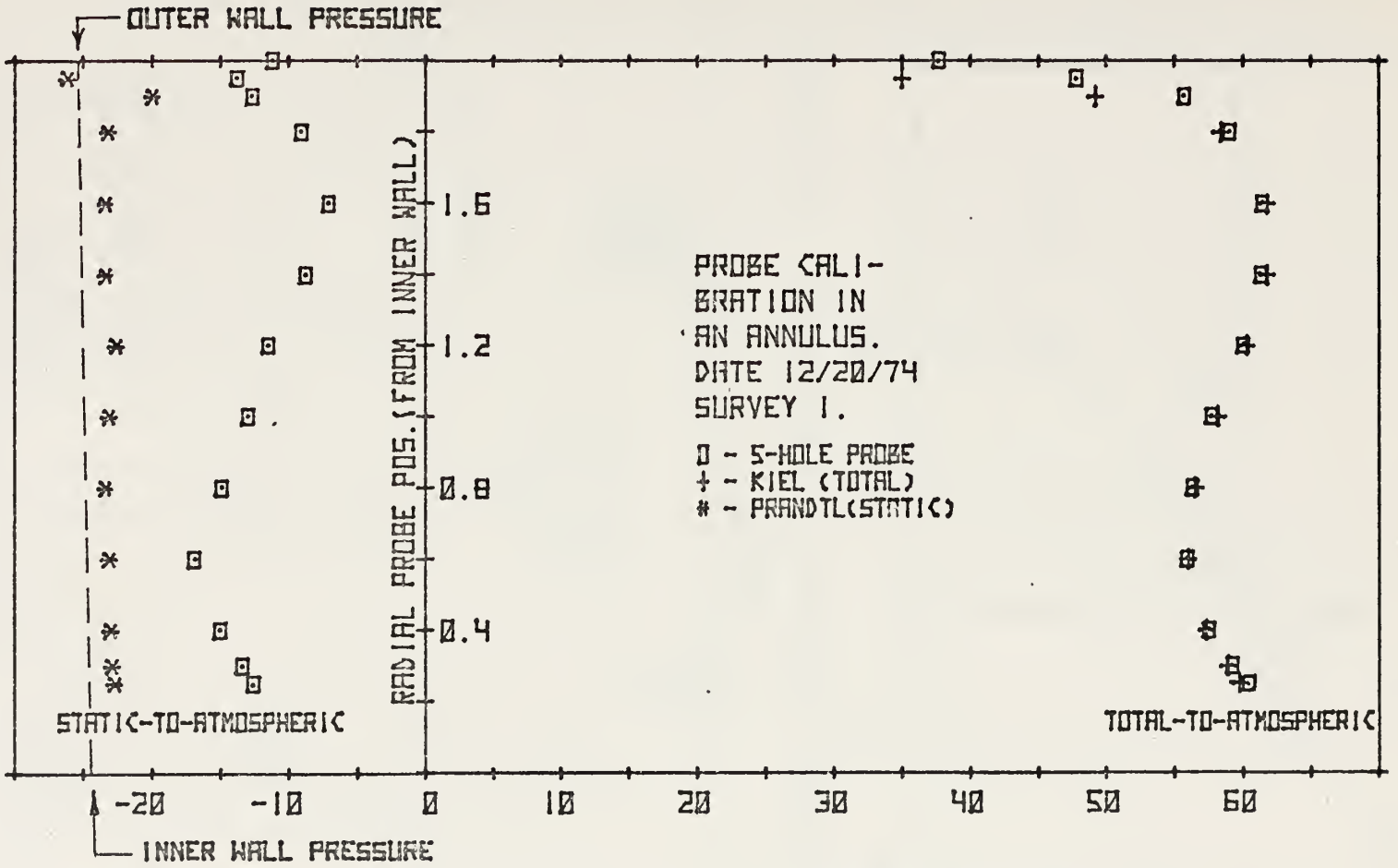

FIGURE A13. RADIAL DISTRIBUTION OF PRESSURE MEASURED IN THE ANNULUS WITH DIFFERENT PROBES.

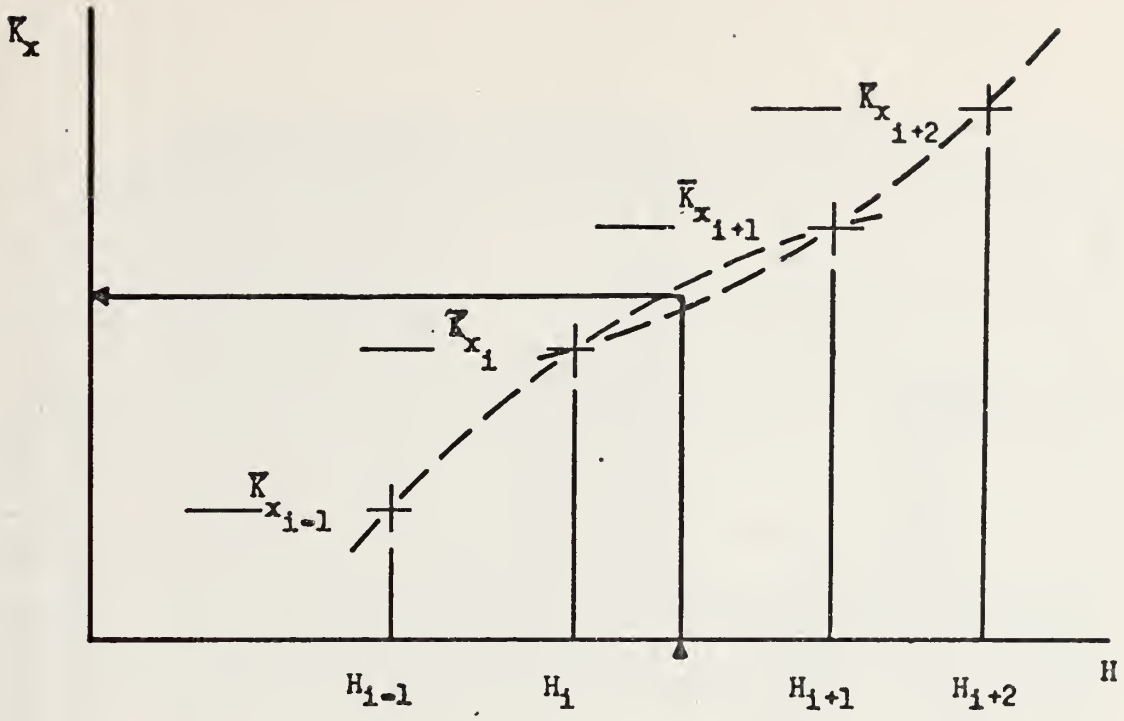

FIGURE A14. ILLUSTRATION OF QUADRATIC INTERPOLATION METHOD

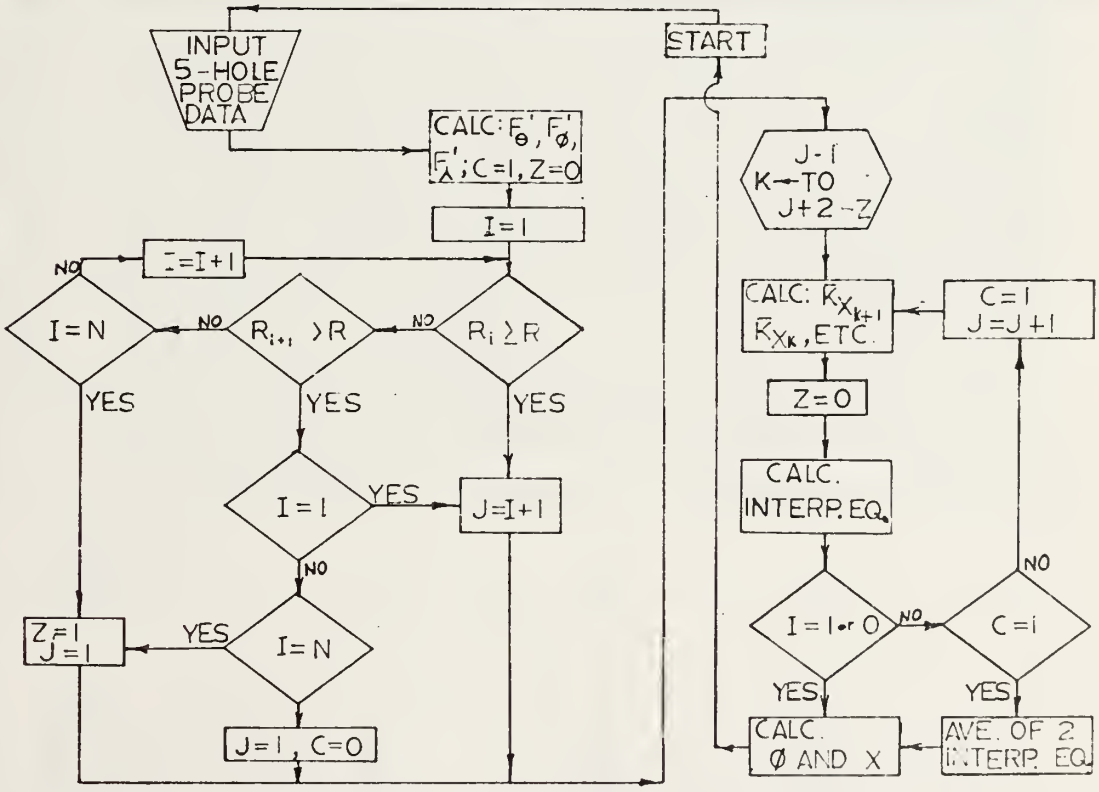

FIGURE A15. FLOW CHART TO CORRECT PROBE CALIBRATION FOR MEASUREMENTS IN AN ANNULUS

TABLE A1. RESULTS OF PROBE CALIBRATION IN A JET.

SURV. NO.	BAROM. (IN. Hg.)	T_{t_1} (°F)	Ø	U-TUBE WATER MANOMETER COLUMN HEIGHT IN INCHES									
				p_A	p_1	$p_{2/3}$	p_1	p_4	p_5	p	p_t	p_t	p_A
1	29.86	102	-5	44.20	39.45	44.30	36.30	43.30	42.20	47.15	38.30	39.60	44.70
			0	44.20	39.45	44.25	36.30	42.90	42.6	47.15	38.30	39.60	44.65
			5	44.20	39.45	44.25	36.30	42.55	43.00	47.15	38.30	39.60	44.65
			10	44.20	39.45	44.25	36.30	42.20	43.30	47.15	38.30	39.60	44.65
			20	44.15	39.50	44.30	36.20	41.55	44.00	47.10	38.30	39.60	44.65
			30	44.20	39.45	44.30	36.20	40.75	44.80	47.15	38.30	39.60	44.65
			40	44.15	39.55	43.80	36.75	40.00	45.55	47.15	38.30	39.60	44.65
2	29.86	102	-5	47.00	36.90	48.15	32.15	43.80	41.70	52.00	33.70	36.90	47.40
			0	47.00	36.85	48.40	31.85	43.00	42.50	52.00	33.70	↓	↓
			5	46.95	36.90	48.25	32.00	42.20	43.30	52.00	33.70		
			10	46.95	36.90	48.30	31.90	41.50	44.00	52.00	33.70		
			20	46.90	36.95	48.20	32.05	40.10	45.40	52.00	33.70		
			30	46.90	37.00	48.30	32.00	38.55	46.95	52.00	33.70	↓	↓
			40	46.80	37.05	47.50	32.85	37.10	48.50	52.05	33.65	36.95	47.35
3	29.86	102	-5	49.30	34.80	51.35	28.80	44.30	41.00	56.00	29.80	34.70	49.70
			0	49.20	34.85	51.75	28.30	43.20	42.20	↓	↓	↓	↓
			5	49.20	34.80	51.65	28.35	42.05	43.35				
			10	49.25	34.75	51.75	28.30	41.00	44.45				
			20	49.20	34.80	51.60	28.50	39.95	46.50			34.75	49.65
			30	49.15	34.85	51.65	28.50	36.90	48.60			↓	↓
			40	49.05	34.95	50.60	29.50	34.70	50.85	↓	↓		
4	29.86	102	-5	51.45	32.75	54.40	25.60	44.80	40.50	59.90	26.00	32.60	51.90
			0	51.50	32.70	55.25	24.80	43.35	42.00	59.90	26.00	↓	↓
			5	51.50	32.70	55.05	24.95	41.90	43.50	60.00	25.90		
			10	51.50	32.70	55.15	24.85	40.45	44.95	↓	↓		
			20	51.40	32.80	54.60	25.40	37.90	47.50				
			30	51.40	32.80	55.05	25.00	35.20	50.25				
			40	51.30	32.90	53.80	26.35	32.90	52.80	↓	↓	↓	↓

TABLE A1.(CONT.)

SURV. NO.	BAROM. (IN. Hg.)	T_{t1} (°F)	Ø	p_A	p_1	$p_{2/3}$	p_1	p_4	p_5	p	p_t	p_t	p_A
5	29.87	100	-5	53.90	30.60	57.70	22.10	45.30	39.90	64.00	21.90	30.30	54.25
			0	53.85	30.60	58.70	20.90	49.60	41.70	64.10	21.80	30.30	54.25
			5	53.80	30.65	58.60	21.00	41.70	43.60	64.10	21.80	30.35	54.30
			10	53.75	30.70	58.25	21.45	39.95	45.40	64.10	21.80	30.40	54.20
			20	53.70	30.75	57.70	22.05	36.75	48.70	64.00	22.00	30.50	54.10
			30	53.65	30.80	58.05	21.65	33.60	51.90	↓	↓	30.55	54.15
			40	53.60	30.80	56.70	23.10	30.85	54.85			30.50	54.20
6	29.87	100	-5	55.90	28.55	60.50	18.90	45.80	39.40	67.80	18.10	28.20	56.40
			0	55.95	28.50	61.80	17.50	43.80	41.50	67.90	18.00		
			5	↓	↓	61.70	17.60	41.55	43.75				
			10			61.60	17.75	39.40	45.90				
			20	55.85	28.60	61.00	18.40	35.50	49.80				
			30	55.85	28.60	61.10	18.25	31.85	53.70	68.00	17.85		
			40	55.90	28.55	59.15	20.45	29.30	56.60	67.95	17.90		
7	29.87	99	-5	58.20	26.25	63.70	15.40	46.50	38.65	72.00	13.95	25.90	58.65
			0	58.15	26.15	65.20	13.55	44.20	41.00	71.90	14.00	25.90	58.65
			5	58.20	26.10	65.10	13.70	41.80	43.60	72.00	13.90	25.80	58.70
			10	58.10	26.20	64.85	14.00	39.10	46.15	72.00	13.90	25.80	58.70
			20	58.10	26.70	64.15	14.90	34.60	50.70	71.90	13.95	25.90	58.60
			30	58.20	26.20	64.05	15.00	30.40	55.25	71.90	14.00	↓	↓
			40	57.95	26.40	61.50	17.80	26.70	59.15	71.90	14.00		
8	29.87	99	-5	60.65	23.50	67.40	11.40	47.20	37.90	76.60	9.40	23.25	61.25
			0	60.70	23.50	68.85	9.40	44.50	40.65	76.60	9.40	23.20	61.25
			5	60.75	23.50	68.95	9.35	41.50	43.70	76.65	9.30	23.25	61.30
			10	60.80	23.55	68.45	9.90	38.65	46.60	76.70	9.30	23.20	61.25
			20	60.55	23.70	67.70	10.85	32.95	52.60	76.75	9.35	23.25	61.30
			30	60.65	23.55	67.90	10.65	28.45	57.30	76.80	9.10	23.10	61.40
			40	60.60	23.85	64.95	14.10	23.95	62.20	76.70	9.25	23.25	61.25
9	29.87	100	-5	62.80	21.50	69.60	8.50	48.20	36.90	81.10	6.00	21.00	63.35
			0	62.60	21.30	71.55	6.55	44.85	40.25	81.15	5.95	20.85	63.45
			5	62.75	21.05	72.40	6.15	41.65	43.55	81.50	5.75	20.80	63.60
			10	62.80	21.45	71.65	6.50	38.45	46.80	81.20	6.10	21.00	63.45
			20	62.80	21.40	70.55	7.45	32.00	53.40	81.35	6.00	21.00	63.50
			30	62.80	21.45	70.15	8.00	27.00	58.80	81.35	5.90	21.05	63.40
			40	62.50	21.65	67.05	11.40	21.65	64.45	81.15	6.10	21.05	63.35

TABLE A2. RESULTS OF PROBE CALIBRATION IN AN ANNULUS

UNITED SENSOR 5-HOLE PROBE DA-125(847-2) BAROMETER (p_A): 30.17 IN.Hg.

SURV NO.	PRESS. DIFF. ($IN.H_2O$)	DISTANCE FROM HUB (INCHES) 0.25	0.30	0.40	0.60	0.80	1.00	1.20	1.40	1.60	1.80	1.90	1.95	2.00
1	p_1-p_A	60.4	59.2	57.5	55.9	56.3	57.7	60.0	61.3	61.4	59.0	55.7	47.8	37.7
	$p_{23}-p_A$	-12.6	-13.4	-15.0	-16.9	-14.9	-13.0	-11.5	-8.8	-7.1	-9.1	-12.7	-13.8	-11.2
	p_4-p_5	-3.6	-4.4	-5.5	-7.0	-7.2	-7.2	-6.9	-6.0	-4.1	0.4	4.7	9.2	17.9
2	p_1-p_A	52.7	51.8	50.6	49.8	50.0	51.5	53.1	53.6	53.3	51.1	49.1	42.3	33.3
	$p_{23}-p_A$	-10.7	-11.6	-13.8	-14.7	-12.9	-11.2	-9.8	-7.7	-6.1	-8.4	-10.6	-12.0	-10.0
	p_4-p_5	-2.5	-3.3	-4.5	-5.9	-6.0	-5.9	-5.5	-4.7	-3.0	1.0	3.8	7.2	14.7
3	p_1-p_A	46.2	45.7	44.5	44.0	44.4	45.8	47.0	47.4	47.1	44.8	41.5	36.5	28.7
	$p_{23}-p_A$	-9.5	-10.4	-12.7	-13.4	-11.6	-10.0	-8.9	-6.8	-5.5	-7.7	-10.0	-10.9	-9.1
	p_4-p_5	-2.0	-2.6	-3.9	-5.0	-5.1	-5.0	-4.7	-3.9	-2.4	1.1	3.5	6.2	12.5
4	p_1-p_A	40.4	39.6	38.6	38.0	38.3	39.5	40.8	41.5	41.4	39.3	36.5	31.6	24.2
	$p_{23}-p_A$	-8.5	-9.1	-11.9	-11.9	-10.5	-9.1	-8.1	-6.3	-4.9	-6.6	-9.2	-9.5	-7.6
	p_4-p_5	-1.6	-2.2	-3.5	-4.2	-4.4	-4.2	-4.0	-3.4	-2.1	0.8	3.0	5.5	11.7
5	p_1-p_A	34.5	34.0	33.1	32.1	31.9	32.8	34.0	34.7	34.4	33.0	30.4	26.5	19.3
	$p_{23}-p_A$	-7.3	-7.7	-10.2	-10.1	-9.1	-7.9	-7.0	-5.4	-4.2	-5.2	-7.4	-7.8	-6.3
	p_4-p_5	-1.3	-1.9	-2.8	-3.3	-3.7	-3.5	-3.3	-2.7	-1.8	0.3	2.6	4.7	10.2
6	p_1-p_A	28.4	28.0	27.3	26.6	26.5	27.3	28.2	28.7	28.4	27.1	25.1	21.2	15.9
	$p_{23}-p_A$	-6.0	-6.7	-8.6	-8.4	-7.8	-6.7	-5.9	-4.7	-3.6	-4.4	-5.8	-6.4	-5.2
	p_4-p_5	-1.2	-1.6	-2.3	-2.7	-2.9	-2.8	-2.6	-2.2	-1.3	0.5	2.0	3.8	7.9
7	p_1-p_A	22.3	22.0	21.4	20.9	20.9	21.4	22.1	22.5	22.2	20.2	19.5	16.5	12.2
	$p_{23}-p_A$	-4.8	-5.3	-6.7	-6.5	-6.1	-5.3	-4.6	-3.7	-2.8	-3.7	-4.7	-5.0	-4.2
	p_4-p_5	-0.8	-1.2	-1.8	-2.1	-2.2	-2.1	-2.1	-1.7	-0.9	0.6	1.6	3.1	6.2

TABLE A2. (CONT.)

KIEL PROBE — BAROMETER (p_A): 30.17 IN.Hg.

SURV NO.	PRESS. DIFF. ($IN.H_2O$)	DISTANCE FROM HUB (INCHES) 0.25	0.30	0.40	0.60	0.80	1.00	1.20	1.40	1.60	1.80	1.90	1.95	2.00
1	p_t-p_A	59.8	58.9	57.3	56.0	56.5	58.2	60.3	61.8	61.8	58.4	49.2	35.0	-
	p_t-p	83.9	83.0	81.5	80.3	80.9	82.7	84.8	86.4	86.5	83.2	74.1	59.9	
7	p_t-p_A	22.3	22.0	21.5	21.0	20.9	21.5	22.2	22.5	22.3	20.9	17.4	12.6	
	p_t-p	20.2	20.3	20.4	20.6	20.8	21.0	21.2	21.4	21.6	21.8	21.9	22.0	

p=wall pressure.

PITOT-STATIC PROBE — BAROMETER (p_A): 30.17 IN.Hg.

1	p_s-p_A	-22.7	-22.9	-23.0	-23.1	-23.4	-32.1	-22.6	-23.4	-23.4	-23.2	-20.0	-26.2	-
7	p_s-p_A	-7.8	-7.5	-7.4	-7.4	-7.4	-7.3	-7.3	-7.4	-7.3	-7.3	-7.7	-8.5	-

p_s= probe static pressure.

TABLE A3. COEFFICIENTS FOR EQ. A(14)

ORDER OF COEFFICIENT	EQ. 14(a) a(x)	EQ. 14(a) b(x)	EQ. 14(a) c(x)	EQ. 14(b) f(ø)	EQ. 14(b) g(ø)	EQ. 14(b) h(ø)
ZEROTH	-0.004046	-0.0001054	5.1653×10^{-6}	0.04995	1.7027	-3.5102
FIRST	0.073024	0.0010741	-4.1165×10^{-5}	1.7255×10^{-4}	-0.00644	0.001453
SECOND	-0.43267	0.055827	-1.0657×10^{-4}	-2.17×10^{-5}	5.328×10^{-4}	1.25×10^{-4}
THIRD	0	0	0	4.6×10^{-7}	-8.0×10^{-6}	0

EXAMPLE: $a(x) = -0.004046 + (0.073024).X - (0.43267).X^2$

TABLE A4. COEFFICIENTS IN EQ. A(16)

J	K	L	M
2.389	51.013	19.813	-27.708

TABLE A5. COEFFICIENTS FOR EQ. A(19)

R(IN.)	i	q_i	r_i	s_i	t_i	u_i	v_i
0.25	1	0.2665	-3.2028	9.3584	0	0	0
0.3	2	0.2334	-2.9667	8.8060			
0.4	3	0.4412	-5.7011	16.5125			
0.6	4	0.3419	-4.4082	12.4122			
0.8	5	0.2663	-3.5527	10.3881			
1.0	6	0.2577	-3.2609	9.5088			
1.2	7	0.2860	-3.4314	9.9040			
1.4	8	0.2565	-2.9199	8.6109			
1.6	9	0.2674	-2.7889	8.1486			
1.8	10	1.5690	-38.4439	361.1053	-1510.6201	2365.1646	
1.9	11	-5.3574	124.4065	-1060.0796	3932.2165	-5356.9732	
1.95	12	9.0701	-284.4704	3543.1654	-21818.4473	66267.8659	-79303.1550

TABLE A6. COEFFICIENTS FOR EQ. A(22)

z_1	z_2	z_3	z_4	z_5	z_6	z_7
-0.0543	0.6963	-3.5519	10.2028	-16.5283	13.9093	-4.7455

TABLE A7. RESULTS OF APPLYING ANALYTICAL CORRECTION TO CALIBRATION MEASUREMENTS IN AN ANNULUS.

	SURVEY # 3			
R/R0	X(UNMOD)	X(ACTUAL)	X(MOD)	% ERROR
0.1250	0.2048	0.2053	0.2054	0.0619
0.1500	0.2059	0.2045	0.2050	0.2498
0.2000	0.2088	0.2027	0.2028	0.0562
0.3000	0.2099	0.2018	0.2025	0.2977
0.4000	0.2073	0.2023	0.2025	0.0954
0.5000	0.2066	0.2043	0.2045	0.1033
0.6000	0.2063	0.2060	0.2063	0.1350
0.7000	0.2027	0.2065	0.2065	0.0111
0.8000	0.1990	0.2059	0.2062	0.1355
0.9000	0.1981	0.2024	0.2027	0.1339
0.9500	0.1965	0.1974	0.1974	0.0122
0.9750	0.1893	0.1894	0.1895	0.0127

APPENDIX B: DETERMINATION OF BLOCKAGE FACTOR FOR FLOW INTO THE ROTOR

B.1. INTRODUCTION

The analysis in Reference 1 established a blockage factor for the flow into the TRANSX compressor rotor which was used to correct inviscid mass flow calculations. The blockage factor at station 1 was defined as,

$$K_B = \frac{\dot{w}_m}{\dot{w}} = \frac{\text{measured flow rate}}{\text{inviscid flow rate}} \qquad B(1)$$

and K_B was shown to be related to the displacement thickness of the boundary layer. Preliminary measurements were made ahead of the TRANSX compressor rotor to determine the boundary layer thickness at the outer wall [Reference 1]. From the measurements, ignoring the hub wall boundary layer, and assuming that the inviscid flow field was described correctly, the result obtained was,

$$K_{B_1} = 0.989$$

Then the flow into the rotor was described by the inviscid flow calculation for a total flow rate ($\dot{w}$) which was related to the measured flow rate ($\dot{w}_m$) by the relation

$$\dot{w} = \dot{w}_m / K_{B_1} \ .$$

The purpose of the present study of the flow into the rotor was to measure the inviscid flow

field, as well as the boundary layer region, and to relate the measurements to the analytical description. It was necessary therefore to change the definition of blockage factor, from that involving only boundary layers, to obtain the desired relationship. In the following sections, necessary parts of the analysis given in Reference 1 are repeated, and the method is given for relating the analytical distribution of mass flux and flow angle to the distributions measured using the 5-hole probe.

B.2. ANALYTICAL BACKGROUND AND METHOD

Referring to Fig. B1, and assuming that streamlines are axisymmetric, continuity at station 1 gives

$$\dot{w} = \int_{r_i}^{r_o} \rho V \cos\lambda \cdot (2\pi r)\, dr \qquad B(2)$$

Non-dimensionalizing Eq. B(2),

$$\overline{W}_t = \frac{\dot{w}}{\rho_t V_t \pi r_o^2} = \int_{r_i^2}^{r_o^2} \frac{\rho V}{\rho_t V_t} \cos\lambda \; d\left(\frac{r}{r_o}\right)^2 \qquad B(3)$$

The definition of the total flow function is given in Reference 7 as

$$\Phi = \frac{\rho V}{\rho_t V_t} = X(1-X^2)^{\frac{1}{\gamma-1}}, \text{ where}$$

$$X = V/V_t \text{ and } V_t = \sqrt{2c_p T_t}\,.$$

Writing $R = r/r_o$, Eq. B(3) taken between R_1 and R_2

becomes

$$\overline{W} = \int_{R_1^2}^{R_2^2} \Phi \cos\lambda \, d(R^2) \, .$$

Introducing the values of the flow function and flow angle at the outer wall, indicated by a "o" subscript, the above equation becomes

$$\overline{W} = \Phi \cos\lambda_o \int_{R_1^2}^{R_2^2} \frac{\Phi}{\Phi_o} \quad \frac{\cos\lambda}{\cos\lambda_o} \, d(R^2)$$

In the TRANSX compressor $\lambda_o = 0$, therefore

$$\overline{W} = \Phi_o \int_{R_1^2}^{R_2^2} \left(\frac{\Phi}{\Phi_o}\right) \cos\lambda \, d(R^2) \qquad B(4)$$

The assumption is then made, in Reference 1, that the pattern of streamlines does not depend on the flow rate, that $\overline{\Phi} = \Phi/\Phi_o$ is a function of R only and $\cos\lambda$ is another function of R. Based upon functions derived from a computer solution of the compressible flow, for $R_1 = R_i$ and $R_2 = R_o$, it is shown that

$$\xi = \int_{R_i^2}^{R_o^2} \overline{\Phi} \cos\lambda \, d(R^2) = 0.70836 \qquad B(4a)$$

where, using Eq. B(4),

$$\overline{W}_t = \Phi_o \xi \,. \qquad \text{B(4b)}$$

Therefore the "theoretical" flow rate is proportional to the value of the analytical flow function at the outer wall.

In order to relate the analytical description of the flow to the measured distributions of the flow function and angle, the "theoretical" mass flux was integrated and set equal to the integral of the measured distribution of the mass flux over that region of the flow where the measurements were valid. The probe measurements were considered to be free of "immersion" or "wall" effects from 20% to 80% of the hub-to-tip survey. Therefore, using Eq. B(4)

$$\int_{R_1^2}^{R_2^2} \Phi_m \cos\lambda_m d(R^2) = \Phi_o \int_{R_1^2}^{R_2^2} \overline{\Phi} \cos\lambda \, d(R^2) \qquad \text{B(5)}$$

defines a value of the analytical flow function at the outer wall which corresponds to the measured flow conditions. Equation B(4b) then gave the "theoretical" flow rate corresponding to the measured flow rate, and Eq. B(1) was again used to evaluate a blockage factor.

B.3. PROCEDURE

The analytical distribution of the total flow function [Ref. 1] is represented as

$$(1-R^2) = a_1(1-\bar{\Phi})^{n_1} + m_1(1-\bar{\Phi}), \qquad B(6)$$

where a_1, n_1, m_1 are coefficients, listed in Table B1, which were evaluated in Reference 1 from a computer solution using a curve fitting technique. $\bar{\Phi}$ is unknown for a given R and must be determined as follows:

1) Choose an initial value for $\bar{\Phi}$ which does not exceed unity. Take
   $\bar{\Phi}_1 = 1-.03(1-R_1^2)^2$, R_1 given.
2) Set $Y = 1-\bar{\Phi}_i$, i=1, 2,..., n
3) Calculate $R_i^2 = 1-a_1Y^{n_1}-m_1Y$
4) Test for convergence of calculated R^2;
   ? $\left|R_1^2 - R_i^2\right| < \mathcal{E}$, $\mathcal{E}$ = convergence limit.
   If yes, the solution is complete.
   If no, continue to step 5.
5) Calculate the slope
   $d(R_i^2)/dy = -a_1n_1Y^{n_1-1} - m_1$, and calculate
   $$\bar{\Phi}_{i+1} = \bar{\Phi}_i - \left[\frac{R_1^2-R_i^2}{d(R_i^2)/dy}\right]$$
6) Repeat steps (2) through (5) until convergence occurs.

Using this procedure the value of $\bar{\Phi}$ could be calculated

for each probe position R.

A quantity K_o was defined such that

$$K_o = \int_{R_1^2}^{R_2^2} \bar{\Phi} \cos\lambda \cdot d(R^2) \ . \qquad B(7)$$

K_o was determined for a given R_1 and R_2 using numerical integration applied over unequal intervals. R_1 was chosen to be the first point greater than 20% of the distance from hub to tip and R_2 was chosen to be the last point before 80% of the distance from hub to tip.

The analytical distribution for the flow angle (λ) used in Eq. B(4a) was evaluated in Reference 1 as

$$\cos\lambda = a_2 (1-R^2)^{n_2} + m_2 (1-R^2) \qquad B(8)$$

where the coefficients are given in Table B1.

Using Eq. B(5), Eq. B(4b) and Eq. B(3) with the perfect gas equation of state in Eq. B(7),

$$K_o = \frac{\frac{g}{J} K_{B_1} \pi r_o^2 V_t}{\dot{w}_m R_G T_t} \int_{R_1^2}^{R_o^2} p_t \, \Phi_m \cos\lambda_m \, d(R^2) \qquad B(9)$$

p_t, λ_m and Φ_m are given from measurements at each point in the probe survey and all other quantities in Eq. B(9) are constant for the survey. Since slight variations in the flow rate were noted during the survey, a correction was introduced. The measured flow

rate, $\dot{w}_m$, in Eq. B(9) was the average of data reduced from scans of fixed instrumentation taken before and after each survey. The value of $\dot{w}_m$ corresponded to a differential pressure, Δh_r, across a flow nozzle. Since the flow rate at any time was proportional to the square root of this differential pressure, Δh, the value of Δh was recorded at each survey point. Rearranging Eq. B(9), with the correction introduced into the integration, the blockage factor is given by

$$K_{B_1} = \frac{K_o \dot{w}_m R_G T_t}{\pi r_o^2 V_t} \left[\frac{1}{\int_{R_1^2}^{R_2^2} \sqrt{\frac{\Delta h_r}{\Delta h}}\, p_t \Phi_m \cos\lambda_m \, d(R^2)} \right] \qquad B(10)$$

Eq. B(6), B(7) and B(10) were programmed to calculate the blockage factor for flow at the rotor inlet from probe survey measurements.

The correction for slight variations in the flow rate was also included in comparing the measured and analytical distributions of the mass flux (or flow function). The left hand side of Eq. B(5) is written, with the addition of the flow correction, as

$$K_m = \int_{R_1^2}^{R_2^2} \Phi_m \sqrt{\frac{\Delta h_r}{\Delta h}} \cos\lambda_m \, d(R^2) \qquad B(11)$$

so that with Eq. B(7), Eq. B(5) becomes

$$K_m = \Phi_o K_o.$$

The analytical flow function, which was included on plots of the measured flow function, was obtained from

$$\overline{\Phi}(R) = \overline{\Phi}\,(R)\left(\frac{K_m}{K_o}\right) \qquad B(12)$$

where $\overline{\Phi}$ was obtained from Eq. B(6), K_m was obtained from Eq. B(11) and K_o was already known from Eq. B(7).

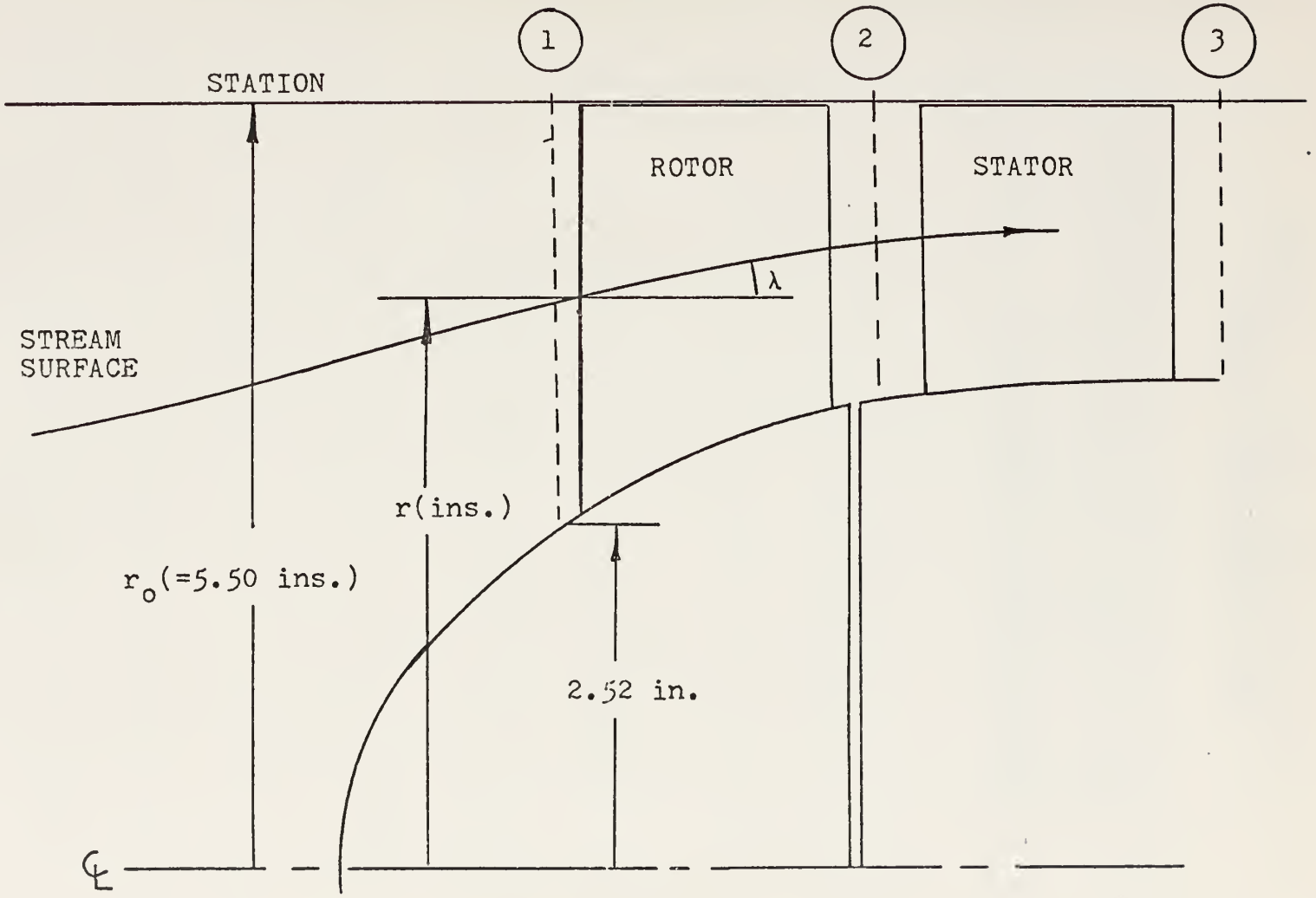

FIGURE B1. SCHEMATIC OF COMPRESSOR GEOMETRY

TABLE B1. CURVE FIT COEFFICIENTS
FOR EQ. B(6) AND EQ. B(8)

EQUATION	i	a_i	n_i	m_i
B(6)	1	1.79864	0.38582	22.3048
B(8)	2	0.98927	3.81679	0.47149

REFERENCES

1. Naval Post Graduate School Report NPS-57Sf4081, Flow Into A Transonic Compressor Rotor, Part-1 Analysis, by R.P. Shreeve, August 1974.

2. NASA Technical Note TN D-4816, A Small Combination Sensing Probe for Measurement of Temperature Pressure, and Flow Direction, by G.E. Glawe, L.M. Krause and T.J. Dudzinski, October 1968.

3. Naval Post Graduate School Report NPS-57Va72091A, A Description of the Turbopropulsion Laboratory in the Aeronautics Department at the Naval Post Graduate School, by M.H. Vavra and R.P. Shreeve, September 1972.

4. Naval Post Graduate School Report NPS-57Va73071A, Design Report of Hybrid Compressor and Associated Test Rig, by M.H. Vavra, July 1973.

5. Naval Post Graduate School Report NPS-57Sf73112A, Report on the Testing of A Hybrid (Radial-to-Axial) Compressor, by R.P. Shreeve, November 1973.

6. U.S. Army Aviation Material Laboratories Technical Report 67-30, Element Design and Development of Small Centrifugal Compressor, Volume II, by A.D. Welliver and J. Acurio, August 1967.

7. Naval Post Graduate School Report NPS-57Sf73071A, Calibration of Flow Nozzles Using Traversing Pitot-Static Probes, by R.P. Shreeve, July 1973.

8. United Sensor Corporation, Bulletin 5 "Directional Probes 3-Dimensional". United Sensor and Control Corp., Watertown, Massachusetts.

9. Conte, S.D. and deBoor, C., Elementary Numerical Analysis: An Algorithmic Approach, McGraw Hill (p. 44-49).

10. Shreeve, R.P., "Program to Calculate Non-Uniform Cylindrical Flow in a Compressor Annulus", Memo GA-RPS 7406-1, 20 June 1974 (Unpublished).

INITIAL DISTRIBUTION LIST

		No. Copies
1.	Defense Documentation Center Cameron Station Alexandria, Virginia 22314	2
2.	Library, Code 0212 Naval Postgraduate School Monterey, California 93940	2
3.	Chairman, Department of Aeronautics Naval Postgraduate School Monterey, California 93940	1
4.	Associate Professor R.P. Shreeve, Code 57Sf Department of Aeronautics Naval Postgraduate School Monterey, California 93940	1
5.	Distinguished Professor M. H. Vavra, Code 57Va Department of Aeronautics Naval Postgraduate School Monterey, California 93940	1
6.	Mr. J. E. Hammer, Code 57 Department of Aeronautics Naval Postgraduate School Monterey, California 93940	1
7.	Dr. H. J. Mueller Research Administrator, Code 310A Naval air Systems Command Navy Department Washington, D. C. 20360	1
8.	Turbo-Propulsion Laboratory Naval Postgraduate School Monterey, California 93940	10
9.	LT. D. J. Anderson, USN HC-6, NAS Norfolk, Virginia 23541	1